الجمهورية الجزائرية الديموقراطية الشعبية

Popular and democratic republic of Algeria

وزارة التعليم العالي و البحث العلمي

Ministry of higher education and scientific research

University of Mohamed Khider, Biskra
Faculty of Sciences and Technology
Department of Civil and Hydraulic Engineering
Ref.:……

جامعة محمد خيضر بسكرة
كلية العلوم و التكنولوجيا
قسم الهندسة المدنية و الري
المرجع:……

Thesis presented in order to obtain the degree of

Doctorate in Civil Engineering

Speciality: Geomechanics and structures in interaction

Analyse numérique de la stabilité des pentes renforcées par pieux

Numerical analysis on the stability of slopes reinforced with piles

Presented by:

Imene Bougouffa

Thesis defended publicly on: 13/03/2022

The jury is composed of:

Mr. Abdelhafid Ounis	**Professor**	**President**	**University of Biskra**
Mr. Mekki Mellas	**Professor**	**Supervisor**	**University of Biskra**
Mr. Mohamed Baheddi	**Professor**	**Co-supervisor**	**University of Batna2**
Mr. Mohamed Salah Nouaouria	**Professor**	**Examiner**	**University of Guelma**
Mr. Djamal Benmeddour	**Professor**	**Examiner**	**University of Biskra**
Mr. Abdelhak Mabrouki	**Professor**	**Guest**	**University of Biskra**

To my dearest and precious parents

To my husband and siblings

To all my family members

To my friends

ACKNOWLEDGEMENTS

My deep gratitude goes first to Allah, who never led me astray. Without his guidance and persistent help, this work wouldn't have been accomplished.

I would like to express the deepest appreciations to my supervisor Mr. Mekki Mellas, Professor at the University of Biskra. His encouragements and support conveyed by introducing me precious advices and orientations, served at moving forward in regard to research.

I address my sincere respect and appreciations to Mr. Abdelhak Mabrouki, Professor at the University of Biskra. Who has the attitude and a substance of a genius, expressed by his time and efforts paid in order to give a genuine boost to this dissertation. He continually and convincingly conveyed a spirit of optimism in regard to teaching.

Also, gratitude to my co-supervisor Mr. Mohamed Baheddi, Professor at the University of Batna. Who expertly provided a genuine kindness to help sustain a positive atmosphere, in which to do the research.

My appreciations extend to Mr. Kristian Krabbenhoft, Professor at the University of Liverpool, Ms. Pelin Tohumcu Ozener, Professor at the University of Istanbul, and Pr. Jean-Michel Pereira, manager of research laboratory Navier-CERMES of Paris. Their welcoming and kind hosting are highly esteemed. As well as, their early insights that launched the greater part of this dissertation.

In addition, appreciations go to the head of committee Mr. Abdelhafid Ounis, Professor at the University of Biskra, for accepting judging this dissertation. Thankfulness is extended to all the committee members for reviewing the manuscript, Mr. Mohamed Salah Nouaouria, Professor at the University of Guelma, and Mr. Djamal Benmeddour, Professor at the University of Biskra.

Gratefulness goes to managers of the Civil Engineering laboratory research LRGC of Biskra. By dint of their mentoring throughout all these years.

Above ground, i am indebted to my parents and husband, whose value to me only grows with age. Their mental and physical support throughout my educational path are highly appreciated. Because they literally shared the excitement of years of discovery. Their personal generosity served at making my time pleasurable.

Abstract

The assessment of slope stability is attributed to various critical conditions; one of which is the self-weight sliding stimulus, and the other one induces failure caused by a surface load condition (shallow foundation). In the particular case of a shallow foundation situated on a slope crest, the bearing capacity is significantly reduced. Therefore in practice, anti-slide piles are used to enhance the performance of the nearby footing. Whereas, the studies tend to rely on the hypothesis of purely vertical surface load condition. The present dissertation aims to contribute to the numerical and stochastic analyses by inducing vertical retaining structures, in order to deal with the group problem of slope stability and bearing capacity of an adjacent combined loaded strip footing. Firstly, a bibliographical research is presenting the most common deterministic and probabilistic methods, pertaining to slope stability assessment and bearing capacity of a shallow foundation. Followed by a presentation of bibliographical synthesis concerning studies published in the literature. The second part furnishes a contribution to the numerical analysis using the finite element software OptumG2. The investigation of the factor of safety is conducted under various conditions of a pile row, using elastoplastic shear strength reduction method. Thence after, a conducted study is done on the effect of reinforcing a cohesive slope by a row of multiple number of piles and a sheet pile wall on the undrained bearing capacity of a rigid strip footing, using the limit analysis.

Key words:

Factor of safety, Pile-stabilized slope, Sheet pile wall, Shallow foundation, Bearing capacity improvement, Inclined loading.

Résumé

La stabilité des pentes dépend du poids propre et les conditions de chargement surfacique. Dans le cas particulier d'une fondation superficielle située au bord d'une pente, la capacité portante est réduite significativement. En conséquence, l'utilisation des pieux comme une technique de renforcement peut montrer une excellente amélioration. Dans ce cas, les études ont tendance de s'appuyer sur l'hypothèse d'une fondation soumise à un chargement vertical centré. La présente thèse, vise à contribuer à l'analyse numérique et stochastique, concernant le problème combiné de la stabilité des pentes et la capacité portante d'une semelle filante sous chargement incliné. En considérant, le renforcement par des structures de soutènement verticales. Tout d'abord, une recherche bibliographique est consacrée à la présentation des méthodes déterministes et probabilistes, pour la détermination de la stabilité du talus et la capacité portante d'une fondation superficielle; ainsi que les travaux publiés sur ce sujet. La deuxième partie, présente des contributions à l'analyse numérique en utilisant le code en éléments finis OptumG2. Des investigations du facteur de sécurité sont appliquées sous diverses conditions d'une rangée de pieux, en utilisant la méthode élastoplastique de la réduction de la résistance au cisaillement. Egalement, une analyse limite est adoptée pour évaluer les facteurs influençant la capacité portante d'une semelle filante rigide, située au bord d'un talus purement cohérent renforcé par une rangée de pieux ou un rideau de palplanche.

Mots clés :

Facteur de sécurité, Pente renforcée par pieux, Rideau de palplanche, Fondation superficielle, Amélioration de la capacité portante, Chargement incliné.

ملخص

إن تقييم استقرار المنحدرات يعود الى عدة شروط حرجة، من بينها الوزن الذاتي المتسبب في إنزلاق التربة؛ و الآخرمتمثل في تواجد حمولة زائدة سطحية (أساس سطحي). الأساسات التي تقع عادة على قمم المنحدرات؛ قدرة تحملها تنقص بشكل ملحوظ. عمليا، استعمال الأعمدة المضادة لإنزلاق التربة يرفع كثيرا من قدرة التحمل. في حين أن الدراسات التي أجريت تعتمد على فرضية كون الحمولة عمودية بحتة، هذه الأطروحة تهدف إلى المشاركة في التحليل العددي والعشوائي لمجموعة من المشاكل، المتمثلة في استقرارية المنحدر و قدرة تحمل الأساس المجاور بوجود حمولة مائلة. و ذلك يتم عن طريق استعمال أعمدة و جدران تدعيمية. في الجزئية الأولى، بحث يعرض أشهر الطرق الحتمية و الافتراضية لتقييم استقرارية المنحدر و قدرة تحمل الأساس السطحي، متبوعا بملخص بيبليوغرافيكي للدراسات المنجزة. الجزئية الثانية تتمثل في المشاركة العلمية في التحليل العددي بواسطة برنامج العنصرالنهائي. دراسة فحص معامل الأمان تمت من خلال استعمال طريقة تخفيض قوة القص. ثم بعد ذلك، دراسة أجريت باستعمال طريقة التحليل الحدي، حول العوامل المؤثرة في قدرة تحمل الأساس السطحي المجاور لمنحدر مدعم و مكون من تربة متماسكة.

الكلمات المفتاحية

معامل الأمان، منحدر مدعم بأعمدة تثبيتية ، جدار تدعيمي، أساس سطحي، تحسين قدرة التحمل، حمولة مائلة.

Table of Contents

General introduction 1

Chapter 1: Principle of different slope analyses by virtue of the sliding stimulus 4

1.1 Introduction 4

1.2 The principle of calculating the factor of safety based on the self-weight failure stimulus 5

1.3 Classical methods of estimating the factor of safety 5

1.3.1 Single body method 6

1.3.2 Method of slices 6

1.3.2.1 Method of Fellenius 6

1.3.2.2 Method of Bishop 7

1.4 Principle of calculating the bearing capacity of shallow foundations by virtue of loading failure stimulus 7

1.4.1 Basic concepts 7

1.4.2 Theories of bearing capacity for strip footings 9

1.4.2.1 Theory of Prandtl 9

1.4.2.2 Theory of Terzaghi 10

1.5 Concept of slope stability by virtue of random variable soil parameters 13

1.5.1 Key factors of uncertainty and spatial variability of soil properties 13

1.6 Concept of probabilistic soil parameters attributed to the spatial variability 14

1.6.1 The mean value or centre of gravity pertaining to the probability density function 14

1.6.2 The variance and standard deviation 15

1.6.3 Correlation structure 16

1.6.4 Continuous probability distribution of random soil parameters 17

1.6.4.1 Normal and standard normal distributions 17

1.6.4.2 Standard lognormal and shifted distributions 18

1.7 Stochastic analysis and random field generation 19

1.7.1 Types of stochastic analyses based on the sought purpose 19

1.7.2 The Monte Carlo simulation method adopted for the random field generation in OptumG2 software 19

1.7.2.1 Karhunen- Loeve expansion integrated in OptumG2 software 20

1.8 Conclusion 21

Chapter 2: Stability assessment of pile-stabilized slope based on analytical and numerical methods 22

2.1 Introduction 22

2.2 Analytical methods for the stability assessment of pile-stabilized slope based on the limit equilibrium method 23

2.2.1 Theoritical background 23

2.3 Numerical computations for the stability estimation of pile-stabilized slope 25

2.3.1 Shear strength reduction method SSR 25

2.3.2 Limit analysis LA 27

2.4 Demonstration of the employed methodology integrated in OptumG2 and finite element modelling 27

2.4.1 General notions 28

2.4.1.1 The yield and stress state 28

2.4.1.2 Classic decomposition of strains 29

2.4.2 Elastoplasticity 30

2.4.2.1 The principle of the lower bound: 30

2.4.2.2 The principle of the upper bound 31

2.4.2.3 Elastoplastic strength reduction analysis 31

2.4.3 Rigid plastic Limit analysis 32

2.4.3.1 Lower bound theorem 32

2.4.3.2 Upper bound theorem 33

2.4.4 Definition of yield criterions 33

2.4.4.1 Mohr-Coulomb criterion 33

2.4.4.2 Tresca criterion 34

2.5 Reliability analyses for the determination of failure probability of a reinforced slope 36

2.6 Conclusion 38

Chapter 3: Bearing capacity assessment of shallow foundations near slopes before and after reinforcement 40

3.1 Introduction 40

3.2 Evaluation of the bearing capacity of shallow footings near unreinforced slopes 41

3.2.1 Deterministic methods for the bearing capacity of shallow footings near unreinforced slopes under vertical and inclined loading condition 41

3.2.2 Stochastic analyses for the determination of the bearing capacity of shallow footings 43

3.3 Bearing capacity of shallow footings near stabilized slopes 46

3.3.1 Deterministic analyses for stabilized slopes under purely vertical surface loads 46

3.4 Conclusion 48

Chapter 4: Strength reduction analysis on the safety factor of a slope reinforced with one row of piles 50

4.1 Introduction 50

4.2 Principle of Sluis integrated in OptumG2 software 51

4.2.1 The pile row properties by virtue of the out of plane direction 52

4.2.2 The properties pertaining to the soil-pile interface 52

4.3 Study on the factor of safety pertaining to a pile- stabilized slope 53

4.3.1 Presentation of the studied problem 53

4.4 Numerical procedures 54

4.5 Results and discussion 54

4.5.1 Comparison of the factor of safety 54

4.5.2 Effect of pile rigidity for various head conditions 55

4.5.3 Effect of pile spacing for various head conditions 57

4.6 Conclusion 59

Chapter 5: Probabilistic analysis on pile-stabilized slope under purely vertical loading 60

5.1 Introduction 60

5.2 Definition of the numerical problem 61

5.3 Comparison of various correlation lengths 62

5.4 Stochasttic computations 62

5.5 Conclusion 66

Chapter 6: Numerical analysis on sheet pile wall reinforcement of a slope with an adjacent inclined loaded strip footing 67

6.1 Introduction 67

6.2 Problem definition 68

6.3 Numerical approach 68

6.4 Numerical analysis of load inclination factors under various slope angles 69

6.4.1 Effect of sheet pile wall location on $i_{c\beta}$ 70

6.4.2 Failure mechanism 71

6.5 Numerical analysis of the load inclintion effect on failure loads under various reinforcement conditions 72

6.5.1 Effect of various sheet pile wall locations d/B within the slope 74

6.5.2 Effect of various sheet pile wall heights 75

6.5.3 Effect of various normalized footing distances 76

6.5.4 Effect of various shear strength ratios $c_u/\gamma B$ 78

6.5.5 Effect of various slope heights 79

6.6 Conclusion 81

General conclusion and perspectives 82

References 86

List of Figures

Figure 1.1: Single body method: (a) forces acting on soil massif, and (b) method of evaluation of the pore pressure u. 6
Figure 1.2: Slice details implemented in the method of slices. 7
Figure 1.3: Types of shallow foundations (Frank, 1999). 8
Figure 1.4: Failure plane of a shallow footing (Prandtl, 1920). 9
Figure 1.5: Failure plane of a shallow foundation (Terzaghi, 1943). 10
Figure 1.6: Inherent spatial variability of soil (Phoon & Kulhawy, 1999). 13
Figure 1.7: Factors influencing the uncertainty pertaining to soil (Phoon & Kulhawy, 1999). 14
Figure 1.8: Two different distributions of the mean value and standard deviation (Fenton & Griffiths, 2008). 15
Figure 1.9: Density functions (Russeli, 2008) attributed to: (a) normal distribution, and (b) lognormal distribution. 17
Figure 1.10: The function transformation from the lognormal distribution to its corresponding standard normal distribution (Russeli, 2008). 19
Figure 1.11: PDF and CDF pertaining to a continuous random variable (Russeli, 2008). 20
Figure 2.1: Soil-pile system (Won et al., 2005): (a) driving forces acting on a pile row, and (b) reaction forces induced by piles. 23
Figure 2.2: Comparison of the finite element method with Bishop's simplified method: (a) optimal pile position, and (b) most effective pile spacing. 25
Figure 2.3: Effect of the embedded pile length on Fs for: (a) free head condition, and (b) fixed head condition. 26
Figure 2.4: Convex of the yield plane. 28
Figure 2.5: Applied traction on the material boundary S. 29

Figure 2.6: Load surfaces of Mohr-Coulomb criterion. 34
Figure 2.7: Failure surface pertaining to generalized Tresca model: (a) deviatoric plane, and (b) principal stress plane for a value as high as sue/suc. 36
Figure 2.8: Variation of the probability of failure with: (a) horizontal correlation lengths, and (b) vertical correlation lengths. 38
Figure 2.9: Variation of the reliability index with different pile locations: (a) effect of various spacings, and (b) comparison between the factor of safety and β with $D_1/D=3$. 38
Figure 3.1: Problem definition (Georgiadis, 2010). 42
Figure 3.2: Types of failure mechanism assumed by Georgiadis (2010). 43
Figure 3.3: Comparison of the developed equation pertaining to the load interaction diagram with the upper bound solutions (Georgiadis, 2010). 43
Figure 3.4: Definition of the problem (Brahmi et al., 2018). 45
Figure 3.5: The variation of COV with: (a) surfaces of normalized failure loads, and (b) curves of load interaction. 45
Figure 3.6: The variation of Θ with: (a) surfaces of normalized failure loads, and (b) curves of load interaction. 46
Figure 3.7: Definition of the problem (Sharafi & Sojoudi, 2016). 47
Figure 3.8: Effect of soil interlayer on Fs (Sharafi & Sojoudi, 2016). 47
Figure 3.9: Effect of pile location on the bearing capacity improvement (Sharafi & Sojoudi, 2016). 48
Figure 3.10: Comparison of the best performance between sheet pile walls and pile rows (El Sawwaf, 2005). 48
Figure 4.1: The 2D interaction between soil and piles in a row (Sluis et al., 2014). 51
Figure 4.2: The problem geometry associated with FE mesh. 53
Figure 4.3: Comparison of F_s for various pile head conditions (E_p= 60 GPa). 54
Figure 4.4: Pile behaviour for different pile head conditions and bending stiffnesses (S/Ø=3). 56
Figure 4.5: Pile behaviour for various head conditions and centre-to-centre spacings. 58
Figure 5.1: Model slope and reinforcing system. 61
Figure 5.2: Comparison of various correlation lengths, for COV_{cu}=50%: (a) μ_{Nc}, and (b) COV_{Nc}. 62
Figure 5.3: Effect of Θ on: (a) μ_{Nc}, and (b) COV_{Nc}. 63
Figure 5.4: Effect of COV_{cu} on: (a) μ_{Nc}, and (b) COV_{Nc}. 64

Figure 5.5: Distributions of the complementary cumulative probabilities pertaining to the random bearing capacity $N_{c,rand}$. 65
Figure 5.6: Shear strength distribution: (a) Θ=1, and (b) Θ=8. 65
Figure 6.1: Definition of the problem: (a) geometry, and (b) mesh adaptivity. 68
Figure 6.2: Effect of d/B ratios on load-displacement plots, for β=40°, and θ=0° and 10°. 70
Figure 6.3: Variation of N_c* factors with θ, for β=40°. 70
Figure 6.4: Effect of various ranges of θ and d/B on $i_{c\beta}$, captured for various slope angles. 71
Figure 6.5: Pattern of failure captured for β=40°, 0°≤θ≤10°, and d/B=0 and 1. 72
Figure 6.6: Load-displacement plots captured for β=45°, θ=0°, λ=0 and d/B=0: (a) effect of the flexural rigidity of the reinforcement, (b) effect of various ratios of L/B. 73
Figure 6.7: Failure plane captured for a footing situated on (a) horizontal ground surface, and (b) slope of β=30°. 73
Figure 6.8: Bearing capacity improvement in terms of various normalized sheet pile locations, for $c_u/\gamma B$=1, λ=0, and β=40°. 74
Figure 6.9: The pattern of failure captured for β=40°, θ=0° and λ=0: (a) unreinforced slope and (b) reinforced slope, with L/B=5. 74
Figure 6.10: Effect of various sheet pile positions, captured for $c_u/\gamma B$=1 and β=45°: (a) normalized failure load planes, and (b) load interaction surfaces. 75
Figure 6.11: Bearing capacity improvement in terms of various sheet pile heights L/B, captured for $c_u/\gamma B$=1, λ=0, and β=40°. 76
Figure 6.12: Effect of various sheet pile heights, captured for $c_u/\gamma B$=1 and β=45°: (a) normalized failure load planes, and (b) load interaction surfaces. 76
Figure 6.13: Bearing capacity improvement in terms of various normalized footing distances, captured for $c_u/\gamma B$=1, d/B=0, and β=40°. 77
Figure 6.14: Effect of various normalized footing distances, captured for $c_u/\gamma B$=1 and β=45°: (a) normalized failure load surfaces, and (b) load interaction curves. 77
Figure 6.15: Effect of various $c_u/\gamma B$ ratios on normalized failure surfaces, captured for: (a) β=15°, (b) β=30°, and (c) β=45°. 78
Figure 6.16: Effect of various $c_u/\gamma B$ ratios on load interaction curves, captured for: (a) β=15°, (b) β=30°, and (c) β=45°. 79

Figure 6.17: Effect of various Z/B ratios on normalized failure surfaces, captured for λ=1: (a) β=30°, and (b) β=45°. 79
Figure 6.18: The pattern of failure pertaining to the unstabilized slope for Z/B=3, λ=1, $c_u/\gamma B$=1 and β=30°: (a) overall failure at θ=0°, and (b) bearing capacity failure at θ=10°. 80
Figure 6.19: The patter of failure pertaining to the stabilized slope for Z/B=3, λ=1, $c_u/\gamma B$=1 and β=30°: (a) overall slope failure at θ=0°, and (b) bearing capacity failure at θ=10°. 80
Figure 6.20: Effect of various Z/B ratios on load interaction curves, captured for λ=1: (a) β=30°, and (b) β=45°. 80

List of Tables

Table 1.1: Different expressions of bearing capacity factors. 11
Table 1.2: Load inclination factors for purely cohesive soil. 12
Table 1.3: load inclination factors by virtue of the sloping ground. 12
Table 2.1: Limit equilibrium based methods for the assessment of pile-stabilized slope stability. 24
Table 2.2: Some studies conducted for the reliability analysis of reinforced slopes. 37
Table 3.1: Theoretical and experimental methods conducted for the limit load of strip footings susceptible to purely vertical loading. 41
Table 3.2: Various probabilistic methods conducted for the bearing capacity of shallow foundations. 44
Table 4.1: Material properties. 54

Symbols and notations

We provide below the main notations used in this dissertation:

F_s: factor of safety.

φ: friction angle.

c: cohesion (c_u: undrained shear strength).

Ø: pile diameter.

S: centre-to-centre pile spacing.

L: embedded pile length.

d: location of pile relative to the slope crest.

β: Slope angle.

Z: slope height.

B: footing width.

λ: relative distance between the footing and the slope crest.

N_{cu}: undrained bearing capacity factor.

q_u: undrained bearing capacity (q_{us}: undrained limit load of the stabilized slope).

BCI: bearing capacity improvement factor.

$i_{c\beta}$: load inclination factor relevant to the slope.

θ: load inclination angle.

σ_{cu}: standard deviation of the undrained cohesion.

μ_{cu}: mean value of the undrained cohesion.

Θ: isotropic correlation length.

COV_{cu}: coefficient of variation of the undrained cohesion.

CDF: cumulative distribution function.

CCDF: complementary cumulative distribution function.

FELA: finite element limit analysis.

RFEM: random finite element method.

General introduction

The slope failure is likely developed in loose materials or generally cohesive soils, due to the insufficiency of soil characteristics in upholding its own weight. Although the action of gravity is the prime force for a landslide to take place, there is another contributing factor identified as a surface load action (i.e. nearby shallow foundations). The failure surface can be significantly stopped from prolonging to the sloping ground by dint of using discrete retaining structures (pile row) within the slope (Chen & Poulos, 1997; Ito et al., 1981; Li & Liang, 2014; Nimityongskul et al., 2018; Poulos, 1995; Qin et al., 2017; Won et al., 2005) or continues structures (sheet pile wall) (Ahmed, 2004; El Sawwaf, 2005; Gazetas et al., 2016; Lin et al., 2018). Beyond which the displacements are significantly limited to acceptable values. Numerical methods are quite effective in the consideration of the pile behavior, soil-pile interaction and the description corresponding to lateral load distributions along the pile row (Chow, 1996; Jeong et al., 2003; Kourkoulis et al., 2012; Pirone & Urciuoli, 2018; Sanping & Robert, 2002; Xiao, 2020; Yamin & Liang, 2010; Yang & Zhang, 2020). It should be mentioned that the investigation of the slope surface load action, necessitates a good understanding of the theory of bearing capacity. In practice, the bearing capacity is determined based on the classical equation of (Terzaghi, 1943). However, the effect of inclined loading on the bearing capacity is investigated through several methods; one of which is the kinematic approach integrated in limit analysis (Chen, 2013; Georgiadis, 2010; Michalowski, 1997).

In geotechnical engineering, the soil is accounted for as anisotropic and heterogeneous field with variable characteristics. The combination of both the theory of random fields and the deterministic finite element method gives the ability to consider the probability distributions for more than one soil parameter. This is done by the generation of random fields relevant to spatial variables. Stochastic analyses were firstly developed by (Griffiths and Fenton ; 1993) using the random finite element method (RFEM). Hence, this latter had been combined with the limit analysis by several researchers in the current decade (Ali et al.,

2016; Ali et al., 2017; Huang et al., 2013). However, the random finite element analysis might be executed by virtue of Monte-Carlo simulations to conduct a statistical analysis of the results; whereas, the generation of many random fields relevant to the soil domain leads to repeated executions.

The objective of this dissertation, is to contribute to numerical and stochastic analyses treating the problem relevant to slope failure caused by the self-weight, as well as a surface load condition.

The first part of this thesis represents a bibliographical synthesis devoted to the presentation of computation methods concerning the common problem of slope stability assessment; thusly, the problem of bearing capacity of an adjacent shallow foundation. Whereas, deterministic and probabilistic studies published in the literature are mentioned in three chapters.

The first chapter represents basic concepts on the deterministic and probabilistic theories of slope steadiness under various circumstances; namely, sliding generated by the self-weight, sliding generated by a surface load condition (shallow foundation near the slope crest) and spatial variability of soil properties.

The second chapter is regarding the presentation of a bibliographical synthesis of previously conducted studies on the slope stability. We are concerned particularly about studies on mechanical and structural behaviour of a pile row used to reinforce unstable slopes; as well as, several pile conditions affecting the factor of safety. Hence, this chapter represents in particular the principles of OptumG2 code used to elaborate the numerical simulations, as well as, the corresponding yield criterions.

The third chapter is dedicated at the presentation of basic concepts pertaining to the determination of the bearing capacity of shallow footings using classical deterministic and probabilistic methods. The chapter particularly focuses on studies addressing the mechanical behaviour of shallow foundations, subjected to combined loading, situated near a slope crest before and after reinforcement.

The second part of this thesis, represents numerical contributions to deterministic and probabilistic studies, devoted to the assessment of slope stability and bearing capacity of a strip footing adjacent to a slope. The computations consider both slope cases before and after reinforcement using the software OptumG2.

The fourth chapter represents the results pertaining to a deterministic study on the stability of a slope reinforced by a row of piles; the effects of pile spacing, head conditions and rigidity on the factor of safety are investigated.

Chapter five, aims to presenting the pile row technique of reinforcement to help improving the bearing capacity of a strip footing subjected to a combined loading. The study relates the enhancement in the bearing capacity to various pile parameters for various load inclinations. The deterministic analysis is conducted using the finite element limit analysis with its upper and lower bounds. Thus, a probabilistic study combined with the theory of random fields is conducted to examine the effect of stochastic parameters on the undrained bearing capacity.

Finally, **the sixth chapter**, investigates the rate of enhancement in the undrained bearing capacity when adopting the sheet pile wall reinforcement technique; as well as, capturing the alterations in the corresponding load inclination factor. The limit analysis based on the finite element method is employed to investigate the effect of load inclinations on the size and shape of failure envelopes under several geometric and mechanical conditions.

Chapter 1: Principle of different slope analyses by virtue of the sliding stimulus

1.1 Introduction

The subject of analyzing the stability of slopes has received a great attention in the literature according to its importance related to safety and economy. The hazard of sliding increases under various conditions applied on slopes. Specifically, self-weight of slopes with great depths measured from the stratum to ground surface and surface load condition near the slope crest that is generally represented by a nearby shallow foundation undergoing horizontal and vertical loadings. As well as, the soil heterogeneity defined by variable physical and mechanical characteristics, inducing uncertainty to the slope factor of safety or bearing capacity of an adjacent footing.

Nevertheless, the principle of calculating the slope stability using equilibrium methods is based on the determination of the minimum factor of safety; in which it relies on balancing the driving forces with resisting forces. Scholars have developed lots of methods to investigate the safety factor; (Huang, 2014) presented a summary on the most common analytical methods previously developed in the literature. It is important to mention that the case where the slope is subjected to a surface load is one of the important subjects in the geotechnical engineering. This is due to the consistent relationship between the bearing capacity and the subject of safety. In other words, the slope stability increases with the increase of the bearing capacity and the vice -versa. The delve into fundamental theories of bearing capacity pertaining to shallow foundations situated on horizontal grounds (Prandtl, 1920; Terzaghi, 1943) leads to the ability of analyzing problems where footings are near slopes. Thusly proposing solutions to enhance the bearing

capacity and improve the overall stability. In geotechnical practice, the deterministic approach is reported to serve at providing conservative solutions, due to the neglect of the effect of soil uncertainty caused by the variability of parameters and test techniques. Therefore, probabilistic analyses are essential to be side by side with the deterministic estimations.

This chapter, presents different deterministic theories and methods serving at the determination of the slope safety factor; as well as, the bearing capacity pertaining to shallow foundations. Hence, basic concepts of probabilistic theories in describing geotechnical uncertainty are introduced.

1.2 The principle of calculating the factor of safety based on the self-weight failure stimulus

It should be emphasized that the factor of safety is an indicator of the slope mechanical stability. It is defined as a coefficient by which the shear resistance parameters are reduced until reaching a state of limit equilibrium ($F_s \geq 1.5$). The objective of determining the slip surface, is to repair the most likely failure plane pertaining to this specific value of F_s. Slope stability analysis focuses on locating the slip surface, computing normal and tangential stresses and finally estimating the safety factor with respect to the failure criterion using equilibrium equations. It is important to mention that the slip surface is determined numerically using softwares like, Nixwin, Nixes or Talren, or else analytically using charts. Biarez (1965) has developed a chart for the determination of the circular sliding surface that intersects the slope toe.

1.3 Classical methods of estimating the factor of safety

The equilibrium equations are developed following two methods:

1) Method of single body (Method of TAYLOR (1937), CAQUOT (1954), and BIAREZ (1960)): it is based on the investigation of the force equilibrium corresponding to the failure zone. It is worthy to mention that usually the slip surface is assumed circular.

2) Method of slices (FELLENIUS (1927) and BISHOP (1955)): the method decomposes the slope into slices, where the individual equilibrium should be studied before globalizing the results. Thus, certain simplifications are introduced.

1.3.1 Single body method

The method assumes homogeneous and isotropic conditions defined by the unit weight γ, friction angle φ, cohesion c and pore pressure u for the case of a nearby water table. The calculations are carried out with admitting that the massive soil is in limit equilibrium and indeformable. The hypothesis relies on assimilating the slip surface to a circle with the centre O, as shown in Figure 1.1. Consequently, the equilibrium of moments is given by eq. (1.1).

$$W.OH - \frac{2c'\alpha R^2}{F_s} - \frac{R_N \ tan\,\varphi' \, R}{F_s} + \vec{u} = 0, \qquad (1.1)$$

where W, OH, c′, α, R, R_N, φ′ and $\vec{u}$ are respectively the soil weight, lever arm, effective cohesion, the angle located at the centre O connecting the top of slope with the centre of the slip circle, radius, normal force, effective friction angle and pore pressure ($\vec{u}=\gamma_w(Z_M-Z_P)$).

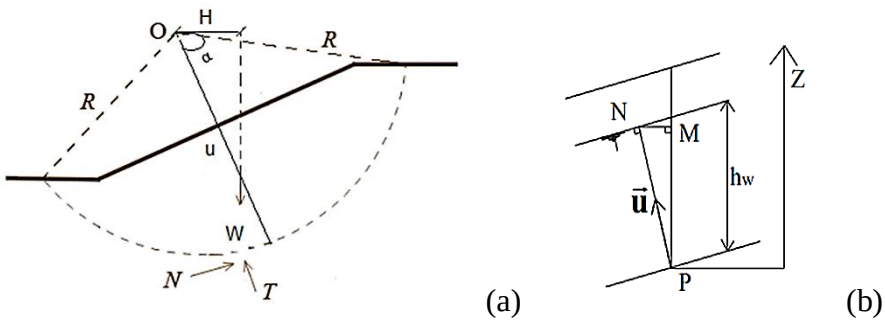

Figure 1.1: Single body method: (a) forces acting on soil massif, and (b) method of evaluation of the pore pressure u.

1.3.2 Method of slices

It is also called the Swedish method, named after the Swedish founder Paterson (1916). Thus, Fellenius (1927) and Bishop (1955) adopted the method to account for the circular failure type. Thenceforth, Nonveiller (1965) extended the method to the noncircular failure type. In nature, the slip surface is rarely formed as a circle and the soil massive is not homogeneous. Therefore, it was necessary to divide the soil massive into vertical and relatively thin slices, as shown in Figure 1.2. Each slice owns its simple slip surface and homogeneous soil.

1.3.2.1 Method of Fellenius

The definition of Fellenius (1927) is commonly recognised in the literature. The method assumes that the limit equilibrium pertaining to the unstable layer (above the slip surface) is obtained when the system

of applied mobilized forces mobilizes the ratios corresponding to the true values of soil friction angle $\tan\varphi/F_s$ and cohesion c/F_s:

$$F_s = \frac{\sum cb + (W\cos^2\theta - ub)\frac{\tan\varphi}{\cos\theta}}{\sum W\sin\theta}, \tag{1.2}$$

where b and θ are the slice width and angle between the centre of the slice to its edge.

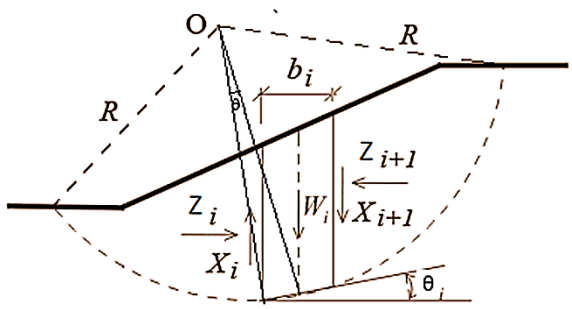

Figure 1.2: Slice details implemented in the method of slices.

1.3.2.2 Method of Bishop

It is important to mention that the maximal value of the shear stress τ distributed along the slip surface is referred to as the shear resistance τ_f. Consequently, prior to failure the system of force applied on the stable layer brings down τ compared to τ_f. Therefore, Bishop (1955) defines the factor of safety as follows:

$$F_s = \frac{\tau_f}{\tau}, \tag{1.3}$$

$$F_s = \frac{\sum[c'b + (W - ub)\tan\varphi']\frac{1}{\cos\alpha\,(1 + \tan\varphi'/F_s}}{\sum W\sin\alpha}. \tag{1.4}$$

1.4 Principle of calculating the bearing capacity of shallow foundations by virtue of loading failure stimulus

1.4.1 Basic concepts

In geotechnical engineering, the foundation represents the bottom part of the structure, where the contact with soil takes place. Its role is to transmit loads induced by the structure to soil. They are generally classified into different categories based on the footing embedment depth D; beyond which it depends on the nature of soil and the type of structure. There are semi-deep foundations, deep foundations (i.e. pile rows and sheet pile wall) and shallow foundations. The last two types together are the subject of

interest of this thesis. The shallow foundations are basically used when the soil layer that is supporting the construction loads is of small depths based on the target structure. The footing is generally called shallow when the embedment length D is less than 1.5 B. Shallow foundations are three categories, isolated foundation (Figure 1.3(a)), with a rectangular shape of identical length L and width B or circular shape with diameter B; strip footing (Figure 1.3(b)), generally of higher length L comparing to the width B (L/B>10); also, raft foundation (Figure 1.3(c)), with important dimensions of L and B.

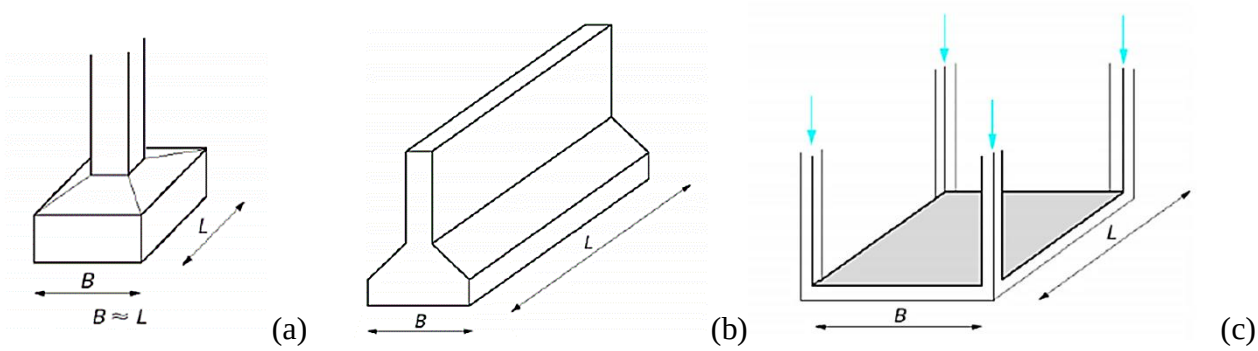

Figure 1.3: Types of shallow foundations (Frank, 1999).

The bearing capacity (limit load) has been widely investigated based on the classical equation of Terzaghi (1943). Shallow foundations has been accounted for using the laboratory based tests known as classical methods relevant to c and φ, or another analytical and numerical methods, namely:

- The limit equilibrium method (Meyerhof, 1951; Terzaghi, 1943; Vesic, 1973). This method is based on assuring a static equilibrium of external and internal forces.

- The characteristic method based on slip surfaces (Bolton & Lau, 1993; Hansen, 1970; Martin, 2003). This method comprises the equity of equilibrium equation with the condition imposed by the soil resistance.

- The elastoplastic analyses based on finite element or finite difference methods (Erickson & Drescher, 2002; Frydman & Burd, 1997). The method provides the ability to follow the elastoplastic development from the state of initial stresses till the plastic failure during process of loading. This feature provides the ability to dress load-displacement curves.

- Kinematic approach integrated in limit analysis (Chen, 2013; Michalowski, 1997). This method considers the kinematic principles relevant to deformations in the failure analysis; as well as, the boundary conditions of displacements. Following Chatzigogos (2007), the upper bound of limit analysis

refers to that the external loading is equal or higher than the limit load, whenever this condition is applicable for an admissible cinematic velocity field: “potency of external loads ≥ rate of dissipation of internal energy”. In contrast, the static approach furnishes inferior bounds than the limit load forming a stress field that is admissible statistically and plastically. It is of interest to know that this method is limited at furnishing the field relevant to real applied stresses and deformations; nonetheless, it only bounds the limit load.

It is worthy to note that the use of limit analysis conducted with finite elements combines the power of finite element discretization relevant to complex geotechnical modes with limit plasticity theorem corresponding to bounding the exact limit load (Krabbenhoft et al., 2005). This method is adopted in the current dissertation using OptumG2 code. Further details concerning the method are mentioned in Chapter 2.

1.4.2 Theories of bearing capacity for strip footings

1.4.2.1 Theory of Prandtl

Prandtl (1920) suggested a theory of bearing capacity based on analyzing the strip footing with a smooth base driven towards the bottom. Figure 1.4, indicates the failure surface of a shallow footing; by which, zone I forms a corner situated below the footing and pushing laterally zone II, causing by that zone III to upheave. Both zones II and III are in plastic equilibrium; where the slip surface pertaining to zone II is log-spiral.

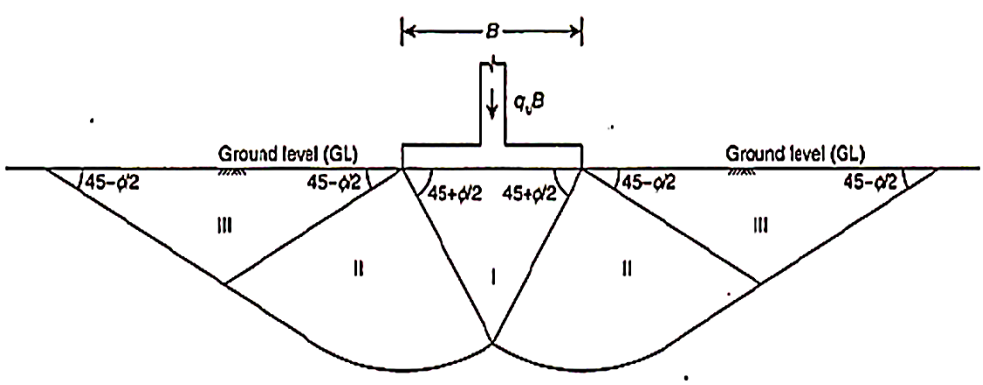

Figure 1.4: Failure plane of a shallow footing (Prandtl, 1920).

Based on the theory of plasticity, Prandtl (1920) derived the following expression of ultimate bearing capacity:

$$q_u = \frac{c}{tan\varphi}[\{tan^2(45+\varphi/2)e^{\pi\, tan\varphi}\} - 1]. \tag{1.5}$$

For purely cohesive soil (φ=0), the log-spiral takes the shape of an arc of circle with an ultimate bearing capacity of $q_u = (\pi+2)\, c_u$.

1.4.2.2 Theory of Terzaghi

Terzaghi (1943) derived a general expression for the limit load of strip footings assuming a two dimensional problem. The suggested bearing theory is based on the previous theory of Prandtl (1920). The footing base is assumed rough, thus the corner abc shown in Figure 1.5 doesn't undergo any lateral displacement. The ultimate limit load is reached when the footing is undergoing the pressure q_u.

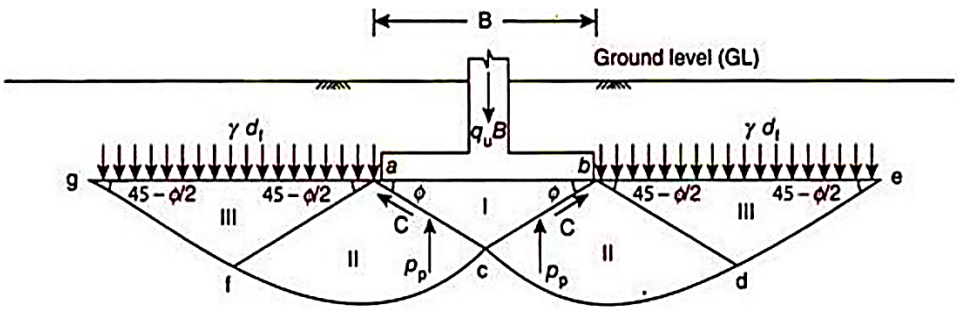

Figure 1.5: Failure plane of a shallow foundation (Terzaghi, 1943).

The expression of limit load (eq. (1.6)) considers group factors; namely, the forces acting on abc, superposition technique to combine the effects of cohesion, overload, and soil weight.

$$q_u = \frac{Q_{ult}}{B} + c\, N_c + \gamma D N_q + \frac{1}{2}\gamma B N_\gamma, \tag{1.6}$$

where Q_{ult} and D are respectively the ultimate load per unit length and embedded depth of footing; hence, N_c, N_q and N_γ are the factors of bearing capacity depending on the angle φ, as follows:

$$N_c = cot\varphi\left[\frac{a^2}{2\, cos^2(45° + \frac{\varphi}{2})} - 1\right] \tag{1.7}$$

$$N_q = \frac{a^2}{2\, cos^2(\frac{\pi}{4} + \frac{\varphi}{2})},$$

$$a = e^{\left[\left(\frac{3\pi}{4} - \frac{\varphi}{2}\right) tan\varphi\right]}, \tag{1.8}$$

$$N_\gamma = \frac{tan\varphi}{2}\left(\frac{K_{p\gamma}}{cos^2\varphi} - 1\right). \tag{1.9}$$

where $K_{p\gamma}$ is obtained from tables. Nevertheless, the determination of bearing capacity factors has been widely addressed. Sieffert and Bay-Gress (2000) presented various studies conducted on the determination of bearing capacity of shallow foundations in Europe. A large diversity in the estimation of multiplicative factors is presented in Table 1.1.

Table 1.1: Different expressions of bearing capacity factors.

Author	N_c	N_q	N_γ
Vesic (1975)	$(N_q - 1)\ cot\varphi$	$tan^2\left(\frac{\pi}{4}+\frac{\varphi}{2}\right)\ e^{\pi\ tan\varphi}$	$2(N_q - 1)\ tan\varphi$
Hansen (1970)	$(N_q - 1)\ cot\varphi$	$tan^2\left(\frac{\pi}{4}+\frac{\varphi}{2}\right)\ e^{\pi\ tan\varphi}$	$1.5(N_q - 1)\ tan\varphi$
Meyerhof (1963)	$(N_q - 1)\ cot\varphi$	$tan^2\left(\frac{\pi}{4}+\frac{\varphi}{2}\right)\ e^{\pi\ tan\varphi}$	$(N_q - 1)\ \tan\ (1.4\ \varphi)$

Meyerhof (1963) developed a general expression inducing correction factors of load inclination, footing shape and embedment depth:

$$q_u = 0.5\ B\ N_\gamma S_\gamma d_\gamma i_\gamma + cN_c S_c d_c i_c + qN_q S_q d_q i_q, \qquad (1.10)$$

where S_γ, S_c and S_q are the footing shape factors; d_γ, d_c and d_q are the footing embedment factors, and i_γ, i_c and i_q are the load inclination factors.

Several researchers have extended the classical expression of Terzaghi (1943) to account for homogeneous soil (Green, 1954; Hansen, 1961; Meyerhof, 1963; Vesic, 1975) and nonhomogeneous soil (Ouahab et al., 2017) with developing load inclination factors. Table 1.2 shows load correction factors for purely cohesive soil (φ=0). Nevertheless, other researchers have developed expressions that are function of load interaction diagrams (Bransby & Randolph, 1998; Gourvenec, 2007; Loukidis et al., 2008; Taiebat & Carter, 2002; Ukritchon et al., 1998). The limit bearing capacity is computed in terms of combined loading. The interaction of load components (vertical V and horizontal H forces) is explicitly taken into consideration in the determination of the limit load by means of failure envelopes. However, this latter is defined as ultimate surfaces in the loading surface V-H. The approach of failure envelopes assumes that the stability field is inside the failure envelope. It is worthy to mention that two loading techniques are available in geotechnical engineering; following Loukidis et al. (2008) they are known as, 'Swipe' and 'Probe'. The Probe technique consists of loading the footing progressively until collapse under specific inclined loads. Each Probe analysis aims to estimating a unique limit load corresponding

to failure; thus, the failure curves are plotted point by point. The Swipe technique consists of two steps to plot the failure curves in terms of V-H. First step is based on the application of a vertical displacement on all the nodes of footing until the mobilization of the vertical bearing capacity. Thence after, a horizontal displacement is applied until failure, with blocking the vertical displacement of the footing. The second step consists of a direct application of horizontal loads on the footing nodes, until reaching the ultimate horizontal stress. The advantage of Swipe technique over Probe is that the failure curves are dressed rapidly as the Swipe technique permits the determination of several points of failure curves V-H at a time.

Table 1.2: Load inclination factors for purely cohesive soil.

Author	i_c
Green (1954)	$0.5 + (1/N_c)\left[cos^{-1}(H/Bc_u) + \sqrt{1-(H/Bc_u)^2}\right]$
Meyerhof (1963)	$[1-(\theta^{\circ}/90^{\circ})]^2$
Hansen (1961)	$0.5 + 0.5\sqrt{1-(H/Bc_u)}$
Vesic (1975)	$1-(2H/Bc_uN_c)$
Ouahab (2017)	$130.23/[(k+6.37)\theta + 130.23]$

Nevertheless, it is worthwhile to mention that, Footings near slopes require the definition of correction factors pertaining to load inclinations in order to estimate the limit load properly. Table 1.3 represents available expressions of i_c factors in the literature for purely cohesive soil in terms of the inclination of slope β and sloping ground factor g_c.

Table 1.3: load inclination factors by virtue of the sloping ground.

Author	$i_{c\beta}$
Hansen (1961)	$\left[0.5 + 0.5\sqrt{1-(H/Bc_u)}\right] - g_c$, , with $g_c = 2\beta/(\pi+2)$
Vesic (1975)	$[1-(2H/Bc_uN_c)].[1-g_c]$

Furthermore, Hansen (1970) derived an expression (eq. (1.11)) relevant to slope factors $\lambda_{\gamma\beta}$, $\lambda_{c\beta}$ and $\lambda_{q\beta}$:

$$q_u = 0.5\, B\, N_\gamma \lambda_{\gamma\beta} + cN_c\lambda_{c\beta} + qN_q\lambda_{q\beta}, \qquad (1.11)$$

where $\lambda_{\gamma\beta}$, $\lambda_{q\beta}$= $(1-0.5\tan\beta)^2$, $\lambda_{c\beta}$= $(N_q\,\lambda_{q\beta}-1)/(N_q-1)$ for φ>0, and $\lambda_{c\beta}$= $1-g_c$ for φ=0.

1.5 Concept of slope stability by virtue of random variable soil parameters

The uncertainty in geotechnical field may be generated by the variability of soil characteristics or different test techniques. Practical experiences show that deterministic analyses are conducted to resolve problems based on the classical definition of safety giving conservative solutions without considering soil uncertainty. This may lead to a deficiency in the accuracy of estimation of the system stability. Therefore, the accurate estimation of uncertainty related to geotechnical problems is accomplished using a variety of probabilistic methods. It is important to mention that the concept of probabilistic methods rely on the statistic theory. In which, a base of theories is obtained to quantify the uncertainty consistently; Thence after, they are defined in a mathematical way to obtain a logical frame capable of analyzing the reliability and risks.

1.5.1 Key factors of uncertainty and spatial variability of soil properties

Understanding the soil history leads to the causes of geotechnical uncertainty attributed to soil. The soil composition is considered complex as it is formed by various processes that are continuous and may make changes to soil in situ; namely, chemical, physical, geological and environmental processes. Due to these natural processes, all the soil in situ properties will vary horizontally and vertically, as shown in Figure 1.6.

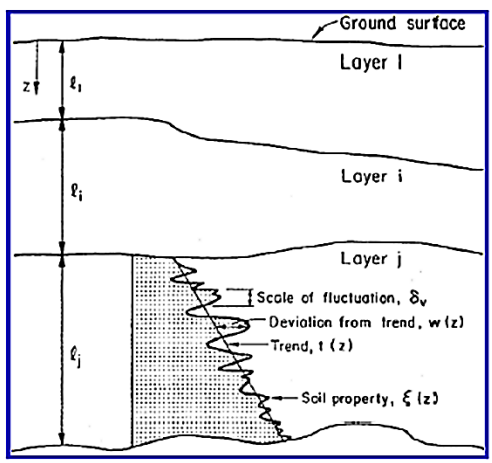

Figure 1.6: Inherent spatial variability of soil (Phoon & Kulhawy, 1999).

The spatial variability is defined as $\xi(z)= t(z)+ w(z)$. In which, $\xi(z)$, $t(z)$ and $w(z)$ are respectively the soil property at depth z, deterministic function that gives the mean value soil property at depth z, and fluctuation component at z (the residual) that represents the inherent variability of soil; it is also referred

to as homogenous random field (Vanmarcke, 1983). The key factors of soil uncertainty are classified by Phoon and Kulhawy (1999) with respect to the following order, as indicated in Figure 1.7:

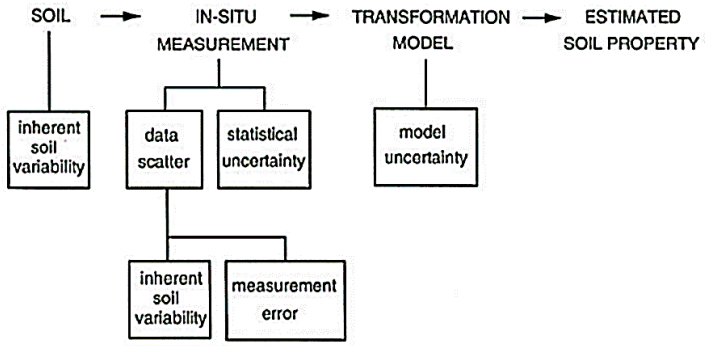

Figure 1.7: Factors influencing the uncertainty pertaining to soil (Phoon & Kulhawy, 1999).

- Inherent variability of soil; the principal factor is the natural geological process causing continues modifications to the soil in situ. This evolutionary process was extended by Tang (1984) to account for a variation in terms of small scale of environmental conditions during deposit, mineral compositions, variation in water content and the history of past stresses.

- Measurement errors due to, equipment, operation procedures and random tests effect. Combining these measurement errors with the inherent variability are described as data dispersion. However, in situ measurements are influenced by statistical uncertainty or sampling errors resulting out of an unlimited number of informations.

- Transformation uncertainty; the measures in the field or laboratory may be transformed to soil properties for the concept of introducing correlation models empirically or else with introducing simplifications and idealizations.

1.6 Concept of probabilistic soil parameters attributed to the spatial variability

Popescu et al. (1997) used the random field theory to define various probabilistic characteristics pertaining to spatial variability of soil parameters:

1.6.1 The mean value or centre of gravity pertaining to the probability density function

The mean value of the random variable (soil parameter) follows an increase or decrease tendency (Figure 1.8). In general, it is defined as the sum of probabilities of each possible result of experience multiplied by its value. It represents the steady mean of all the experimental data by virtue of the corresponding

frequency of occurrence. The mean value of a random soil parameter (i.e., X) with the corresponding probability density functions $f_X(X)$ are given as follows:

$$\mu_X = \int_{-\infty}^{+\infty} X f_X(X)\, dX. \tag{1.12}$$

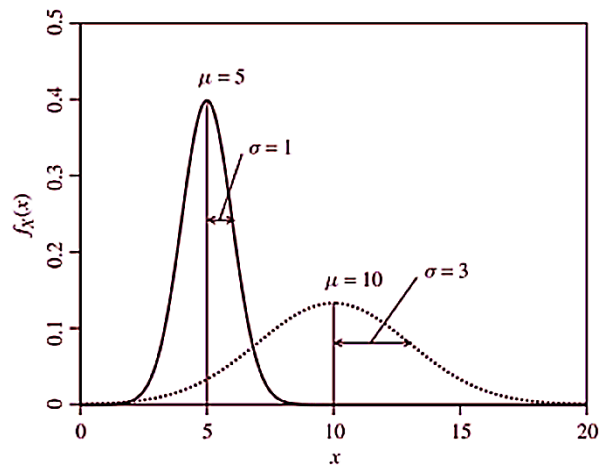

Figure 1.8: Two different distributions of the mean value and standard deviation (Fenton & Griffiths, 2008).

1.6.2 The variance and standard deviation

The variance (Var) measures the degree of dispersion in the fluctuations around the mean value of the parameter (eq. (1.13)). Consequently, the mean value is called the first central moment and the variance is called the second central moment.

$$Var(X) = \sigma_X^2 = \int_{-\infty}^{+\infty} (X - \mu_X)^2 f_X(X) dX, \tag{1.13}$$

where σ_X is the standard deviation; it is obtained by the square root of Var(X). Following Fenton and Griffiths (2008), this probabilistic characteristic refers to the possible deviations around the mean value, as illustrated in Figure 1.8.

However, the coefficient of variation COV describes the size of dispersion of the random variable based on the standard deviation. Basically, the role of this non-dimensional coefficient is to specify small and large dispersions. It is defined as the ratio of the standard deviation to the mean value:

$$COV_X = \frac{\sigma_X}{\mu_X}. \tag{1.14}$$

Phoon and kulhawy (1999) presented approximated values of COV for each soil parameter. This was executed using Cone Penetration Tests (CPT), Vane Shear Tests (VST) and tests made in laboratory (i.e., unconfined compression tests (U-C), triaxial compression tests (unconsolidated-undrained U-U) and

undrained triaxial compression tests (consolidated-isotropic C-I)). As a result, the soil undrained cohesion c_u furnished typical values of COV as high as 10-55%.

1.6.3 Correlation structure

Basically, the rate of linear dependency between two random variables X and Y is expressed by the covariance (eq.(1.15)). This expression may be replaced by that of the normalized covariance (correlation coefficient), shown in eq. (1.16).

$$COV(X,Y) = \int_{-\infty}^{+\infty}\int_{-\infty}^{+\infty}(x-\mu_X)(y-\mu_Y)f_{XY}(x,y), \tag{1.15}$$

$$\rho_{XY} = \frac{COV(X,Y)}{\sigma_X\sigma_Y}, \quad -1 \le \rho_{XY} \le +1. \tag{1.16}$$

It is worthwhile noting that, for statistically independent X and Y, the covariance is zero. Hence, $\rho_{XY}=\pm1$ signifies a linear relation between X and Y that is perfectly positive and respectively negative. While, $\rho_{XY}=0$ signifies uncorrelated random variables.

Nevertheless, the correlation structure representing the inherent variability, highlights the similarity in fluctuations measured at two adjacent points following a similar tendency with respect to a certain degree of consistency. In other words, a function of auto-correlation is developed to account for the consistency of each soil property at two different locations. The function is defined in terms of a correlation distance or scale of fluctuations that represents a significant consistency pertaining to the length between two constant points. Vanmarcke (1983) developed a rational method to asses a group of random and correlated variables pronounced by w(z) assuming a homogeneous random field to analyze the inherent variability. Moreover, the suggested correlation structure of a random field is defined by the function of covariance. The application of random field starts by the choice of distribution of field probability. Fenton and Griffiths (2008) defined the correlation function (covariance function) exponentially in two dimensions as follows:

$$\rho\big((x_1,y_1),(x_2,y_2)\big) = exp\left(-\frac{|x_1-x_2|}{\theta_x}\right) exp\left(-\frac{|y_1-y_2|}{\theta_y}\right), \tag{1.17}$$

where, θ_x and θ_y are respectively the horizontal and vertical correlation lengths. Phoon and kulhawy (1999) presented approximated values for the correlation lengths of soil undrained cohesion c_u using laboratory and in situ tests with respect to the fact that the soil properties vary vertically more than the

horizontal direction. Accordingly, θ_x is in the interval of 40-60 m and θ_y is of 0.5-6 m (generally taken as 1-2 m). However, the isotropic random field is defined as, $\Theta=\theta_v=\theta_h$.

1.6.4 Continuous probability distribution of random soil parameters

Understanding the parameters of the probability density function helps remarkably describing the principal characteristics of the random variable. In practice, the distribution function is unknown, therefore, various approximate distributions are suggested to fill this gap such as normal and lognormal distributions:

1.6.4.1 Normal and standard normal distributions

Also known as the Gaussian distribution; it is widely used in practice for reasons of mathematical simplifications and symmetry. The probability density function for this type is defined as follows:

$$f_X(X) = N(\mu_X, \sigma_X^2) = \frac{1}{\sqrt{2\pi}\sigma_X} exp\left[-\frac{1}{2}\left(\frac{X-\mu_X}{\sigma_X}\right)^2\right], \qquad -\infty < X < +\infty. \tag{1.18}$$

Figure 1.9 shows the density function of the normal distribution. It is noted that, as the mean value is maintained constant, the standard deviation governs the spread out of the plots. Generally, the standard normal distribution is used for reasons of simplifications (Figure 1.9(b)). It is based on replacing the normal variable X by the standard normal variable Z with a corresponding mean value of 0 and standard deviation of 1, pronounced by N(0,1):

$$Z = \frac{X-\mu_X}{\sigma_X}. \tag{1.19}$$

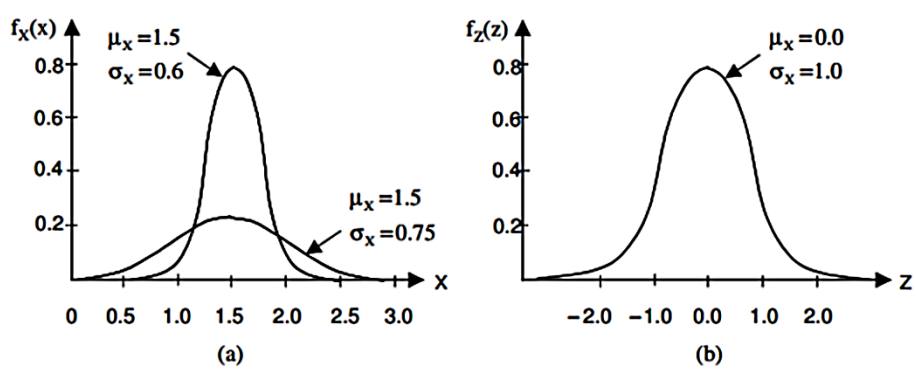

Figure 1.9: Density functions (Russeli, 2008) attributed to: (a) normal distribution, and (b) lognormal distribution.

The corresponding probability density function is given by:

$$\Phi_Z(Z) = \frac{1}{\sqrt{2\pi}} exp\left(-\frac{Z^2}{2}\right), -\infty < X < +\infty. \tag{1.20}$$

Furthermore, the Gaussian distribution admits negative values for soil properties, noting that they are considered physically unrealistic. Therefore, this distribution could only be a rigorous approximation.

1.6.4.2 Standard lognormal and shifted distributions

The lognormal distribution is used to model the soil and rocks properties with simplicity, as it is derived from a simple non-linear transformation of the classical normal distribution (Gaussian distribution). In addition, this type of distribution maintains the random variable always positive. The general form of the probability density function pertaining to the shifted lognormal distribution is given by eq. (1.21) for a random variable X by virtue of a natural algorithm that is normally distributed Y=ln(X).

$$f_x(X) = \frac{1}{\sqrt{2\pi}(X - X_0)\sigma_{ln(X)}} exp\left\{-\frac{1}{2}\left[\frac{l\,n(X - X_0) - \mu_{ln(X)}}{\sigma_{ln(X)}}\right]^2\right\}, \quad X_0 < X < +\infty, \tag{1.21}$$

where X_0 is the shift parameter of the random variable X. For X_0=0, the function is that of the standard lognormal distribution. Hence, the mean value and standard deviation are defined accordingly:

$$\mu_{ln(X)} = l\,n(\mu_X - X_0) - \frac{1}{2} ln\left[1 + \left(\frac{\sigma_X}{\mu_X - X_0}\right)^2\right], \tag{1.22}$$

$$\sigma_{l\,n(X)} = \sqrt{ln\left[1 + \left(\frac{\sigma_X}{\mu_X - X_0}\right)^2\right]}, \tag{1.23}$$

The emplacement parameter X_0 is obtained from the equation of asymmetry (third central moment) v_X, which measures the degree of asymmetry of the probability density function:

$$v_X = 3\frac{\sigma_X}{\mu_X - X_0} + \left(\frac{\sigma_X}{\mu_X - X_0}\right)^3 \tag{1.24}$$

Furthermore, Figure 1.10 shows the transformation of the lognormal distribution to the standard normal distribution. The lognormal distribution provides a realistic modelling of many properties of soil in the space at a time as it is strictly positive. Consequently, the cumulative distribution function CDF is obtained as follows:

$$F(X) = \frac{1}{2} erfc\left(-\frac{ln(X - X_0 - \mu_{lnX}}{\sigma_{lnX}\sqrt{2}}\right), \tag{1.25}$$

where *erfc* is the complementary error function.

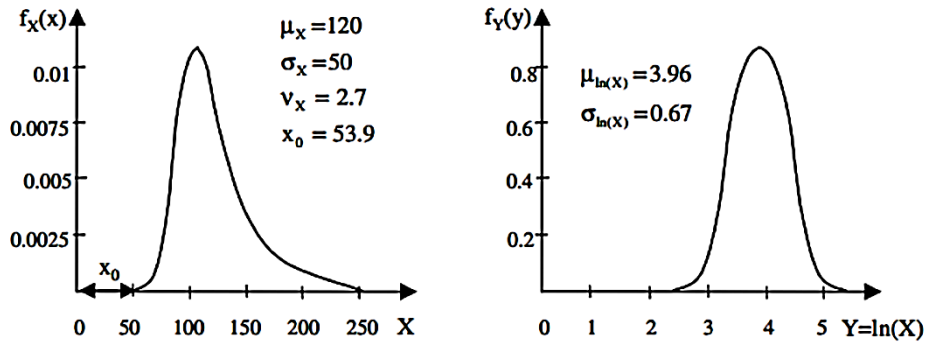

Figure 1.10: The function transformation from the lognormal distribution to its corresponding standard normal distribution (Russeli, 2008).

1.7 Stochastic analysis and random field generation

1.7.1 Types of stochastic analyses based on the sought purpose

Following Schweckendiek (2006), the uncertainty analyses may be conducted based on the sought reason.

- **Analysis based on uncertainty:** its purpose is to estimate the dispersion of results with introducing the principle static moments (mean value and standard deviation).

- **Analysis based on reliability:** this type of analysis is conducted by introducing a failure criterion that describes the unfavourable occurrences. The resulting data are in terms of reliability index β (eq. (1.26)) or probability of failure P_f.

$$\beta = \frac{\mu_{F_s} - 1}{\sigma_{F_s}}. \qquad (1.26)$$

- **Analysis based on risk determination:** this analysis is related to the decision making; it analyzes the possible consequences of the problem.

- **Analysis based on the probabilistic concept:** this analysis addresses basically all the principle methods with considering a rational economic criterion.

1.7.2 The Monte Carlo simulation method adopted for the random field generation in OptumG2 software

The numerical software (Krabbenhoft, 2017) implements the Monte Carlo (MC) simulation due to its simplicity in tackling complex problems analytically. Basically, this method consists of combining all

possible random variable combinations (Kayser & Gajan, 2014). First of all, the problem model has to be identified in order to obtain a deterministic solution. Thenceforth, the type of probability distribution needs to be specified for the input data. The frequency estimation is required with an estimated correlation of input data in order to make the probability distribution reliable. Thus, the MC simulation is conducted for each unique combination of the input and output data of the problem, in order to estimate the mean value, standard deviation, probability distribution function PDF and cumulative distribution function CDF. It is clear that, the function CDF (F_x (X)) is obtained from the sum of all resulting probabilities; in other words, it is obtained from deriving PDF (Figure 1.11):

$$F_X(X) = \frac{df_x(X)}{dX}. \tag{1.27}$$

The MC simulation results in the predicted probability of failure for the output data pertaining to each overtaken probability.

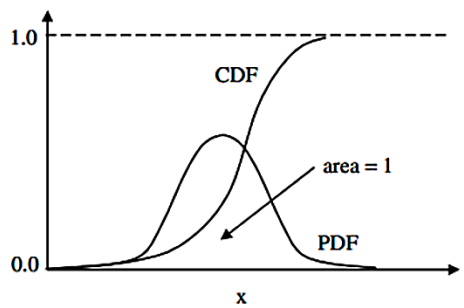

Figure 1.11: PDF and CDF pertaining to a continuous random variable (Russeli, 2008).

1.7.2.1 Karhunen- Loeve expansion integrated in OptumG2 software

According to Zhang and Lu (2004), this method is effective as it identifies analytical solutions for the exponential function of covariance. Generally, the covariance is defined as a measure of linear dependence between two continuous random variables (S,t) or more. For cases where the random variables are completely independent of each other, the covariance is equal to zero. The function of covariance is given based on the theorem of Mercer:

$$C_X(s,t) = \sum_{i}^{\infty} \lambda_i f_i(S) f_i(t), \tag{1.28}$$

where λ_i and f_i are respectively the eigenvalues and the corresponding function of C_x. The derived function in eq. (1.29) is segmented into an infinite number of terms n with a reduced simulated variance.

The eigenvalues are classified from highest to lowest until reaching the sought diminution of the corresponding functions that satisfies the following condition:

$$\frac{\lambda_n}{\lambda_1} \leq TOL, \tag{1.29}$$

where, TOL=10^{-5}. The equation is resolved using the solution provided by Zhang and Lu (2004). It is indicated that an increasing tendency is relevant to the number of terms with the decrease in the correlation lengths.

1.8 Conclusion

This chapter presents in brief the methods of analyzing the slope stability under different conditions; for instance, sliding caused by the self-weight, and sliding caused by a surface load condition (shallow foundation at the slope surface); as well as, spatial variability of soil properties.

The classical stability estimation goes through different stages; firstly, locating the slip surface, determining normal and tangential stresses and eventually computing the factor of security. Furthermore, the bearing capacity is function of mechanical soil properties and footing geometry; this is taken into account by means of correction factors. Various analytical expressions have been derived to provide an accurate estimation for the case of homogeneous soil. To rigorously consider the uncertainty of various soil parameters, the spatial variability is considered in different methods. The probabilistic approach considers each uncertain parameter in the probability distribution, in order to give a factor of safety or limit load by means of mean value, variance, reliability index and probability of failure.

Chapter 2: Stability assessment of pile-stabilized slope based on analytical and numerical methods

2.1 Introduction

Among deterministic methods of analyzing pile-stabilized slopes, several analytical methods have been adopted. One of which is the pressure based method (Broms, 1964; Dong-ping et al., 2017; Ito & Matsui, 1975; Randolph & Houlsby, 1984; Viggiani, 1981); its main objective is to focus on the passive part of piles exposed to horizontal soil pressure. In addition, the displacement based methods have proved accuracy in estimating the pile resistance in terms of soil movements (Chen et al., 2020; Lee et al., 1995; Poulos, 1995). The method estimates the lateral soil movement above the slip surface to be used in evaluating the active pile behavior. Numerical methods have become innovational over the last few decades. They are used to account for complex geometries in 3D analysis and to enhance the description of lateral load distribution along the pile row. This is due to the consideration of both the pile behavior and soil-pile interaction (Chow, 1996; Jeong et al., 2003; Kourkoulis et al., 2012; Pirone & Urciuoli, 2018; Sanping & Robert, 2002; Xiao, 2020; Yamin & Liang, 2010; Yang & Zhang, 2020). Nevertheless, the probabilistic analyses should be conducted side by side with deterministic analyses, as they are a complementary process to enhance the conservative deterministic solutions. The spatial variability of soil parameters based on random field concept are widely taken into consideration by various scholars in the last decade for the case of a slope stabilized by a row of piles (Gong et al., 2019; Jiang et al., 2016; Li & Liang, 2014).

This chapter represents analytical and numerical methods available in the literature, as well as the reliability assessment of a slope stabilized with piles. The numerical simulation of slope stability using

piles necessitates a well adopted numerical tool. For this purpose, the computation code OptumG2 is enlightened in this chapter. The elastoplastic and rigid plastic theorems are represented as the current software permits the use of shear strength and limit analyses in finite elements with their upper and lower bounds. Therefore, the direct determination of the slope stability and the ultimate reaction force induced by piles is furnished.

2.2 Analytical methods for the stability assessment of pile-stabilized slope based on the limit equilibrium method

The slope reinforcement allows the transfer of lateral mobilized loads (active pressure) to greater depths of higher mechanical characteristics (stable layer) by producing passive resistance as shown in Figure 2.1(a).

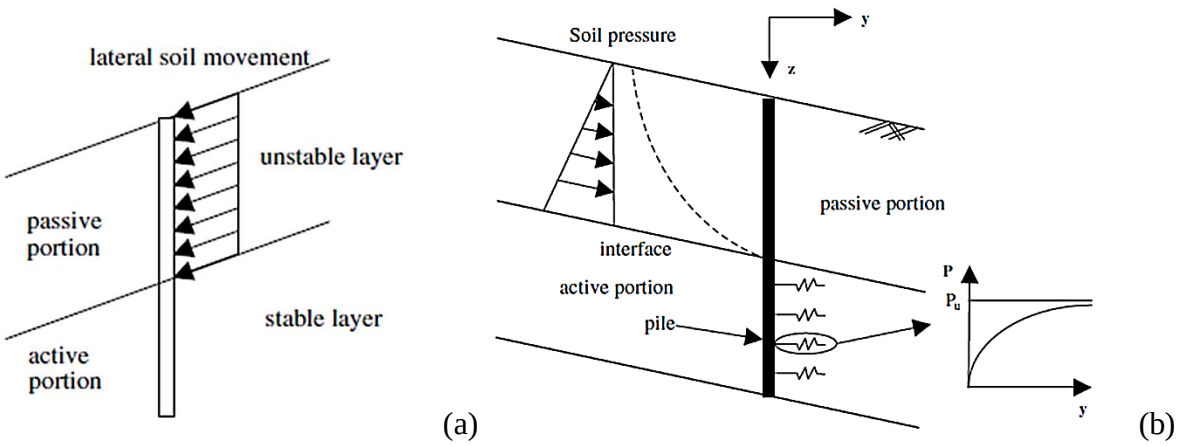

Figure 2.1: Soil-pile system (Won et al., 2005): (a) driving forces acting on a pile row, and (b) reaction forces induced by piles.

The analysis is achieved by extending classical methods used for the slope without reinforcement to the reinforced case, with incorporating the effect of force resistance, as indicated in Figure 2.1(b). However, the piles are subject to two types of solicitations; namely, solicitations generated by a superstructure and others generated by the surrounding soil (breaking action, horizontal pressure, earthquakes, etc.).

2.2.1 Theoritical background

Table (2.1) summarizes the most famous methods published in the literature for the stability assessment of piled slopes. The pressure based methods, rely on the assumption of lateral pressure acting on passive piles following Ito and Matsui (1975). The method assumes rigid piles of an infinite length, yielding to a plastic flow between piles (plastic deformation) during sliding. Thus, the surrounding soil is in a state

of plastic equilibrium, following Mohr-Coulomb yield criterion. It is of interest to mention that the resistance induced by each pile is quite affected by the soil mechanical characteristics, width of single slide and geometrical properties of piles. The pile spacing, overburden pressure, and soil characteristics are considered the key factors to the estimation of the ultimate pressure generated by the soil flow. In contrast, the pile stiffness has no effect at all. Hence, the lateral soil-pile pressure rises with the decreasing trend of pile spacing. It is noted that the pressure-based approach doesn't consider the effect of soil arching between piles, which makes it a limitation for the study of the actual response of flexible piles.

Table 2.1: Limit equilibrium based methods for the assessment of pile-stabilized slope stability.

Author	Condition of piles	Type of soil	Method
Ito et al. (1981)	Laterally loaded piles of Fixed, hinged, unrotated and free head.	c-φ slope	Limit equilibrium
Broms (1964)	Laterally loaded single pile and pile group	Sandy slope	Pressure based
Viggiani (1981)	Laterally loaded pile group	Cohesive slope	Pressure based
Hassiotis et al. (1997)	Laterally loaded drilled piers	c-φ slope	Pressure based
Dong-Ping et al. (2017)	Laterally loaded micropiles	c-φ slope	Pressure based
Poulos (1995)	Laterally loaded single pile	Cohesive slope	Boundary element/ Displacement based
Lee et al. (1995)	Laterally loaded pile row	Cohesive slope	Boundary element/ Displacement based
Chen et al. (2020)	Soil arch force applied on piles	c-φ slope	Displacement based

The approach of displacement based methods relies on the determination of the relative soil-pile movement. It is based on an uncoupled analysis; in which, the piles behaviour and slope failure are computed separately. The prevalence of this method over the pressure based one is that, it depicts the accurate soil-pile interaction; thusly, the mobilized resistance of piles is calculated using the lateral sliding. However, the lateral sliding soil may be directly computed using inclinometer data or with the contribution of other numerical methods and empirical correlations. It is worthwhile noting that this method doesn't account for centre-to-centre spacing in the evaluation of soil-pile pressure. Basically, the pile and soil are assumed to be respectively as elastic beam and its corresponding continuum. Hence, a

large soil mass is considered to be sliding as a block towards the downslope forming a drag zone tolerating vigorous shearing right below. The method computes the lateral behaviour of each pile and the induced maximum shear force with respect to the condition of a free-field soil movement and pile lateral displacement.

2.3 Numerical computations for the stability estimation of pile-stabilized slope

Numerical methods are much more accurate compared to analytical methods, as they rely on conducting coupled analyses by considering both soil and pile interaction. The computations may be carried out without necessarily locating the failure surface previously. The soil-pile interaction has been investigated by several scholars in the last few decades (Jeong et al., 2003; Sanping & Robert, 2002; Yamin & Liang, 2010). The power of numerical methods is in the consideration of complex models; namely, 3D analysis of pile-stabilized slopes, pile group behavior and nonlinearity of pile rows and soil. The only inconvenience is in the time consumption, as usually many calculation stages are required to analyze the soil-pile behavior accurately.

2.3.1 Shear strength reduction method SSR

Cai and Ugai (2000) used the elastoplastic finite element method to predict the piles response, as shown in Figure 2.2:

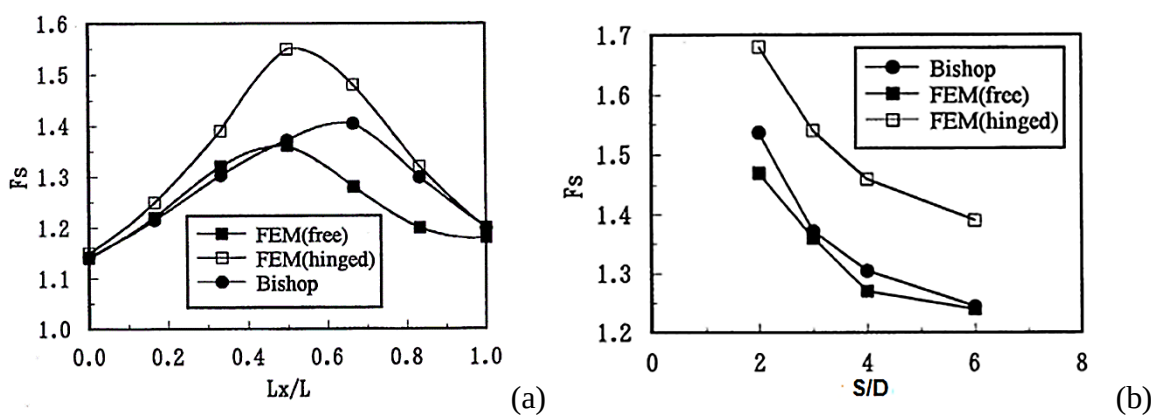

Figure 2.2: Comparison of the finite element method with Bishop's simplified method: (a) optimal pile position, and (b) most effective pile spacing.

The advantage of the adopted method over classical limit equilibrium methods is the ability to account for pile bending stiffness and head condition in the calculations of the factor of safety. Nevertheless, Bishop's simplified method (Bishop, 1955) assumed that the best pile location is near the top of the slope contrasting with numerical methods, where the piles showed higher factors of safety when they are at the

middle of the slope Lx/L=0.5 (Figure 2.2(a)). Hence, the factor of safety resulted from Bishop has shown slightly an over estimation for relatively small spacings, as shown in Figure 2.2(b).

The same model geometry was adopted by Won et al. (2005); the coupled effects has been addressed to compute the safety factor of a pile-stabilized slope using the finite difference analysis. It was deduced that the best stability is obtained for piles with restrained head conditions that are driven at the middle of the sloping ground. Wei and Cheng (2009) found that the slip surface is quite affected by the pile centre-to- centre spacing. This tendency is pronounced by an integral failure surface for relatively high spacings, or might be divided into two parts for relatively smaller spacings. Furthermore, the failure surface for pile-stabilized slope is reported to be shallower compared to that of the unstabilized one. Thus, the optimal pile position is found to be centring the failure surface. Yang et al. (2011) used the finite element elastoplastic analysis to account for the effect of the embedded pile length on the overall stability of the slope.

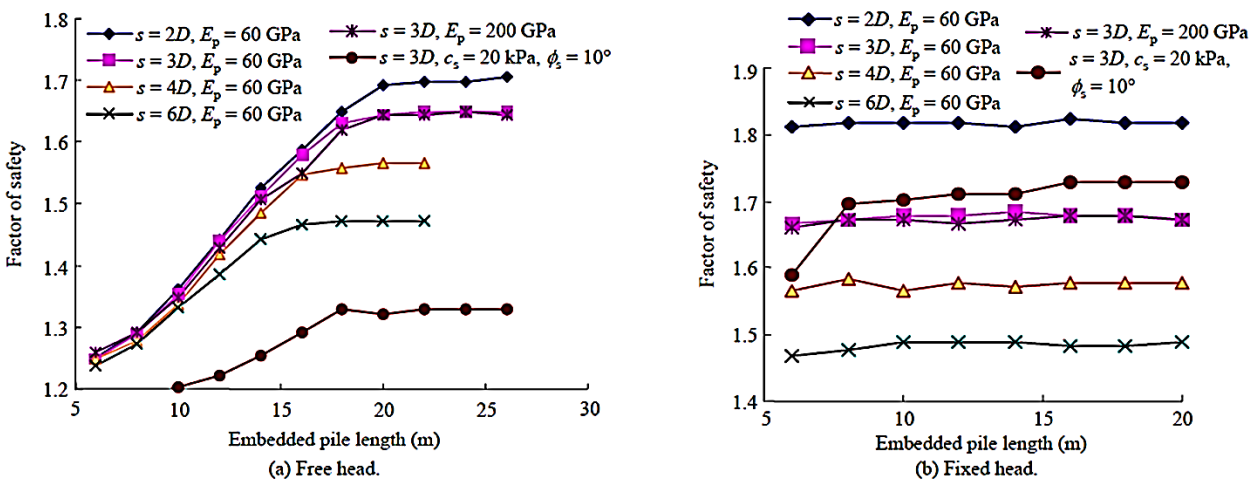

Figure 2.3: Effect of the embedded pile length on Fs for: (a) free head condition, and (b) fixed head condition.

For the free head condition (Figure 2.3(a)), the pile length keeps rising with the raise of F_s independently of the spacing S/D (spacing/pile diameter), until reaching the critical state beyond which the safety factor remains constant. In contrast, for the fixed head condition (Figure 2.3(b)), F_s follows a steady tendency independently of the pile lengths and S/D. In both head conditions, the increase in the spacing S/D leads to the factor of safety to decrease. However, Pirone and Uriuoli (2018) focused on the determination of the ultimate limit load acting on continuous or discrete piles, used to reinforce infinite slopes. It was found that the distribution of stress under ultimate limit state conditions is investigated accurately using

the coefficients of Ranking earth pressure, in spite of the friction pertaining to pile row/wall and soil interface.

2.3.2 Limit analysis LA

Recently, several researchers (Li et al., 2020; Xiao, 2020; Yang & Zhang, 2020) adopted the limit analysis kinematic approach to analyze the stability of a slope reinforced by pile rows. The method served at the purpose of locating the potential failure plane by accounting for the stabilizing force induced by piles. It is important to mention that the principle of the Kinematic approach has been extended from Ausilio et al. (2001) to develop expressions for the sought value of the force used to raise the factor of safety. Furthermore, Yang and Deng (2019) used the upper bound of limit analysis to determine the lateral resisting force with respect to unsaturated flow under vertical and steady conditions. A numerical analysis was conducted to investigate the influence of the ultimate reaction force induced by piles. Nian et al. (2008) made use of both techniques strength reduction and limit analysis to propose analytical expressions for the resisting force induced by piles. This was to raise F_s pertaining to a slope with nonhomogeneous and anisotropic soil strength. Hence, the minimum factor of safety pertaining to the critical slip surface was obtained numerically using the program Fortran 90.

2.4 Demonstration of the employed methodology integrated in OptumG2 and finite element modelling

Technically, OptumG2 is a software of finite elements in 2D based on modern numerical optimizations. The software provides the full ability of modelling a row of piles following Sluis et al. (2014). It is executed by the integration of two independent layers for the piles and the soil, where the soil-pile interaction is simulated by means of axial, base and tangential springs. It is worthwhile to mention that the used numerical code is specially developed for geotechnical applications. The finite element modelling is rapidly realized by dint of user graphical interface. Even though the software have similar characteristics with other finite element programmes, it addresses as well another feature resulting in direct solutions for direct problems without having to get through quite longer analyses. For instance, the shear strength reduction analysis that offers a rapid estimation of the factor of safety pertaining to geostructures and the limit analysis for the direct evaluation of the limit load without having to get through lengthy elastoplastic analyses.

2.4.1 General notions

Elasticity and plasticity are two important definitions in geomaterials, as the characteristics of strain and strength are determined accordingly.

2.4.1.1 The yield and stress state

The limit state is defined in terms of stresses; by which, a threshold is located at a specific point pertaining to the case of σ=0. The yield surface defining stresses permissibility is given by a convex (Figure 2.4).

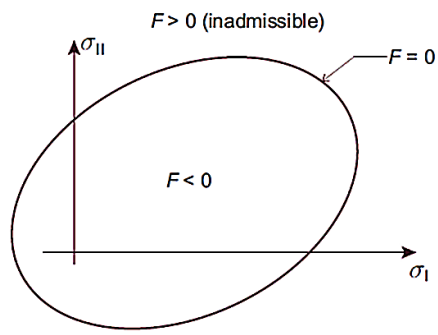

Figure 2.4: Convex of the yield plane.

It is shown that, the yield function defining the limit state F(σ) is pronounced for several cases:

- The zone where stresses are permissible inside the yield surface F(σ)≤0.

- The zone pertaining exactly to the yield surface F(σ)=0.

- The zone of inadmissible stresses outside the yield surface F(σ)>0.

For a structure of volume V yielding to surface tractions αt (α is the load multiplier) on S_σ, and at the same time sustained on S_u (Figure 2.5), infinite displacements are generated at collapse. Therefore, it is important to define a quantity of relevant work or velocity scaling. The equilibrium and limit state conditions are expressed as follows:

$$\nabla^T \sigma + b = 0 \quad in\, V,$$
$$P^T \sigma = t \quad in\, S_\sigma, \tag{2.1}$$

where

$$\nabla^T = \begin{bmatrix} \frac{\partial}{\partial x} & 0 & 0 & \frac{\partial}{\partial y} \\ 0 & \frac{\partial}{\partial y} & 0 & \frac{\partial}{\partial x} \end{bmatrix}, \tag{2.2}$$

$$P^T = \begin{bmatrix} n_x & 0 & n_y \\ 0 & n_y & n_x \end{bmatrix}. \tag{2.3}$$

Furthermore, the failure is assured with respect to the following condition:

$$F(\sigma) \leq 0. \tag{2.4}$$

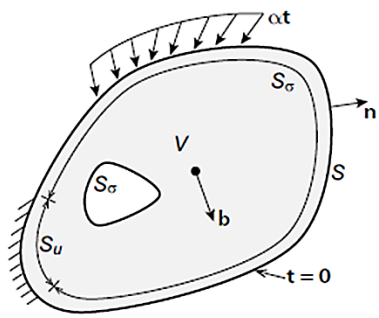

Figure 2.5: Applied traction on the material boundary S.

2.4.1.2 Classic decomposition of strains

The strains ε are given in terms of displacements u:

$$\varepsilon = \nabla u. \tag{2.5}$$

The total strain principle ε, relies on combining two essential parts, elastic strains ε^e and plastic strains ε^p:

$$\varepsilon = \varepsilon^e + \varepsilon^p. \tag{2.6}$$

The Stresses define the elastic strains with inducing a compliance modulus to account for elasticity ℂ as follows:

$$\varepsilon = \mathbb{C}\sigma. \tag{2.7}$$

A flow rule defines the plastic strains changing ratio in terms of a flow potential G and plastic multiplier $\dot{\lambda}$ ($\dot{\lambda} \geq 0$):

$$\dot{\varepsilon}^p = \dot{\lambda}\frac{\partial G}{\partial \sigma}. \tag{2.8}$$

The exact value of $\dot{\lambda}$ is undetermined, therefore it is defined with respect to the yield condition of stresses F(σ)=0:

$$\dot{\lambda}\, F(\sigma) = 0. \tag{2.9}$$

In practice, the potential flow G is obtained based on mathematical experiments, with taking into consideration that G takes the same functionality as F but with another special material properties.

However, G is considered as high as F (G=F) for the associated flow rule, consequently when the opposite tendency happens (G≠F) the non-associativity takes place.

2.4.2 Elastoplasticity

The general definition of thermomechanical formulation to account for elastoplasticity relies on the first and second laws of thermodynamics. The central formulation is expressed by the rate of internal work Ƥ under the condition of isotherm:

$$\begin{gathered} \text{Ƥ} = \sigma^T \dot{\varepsilon} = \dot{\phi} + D, \\ \sigma^T = \left(\sigma_x, \sigma_y, \sigma_z, \tau_{xy}, \tau_{yz}, \tau_{zx}\right), \\ \emptyset = \emptyset(\varepsilon^e, \eta), \\ \dot{\phi} = \nabla_{\varepsilon^e} \emptyset(\varepsilon^e, \eta)\dot{\varepsilon}^e + \nabla_\alpha \emptyset(\varepsilon^e, \eta)\dot{\eta}, \end{gathered} \tag{2.10}$$

where σ^T and Ø are respectively the transposed stress vector and free energy function of Helmholtz that depends on elastic strains ε and strain-like hardening variables η; also, D is the function of dissipation (D≥0). Nevertheless, the finite step formulation may approximates the energy function in time with inducing an initial recognised state $Ø_0$:

$$\text{Ƥ} = \dot{\phi} + D \approx \emptyset - \emptyset_0 + D. \tag{2.11}$$

Although, the majority of simple materials involve a steady yield surface; recently developed materials tend to introduce hardening mechanisms. The finite-step version is derived with respect to an implicit determination of deformation power; inducing both terms of variable pertaining to stress-like hardening *k* and stress σ:

$$\begin{gathered} \text{Ƥ}(\sigma, k) = \sigma^T \Delta\varepsilon - \widehat{\text{Ƥ}}(\sigma, k), \\ \widehat{\text{Ƥ}}(\sigma, k) = (\psi - \psi_0) - \Delta\sigma^T \nabla_{\sigma\psi_0} - \Delta k^T \nabla_{k\psi_0}. \end{gathered} \tag{2.12}$$

The code of material point is expressed with respect to the formulation of finite-step, as follows:

$$\begin{aligned} &maximize \quad \sigma^T \Delta\varepsilon - \widehat{\text{Ƥ}}(\sigma, k) \\ &subject\ to \quad F(\sigma, k) \leq 0. \end{aligned} \tag{2.13}$$

2.4.2.1 The principle of the lower bound:

The governing equations are expressed in terms of lower bound theorem in an equivalent way with assuming a linear elastic perfectly plastic material:

$$\begin{gathered} \hat{P} = \frac{1}{2} \Delta\sigma^T \mathbb{C} \Delta\sigma, \\ \Delta\sigma = (\sigma - \sigma_0). \end{gathered} \tag{2.14}$$

There by:

$$\begin{aligned} &Maximize \quad \alpha - \frac{1}{2}\int \hat{p} \quad dV \\ &subject\ to \quad \nabla^T \sigma + b = 0 \qquad in\, V, \\ &p^T \sigma = \alpha t \qquad in\, S_\sigma, \\ &F(\sigma) \leq 0. \end{aligned} \tag{2.15}$$

2.4.2.2 The principle of the upper bound

The upper bound induces governing equations derived as follows:

$$\begin{aligned} &Manimize \quad \int K^T \Delta\lambda\, dV - \int b^T \Delta u\, dV + \int \frac{1}{2} \varepsilon^{eT} \mathbb{D} \varepsilon^e\, dV \\ &subject\ to \quad \nabla\, \Delta u = \Delta\varepsilon^e + F\Delta\lambda, \quad \Delta\lambda \geq 0, \\ &\int t^T \Delta u\, dS = 1. \end{aligned} \tag{2.16}$$

where ε^e, λ, u and $\mathbb{D}$ *are respectively, the elastic strains, plastic multiplier, displacements and the modulus depicting the rigid plastic behaviour* ($\mathbb{D} = \infty, \varepsilon^e = 0$).

2.4.2.3 Elastoplastic strength reduction analysis

Strength reduction analysis is conducted by a group of realistic loads that address the determination of the actual strength to be used in the final decision of the failure mechanism. The process is achieved by calculating the factor of shear strength reduction, pertaining to the reduced parameters of soil at the stage of initial failure. A strength reduction factor less than 1.5 for slopes implies an unstable ground with the necessity of supplementary strength to prevent failure; also a factor more than 1.5 implies the attaint of stability. The parameters in question are those who may affect the stability of the soil. For instance, Mohr-Coulomb criterion implies a similar rate of reduction to the cohesion c and friction angle φ. Thus, the factor of safety is defined in terms of reduced parameters:

$$F_s = \frac{c}{c_{red}} = \frac{tan\, \varphi}{tan\, \varphi_{red}}. \tag{2.17}$$

The computation of rigorous lower and upper bounds conducted for the analysis are of huge interest as the accurate factor of safety will fall in the interval of both bounds. In other words, it falls exactly at the average value that is greater than the lower bound and lower than the upper bound.

2.4.3 Rigid plastic Limit analysis

The limit analysis assumes rigid plastic materials, by which the maximum magnitude of tractions is investigated at the point before collapse. In other words, the minimum magnitude of tractions causing failure should be well determined. The condition of yielding is given by:

$$F^T\sigma - K \leq 0, \tag{2.18}$$

where F and K are contributors of linear restrictions defined as f_i and k_i (i=1,…,n):

$$f_i^T\sigma - k_i \leq 0. \tag{2.19}$$

Thus, introducing indolent variables in the yield condition leads to the following:

$$F^T\sigma - K + s = 0, \quad s \geq 0. \tag{2.20}$$

The compatibility of the flow rule associated with strains and displacements is given by:

$$\nabla\dot{u} = F\dot{\lambda}, \tag{2.21}$$

with respect to the scaling, the rate of work induced by the incipient tractions t is satisfied:

$$\int_{\sigma_S} t^T\,\dot{u}\,dS = 1. \tag{2.22}$$

Under complemental constrains:

$$S^T\dot{\lambda} = 0, \quad s \geq 0, \dot{\lambda} \geq 0. \tag{2.23}$$

The result of the above governing functions is derived in terms of the load multiplier α. Nevertheless, it was reported that the collapse multiplier is targeted by a group of fields of velocity and distributions of stress. Variational principles may be induced to the above equations to serve the initiation of lower and upper bounds comprising the average solution.

2.4.3.1 Lower bound theorem

The lower bound theorem defines the governing equation with respect to the optimized problem as below:

$$\begin{aligned} &Maximize \quad \alpha \\ subject\ to \quad &\nabla^T\sigma + b = 0 \qquad in\ V, \\ &P^T\sigma = \alpha t \qquad on\ S_\sigma, \\ &F^T\sigma - k + s = 0, \quad s \geq 0. \end{aligned} \tag{2.24}$$

The solution of the above problem presents multipliers of Lagrange to represent the kinematic principle that is not defined in the above. The lower bound principle relies on the establishment of a stress field with respect to the conditions.

2.4.3.2 Upper bound theorem

The upper bound theorem defines the governing equation with respect to the optimized problem as below:

$$\begin{gathered} Minimize \int_V K^T \dot{\lambda}\, dV - \int_V b^T \dot{u}\ dV \\ subject\ to\ \nabla \dot{u} = F\dot{\lambda}, \quad \dot{\lambda} \geq 0, \\ \int_{S_\sigma} t^T\, \dot{u}\, dS = 1. \end{gathered} \tag{2.25}$$

The upper bound principle relies on the establishment of a velocity field with respect to the flow rule. By which, the rate of work induced by incipient tractions equals unity. The sough value of the collapse multiplier is given by subtracting the forces induced by the body from the rate of work.

2.4.4 Definition of yield criterions

2.4.4.1 Mohr-Coulomb criterion

The Mohr-coulomb criterion is pretty much used to depict the failure by soil shear assuming elastic perfectly plastic model. The developed yield function is given in terms of cohesion c (kPa) and friction angle φ (°). Addressing by that, both frictional (sandy soil) and cohesive (clay and limon) soils at short and long terms. The yield envelope is plotted according to the following:

$$\tau = c + \sigma_n \tan\varphi, \tag{2.26}$$

where τ and σ_n are respectively the shear and normal stresses. Three types of elasticity are accounted for linear isotropic, linear anisotropic and nonlinear isotropic. However, this dissertation only addresses the linear isotropy, in which the parameters are defined in two ways:

- Group A involves the young's modulus E (MPa) and poisson's ratio ν:

- Group B involves the Bulk K (MPa) and shear G (MPa) modulus.

$$K = \frac{E}{3(1-2\nu)}, \qquad G = \frac{E}{2(1+\nu)}, \tag{2.27}$$

$$E = \frac{9KG}{3K+G'}, \qquad \nu = \frac{3K-2G}{2(3K+G)}. \tag{2.28}$$

The load function (yield function) of Mohr-Coulomb is expressed in terms of both principal stresses, major σ_1 and minor σ_3 as follows:

$$F = |\sigma_1 - \sigma_3| + (\sigma_1 + \sigma_3) sin\varphi - 2c\ cos\varphi. \tag{2.29}$$

All possible representations of the yield surface pertaining to Mohr-Coulomb in the stress plane are shown in Figure 2.6.

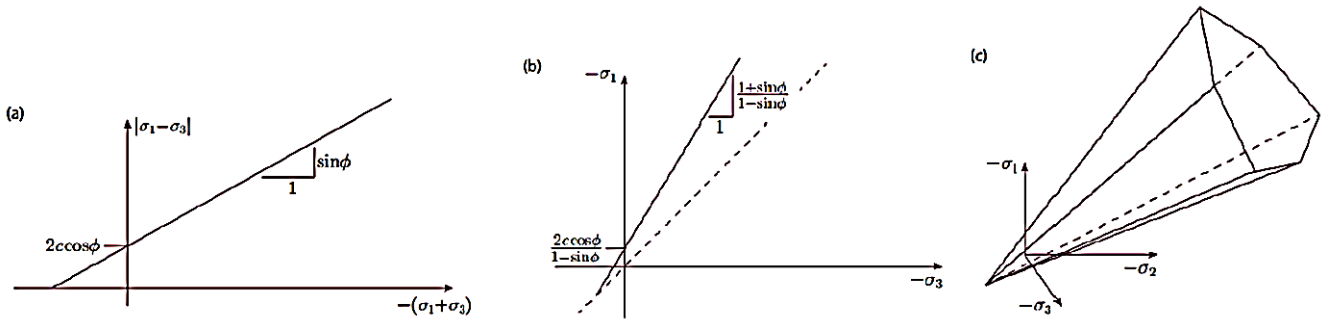

Figure 2.6: Load surfaces of Mohr-Coulomb criterion.

2.4.4.2 Tresca criterion

Tresca criterion is part of Mohr-Coulomb under purely cohesive soils (φ=0), namely saturated soils (clay and limon). The undrained condition is applied under total stresses that are captured at short term with invalid volume changes. Under plane strain conditions, the effective stresses are constants. They may be summed to represent the major and minor effective stresses, inducing the yield function of Mohr-Coulomb:

$$\begin{aligned} |\sigma_1 - \sigma_3| &= 2c\ cos\varphi - (\sigma'_1 + \sigma'_3)_0\ sin\varphi \\ &= 2c\ cos\varphi - \left(\sigma'_x + \sigma'_y\right)_0\ sin\varphi \\ &= 2c\ cos\varphi - (1 + K_0)\ \sigma'_{v,0}\ sin\varphi \\ &= 2S_u, \end{aligned} \tag{2.30}$$

where the initial vertical effective stress $\sigma'_{v,0}=-\sigma_{y,0}$ is positive in compression, also the initial coefficient of soil pressure is induced by $K_0 = \sigma_{x,0}/\sigma_{y,0}$. Two models are extracted from the Tresca model; standard Tresca model and a generalized model. This latter develops a yield function in terms of total stresses following the effective stress model of Mohr-Coulomb with respect to the general stress condition. It is important to mention that under undrained constrains the shear strength is expressed by the cohesion in the Tresca yield function with inducing undrained elastic parameters E_u or G. Two options of Tresca criterion are applicable by virtue of the shear strength:

*** Standard Tresca model**

The shear strength is expressed under undrained conditions s_u (kPa), where the collapse criterion is defined as:

$$F = |\sigma_1 - \sigma_3| - 2s_u. \tag{2.31}$$

The physical significance of s_u is related to the experiments conducted for plane strain conditions or direct simple shear. It is important to respect the direct estimation of s_u in the criterion function without referring to the characteristics. The tenacity of Tresca model with the Mohr-Coulomb reveals for a shear strength developed as below with respect to the condition of initial stresses $\sigma'_x/\sigma'_y=\sigma'_z/\sigma'_y=K_0$:

$$s_u = c\,cos\varphi + \frac{1}{2}(1 + K_0)\,\sigma'_{v,0}\,sin\varphi. \tag{2.32}$$

The standard Tresca model works under plane strain conditions with the ability of the shear strength to increase in deeper graduations of soil. This is due to the dependence of the pertaining vertical stresses. In other words, the shear strength is independent of the collapse stress path and determined directly.

*** Generalized Tresca model**

The key factors to plotting the behaviour of stress with strain are the major soil properties. Therefore, models of total stress are equivalent to that of effective stresses. This is referring to the equivalence of Mohr-Coulomb with standard Tresca model under plane strain, without considering other states of general stress. The shear strength is expressed under undrained conditions differently for triaxial compression s_{uc} (kPa) and triaxial extension s_{ue} (kPa). By which, it depends on the collapse corresponding stress track. However, the yield function is expressed as follows:

$$F = |\sigma_1 - \sigma_3| + \alpha(\sigma_3 - \sigma_2) - k,$$

$$\alpha = \frac{2\,sin\varphi}{3 - sin\varphi'}, \qquad k = \frac{6}{3 - sin\varphi}\left[\frac{1}{3}(1 + 2k_0)\sigma'_{v,0}sin\varphi + c\,cos\varphi\right], \tag{2.33}$$

where the major stresses are directive as of $\sigma_1 \leq \sigma_2 \leq \sigma_3$ and the compressive stresses are given with negative values. It is important to mention that, the relationship between the initial effective stresses is expressed by $\sigma'_{x,0}/\sigma'_{y,0}=\sigma'_{z,0}/\sigma'_{y,0}=k_0$, with referring to the asymmetry of $\sigma'_{x,0}/\sigma'_{y,0}=\sigma'_{\theta,0}/\sigma'_{y,0}=k_0$. Nevertheless, α and k may be expressed by the experimental undrained shear strengths pertaining to triaxial compression (s_{uc}) and extension (s_{ue}).

$$\alpha = \frac{s_{uc}}{s_{ue}} - 1, \quad k = 2s_{uc}. \tag{2.34}$$

Figure 2.7 shows the generalized Tresca model with the yield surface; the nodes indicated in the figure are referring to the triaxial compression TC and triaxial extension TE. The admissible shear strength range required to keep the failure surface convex and assure the proceeding of computations is given by:

$$\frac{1}{2} \leq \frac{s_{uc}}{s_{ue}} \leq 1. \qquad (2.35)$$

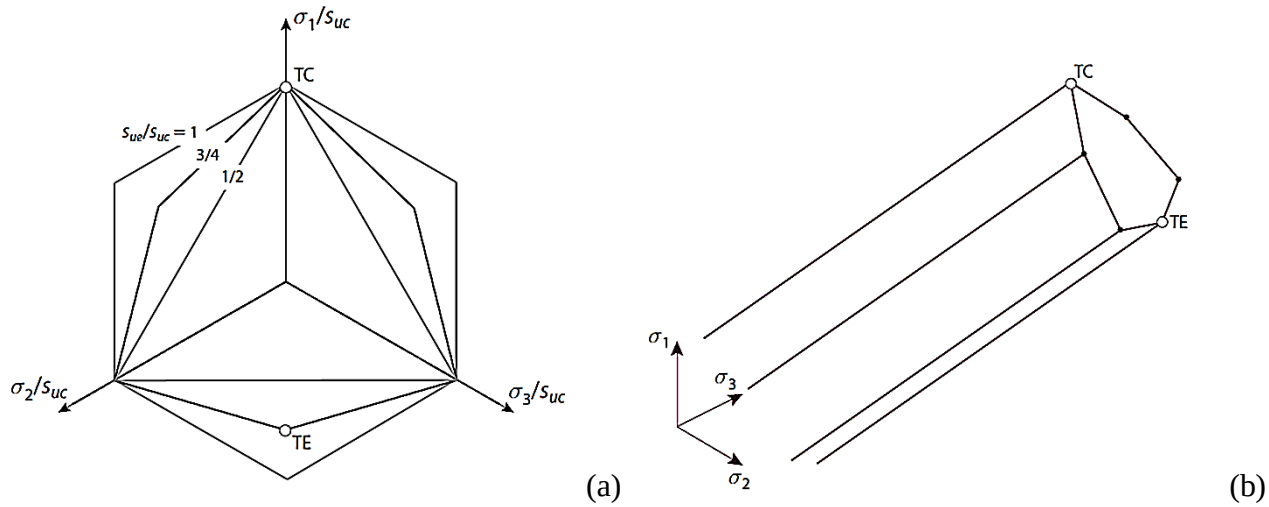

Figure 2.7: Failure surface pertaining to generalized Tresca model: (a) deviatoric plane, and (b) principal stress plane for a value as high as sue/suc.

2.5 Reliability analyses for the determination of failure probability of a reinforced slope

Technically, the factor of safety given by deterministic methods doesn't depict accurately the slope status for naturally heterogeneous soils. This is because several slopes have been reported as having high factors of safety, but in reality they failed many times. For this reason, the soil inherent variability has been widely addressed by several methods to give better estimation of failure probability:

- The first and second order reliability method FOSM; also called, first order reliability method FORM, and second order reliability method SORM.

- Sampling methods; such as, Monte Carlo simulation MC, and importance sampling method

- Latin hypercube sampling method.

- Stochastic expansion methods; such as, Karhunen-Loeve expansion KL, polynomial chaos expansion PCE, and Stochastic Finite element method (SFEM or RFEM). This latter is categorized as follows, perturbation method, Neumann expansion method, Weighted integral method and Spectral stochastic finite element method.

However, Table (2.2) shows some methods conducted for the reliability analysis of reinforced slopes. In which, parametric studies were conducted for the optimal and critical reinforcement conditions within the slope:

Table 2.2: Some studies conducted for the reliability analysis of reinforced slopes.

Author	Type of reinforcement	Method of generation	Type of distribution	Spatial variable shear strength characteristics
Bougouffa et al. (2019)	Row of piles	MC	Lognormal	COV_c=10-40%, COV_φ=5-15%
Sayed et al. (2010)	Pile wall	FOSM	Normal	μ_φ=22°, σ_φ=4.4°, COV_φ=20%
Li and Liang (2014b)	Drilled shaft	MC	Lognormal	μ_c= 0.96-7.42 kPa, μ_φ=11-35° COV_c=20%, COV_φ=10%
Jiang et al. (2016)	Row of piles	FORM	Normal, Lognormal	_
Zhang et al. (2017)	Row of piles	SORM	Lognormal	μ_c= 10-60 kPa, σ_c= 3-18 kPa μ_φ=0-20°, σ_φ=2-4°
Chen et al. (2019)	Row of piles	Latin hypercube sampling	Lognormal	μ_c= 10 kPa, μ_φ=30° COV_c=30%, COV_φ=20% θ_h=5-80 m, θ_v=2-10 m
Gong et al. (2019)	Row of piles	MC	Lognormal	μ_c= 12 kPa, COV_c=10-70% μ_φ=20°, COV_φ=10-40% θ_h=50 m , θ_v=0.25-32 m

Chen et al. (2019) investigated the variation of the horizontal and vertical scales of fluctuation δ on the probability of failure, corresponding to a pile-stabilized slope. Figure 2.8 shows that, the soil properties are distributed uniformly and appear to be more consistent with the increase of correlation lengths. The probability of failure is pronounced better for the case where δ_v is varying compared to δ_h. This is explained by the fact that, the geotechnical properties of the soil vary significantly in vertical directions.

Zhang et al. (2017) proved that, small pile spacings (D_1/D) may lead to larger reliability indexes β as indicated in Figure 2.9(a). When the piles are placed closer to each other they provide a noticeable

resistance to failure. Thus, the optimal pile location (s) is where the maximum reliability index is obtained.

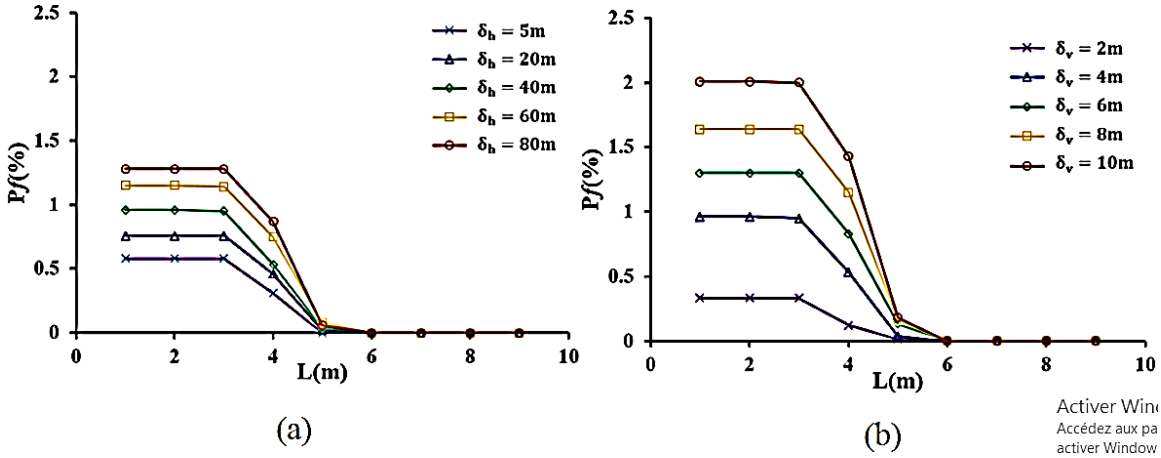

Figure 2.8: Variation of the probability of failure with: (a) horizontal correlation lengths, and (b) vertical correlation lengths.

However, Figure 2.9(b) shows that, the critical pile location when considering special variability depends on the basis that we are comparing to. Which means that the maximum mean value of the factor of safety doesn't necessary refer to the optimal location as the maximum reliability index is captured for a slightly different location. Therefore, the best location is at the interval of s=10-12m.

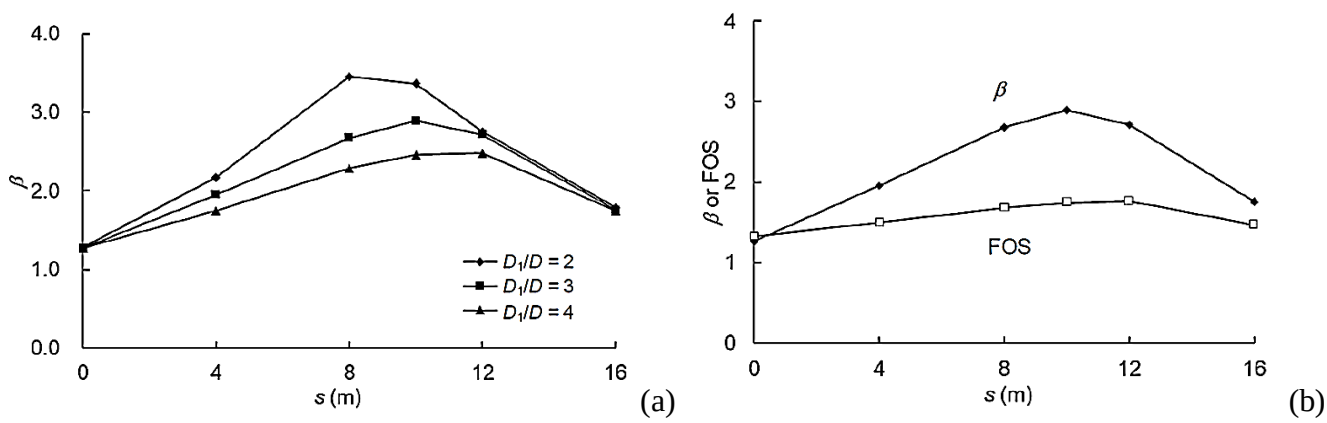

Figure 2.9: Variation of the reliability index with different pile locations: (a) effect of various spacings, and (b) comparison between the factor of safety and β with $D_1/D=3$.

2.6 Conclusion

This chapter aimed at representing various methods of analyzing pile-stabilized slopes. One of which, is the pressure based methods, focusing on the passive part of piles, exposed to horizontal soil pressure. The analysis is basically assuming that, the pile surrounding soil is undergoing a plastic equilibrium state.

This leads to the equations to be limited over very specific center-to-center spacings and few model piles; such as rigid beams with great lengths. The displacement based methods rely on the estimation of pile resistance by virtue of soil movements. The piles are modeled as elastoplastic beams and the soil as an elastic continuum, in order to estimate the lateral soil movement above the slip surface to use it in evaluating the active pile behavior. Nevertheless, analytical methods don't account for the effect of spacing on soil-pile interaction; therefore, it is well studied in 3D numerical methods. These methods have shown great estimations for pile group behavior and nonlinearity of pile rows. Technically, the numerical code OptumG2 gives the possibility of conducting deterministic and probabilistic computations, with respect to the possibility of modelling homogenous and spatial variable soil parameters. This is executed based on the combination of the random field theory with the finite element method. The generation of the random field is conducted by stochastic inputs in OptumG2; namely, probabilistic distribution, mean value, coefficient of variation and correlation lengths. Thusly, the results may be given in terms of reliability index or probability and cumulative distribution functions.

Chapter 3: Bearing capacity assessment of shallow foundations near slopes before and after reinforcement

3.1 Introduction

Inclined loading developed at slope surface may be captured in foundations with respect to two load components, vertical V and horizontal H. Generally, the inclination of the load lead to a reduction in soil bearing capacity, comparing to the slope under purely vertical load condition (Bransby & Randolph, 1998; Gourvenec, 2007; Houlsby & Puzrin, 1999; Taiebat & Carter, 2002; Ukritchon et al., 1998). This tendency amplifies under specific conditions related to the slope angle and height; as well as, the footing position relatively to the crest. To enhance the limit load of slopes susceptible to surface load excitations, the effectiveness of continues and discrete vertical retaining structures was widely reported (Ahmed, 2004; El Sawwaf, 2005; Esser & Dingeldein, 2007; Hon & Demcsak, 2010; Sharafi & Sojoudi, 2016; Sudani et al., 2015). This is due to their remarkable dynamic response, leading to the overall stability to raise with the raise in the lateral stabilizing forces.

For reasons of study simplifications, the assumption of homogeneous soil underneath the footing permits bounding the variation of the corresponding characteristics. This approach adopts representative values of the mechanical soil properties to account for deterministic methods. Recently, the subject of soils that are spatially random has received a great deal of attention in the foundation engineering as it reflects the natural soil status; consequently, the probabilistic analyses are required to study the slope response.

This chapter, firstly introduces deterministic and stochastic methods for the bearing capacity of shallow footings near unreinforced slopes, under both vertical and inclined loading conditions. Then a synthesis is made out of studies in the literature addressing anti-slide piles and sheet pile walls within slopes.

3.2 Evaluation of the bearing capacity of shallow footings near unreinforced slopes

3.2.1 Deterministic methods for the bearing capacity of shallow footings near unreinforced slopes under vertical and inclined loading condition

The sloping ground has a significant impact on the bearing capacity of vertical loaded strip footings. For this reason several theoretical and experimental investigations were conducted as summarized below:

Table 3.1: Theoretical and experimental methods conducted for the limit load of strip footings susceptible to purely vertical loading.

Author	Type of soil	Employed method	Slope angle
Meyerhof (1957)	Clayey and sandy	Limit equilibrium	30° and 40°
Hansen (1970)	Clayey and sandy	Limit equilibrium	30°,35°, 40° 45°
Giroud (1971)	Sandy	Small-scale tests	26°
Lebegue (1973)	sandy	Small-scale tests	40°,35°
Dembicki (1974)	Sandy	Small-scale tests	26°,31.3°,43°
Shields et al. (1977)	Sandy	Small-scale tests	37°,41°
Kusakabe et al. (1981)	Clayey and sandy	Limit equilibrium and Limit analysis	0°, 30°
Bauer et al. (1981)	Sandy	Full-scale tests	45°
Kimura et al. (1985)	Sandy	Centrifugal test	49°
Graham et al. (1988)	Sandy	Analytical method	30°,35°, 40°,45°
Shields and Garnier (1989)	Sandy	Centrifugal test	30,5°, 35,5°
Saran et al. (1989)	Clayey and sandy	Limit equilibrium and Limit analysis	10°,15°,20°; 25, 30°, 35° and 40°
Choudhury and Rao (2006)	Clayey and sandy	Limit equilibrium	30°, 40°
Mabrouki et al. (2010)	Sandy	Finite difference method	35°, 40°, 45°
Keskin and Laman (2013)	Sandy	Experimental and FEM	40.6°, 41.8°, 43.5°
Castelli and Motta (2010)	Sandy	Limit equilibrium	0° up to 40°

It is important to mention that the elastoplastic approach helps keeping up with the history of deformations and stresses; in contrast, the static and kinematic approaches of the limit analysis provide a precise evaluation of the bearing capacity, which minimizes the computation timing.

In practice, footings adjacent to slopes are accounted for by correction factors of load inclinations. In order to determine the exact bearing capacity, numerous methods have been employed; for instance, the centrifuged scale model by Marechal (1999), finite difference method by Baazouzi et al. (2016); as well as, the finite element limit analysis (upper bound) and the stress field methods conducted by Georgiadis (2010). However, the failure envelopes are defined by means of two types of loading space (Bransby & Randolph, 1998; Gourvenec, 2007; Houlsby & Puzrin, 1999; Taiebat & Carter, 2002; Ukritchon et al., 1998). The first type presents the absolute size of failure envelopes; it is defined in terms of bearing capacity factors in horizontal H/Bc_u and vertical V/Bc_u directions. The second type represents the shape of failure envelopes, as it plots the space of loading parameters normalized by their ultimate horizontal and vertical values respectively, H/H_u and V/V_u. Georgiadis (2010) studied the effect of footing undrained inclined loading on slope geometry and properties of the corresponding soil (Figure 3.1). The methods of stress field and upper bound, integrated in finite element analysis were employed.

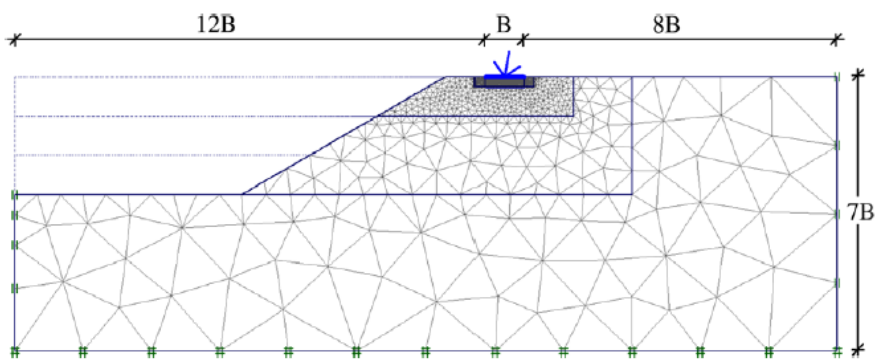

Figure 3.1: Problem definition (Georgiadis, 2010).

Two failure modes were predicted by Georgiadis (2010); a failure mechanism pertaining to the bearing capacity (Figure 3.2(a)) and a failure affecting the overall stability of the slope (Figure 3.2(b)). In addition, an empirical equation was derived for the load interaction diagram of the bearing capacity, for purely cohesive soil slope (eq. (3.1)) with considering different slope angles. Thus, the influence of the strip footing position relatively to the crest was considered in Figure 3.3. It is noted that the plotted curves using the upper bound method agree well with those obtained from the suggested equation.

$$v = \frac{1}{2} + \frac{cos^{-1}(\xi.h) + \sqrt{1-(\xi.h)^2} - \beta}{\pi + 2 - 2\beta},$$

$$\xi = 1 - \beta\left(1 - e^{-\lambda}\right). \qquad (3.1)$$

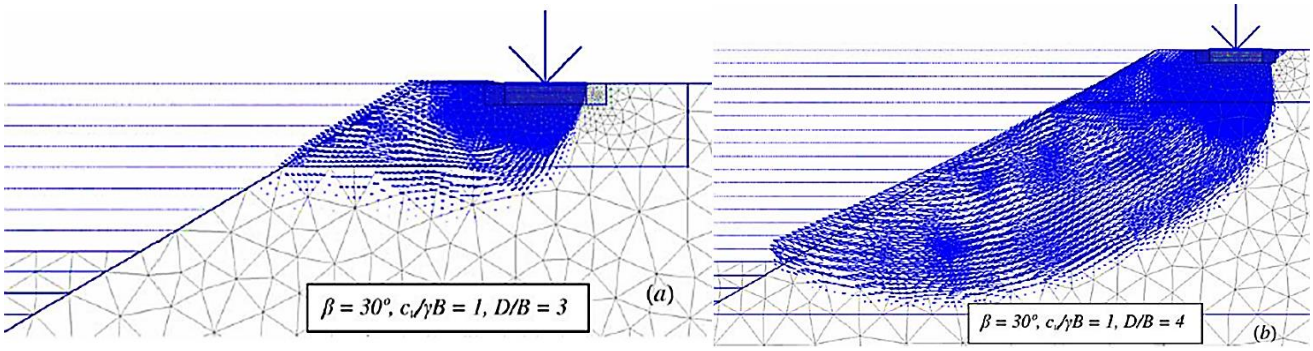

Figure 3.2: Types of failure mechanism assumed by Georgiadis (2010).

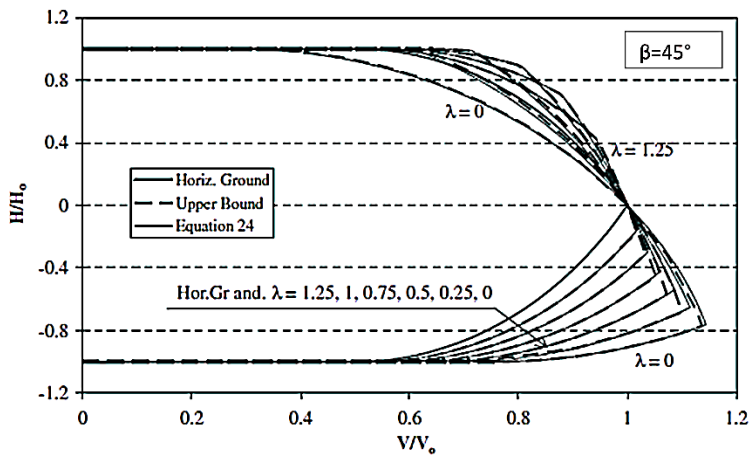

Figure 3.3: Comparison of the developed equation pertaining to the load interaction diagram with the upper bound solutions (Georgiadis, 2010).

3.2.2 Stochastic analyses for the determination of the bearing capacity of shallow footings

The new innovation in geotechnical engineering, relies on extending the concept of reliability for the analysis of slopes to the case of nearby footings. The bearing capacity and footing settlement have received a great attention in the literature. Basically, uncertain parameters were modelled as random procedure with conducting analyses on the effect of spatial variability. Table (3.2) recapitulate several studies conducted to analyze the bearing capacity of a shallow footing, situated on both horizontal and sloping grounds, with employing different probabilistic methods. In the majority of studies, the isotropic correlation length Θ (θ_h=θ_v) is considered with the normalization by the footing width B.

Table 3.2: Various probabilistic methods conducted for the bearing capacity of shallow foundations.

Author	Ground surface	Type of loading	Probabilistic method	Type of distribution	Spatial variable Shear strength characteristics
Griffiths et al (2002)	Cohesive horizontal	Vertical	RFEM and MC	Lognormal	COV_{cu}= 0.125-8 Θ_{cu}= 0.125-8
Srivastava and Babu (2009)	Cohesive horizontal	Vertical	MC	Normal	μ_{Nc}= 5.03 COV_{Nc}= 24%
Abdel Massih and Soubra (2010)	c-φ horizontal ground	Vertical	MC	Lognormal for c and beta for φ	μ_{cu}= 20kPa COV_{cu}= 10-40% μ_{ϕ}= 30° COV_{φ}= 5-15% Θ= 2
Zhalehjoo et al. (2012)	Cohesive horizontal	Vertical	RFDM and MC	Lognormal	μ_{cu}= 25-100 kPa COV_{cu}= 10-75%
Cassidy et al. (2013)	Cohesive horizontal	Inclined	RFEM	Lognormal	COV_{cu}= 10-50%
Huang et al. (2016)	Cohesive horizontal	Inclined	RFELA (limit analysis) and MC	Lognormal	μ_{cu}= 10 kPa COV_{cu}= 50% Θ= 0.125-4
Luo and Buthurst (2017)	Cohesive slope	Vertical	RFEM and MC	Lognormal	μ_{cu}= 20 kPa COV_{cu}= 10-50% Θ_{cu}= 0.125-8
Brahmi et al. (2018)	Cohesive slope	Inclined	MC	Lognormal	μ_{cu}= 20 kPa COV_{cu}= 10-50% Θ_{cu}= 0.125-8

Brahmi et al. (2018) investigated the effect of spatial variability on the mean bearing capacity corresponding to a strip footing, situated at a slope crest (Figure 3.4). The random finite element limit analysis RFELA integrated in OptumG2 software was conducted. The study accounted for the Monte Carlo simulation, with respect to the Karhunen-Loeve expansion. The load inclination effect on the mean

failure envelopes was calculated for Lognormally distributed undrained shear strength with a mean value of μ_{cu}= 20 kPa.

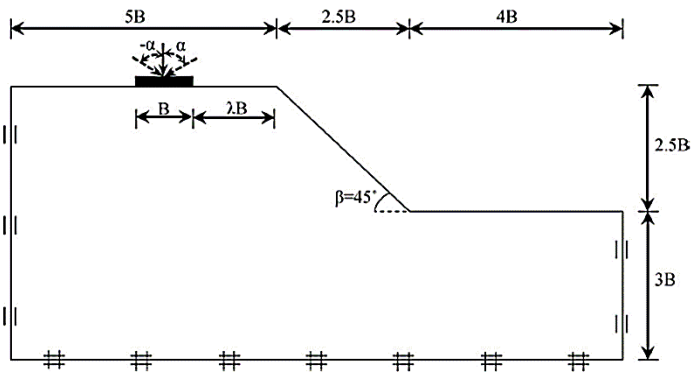

Figure 3.4: Definition of the problem (Brahmi et al., 2018).

Figures 3.5 and 3.6 represented the size and shape of failure envelopes in terms of coefficient of variation and normalized correlation lengths, respectively. It was found that, the failure envelopes plotted in terms of bearing capacity factors H/B_{cu}-V/B_{cu} describing the size (Figure 3.5(a)) are following a decreasing trend with the increase of the COV from 10% to 50%. However, the shape of spatial variable failure envelopes is much more conservative than the deterministic one (Figure 3.5(b)).

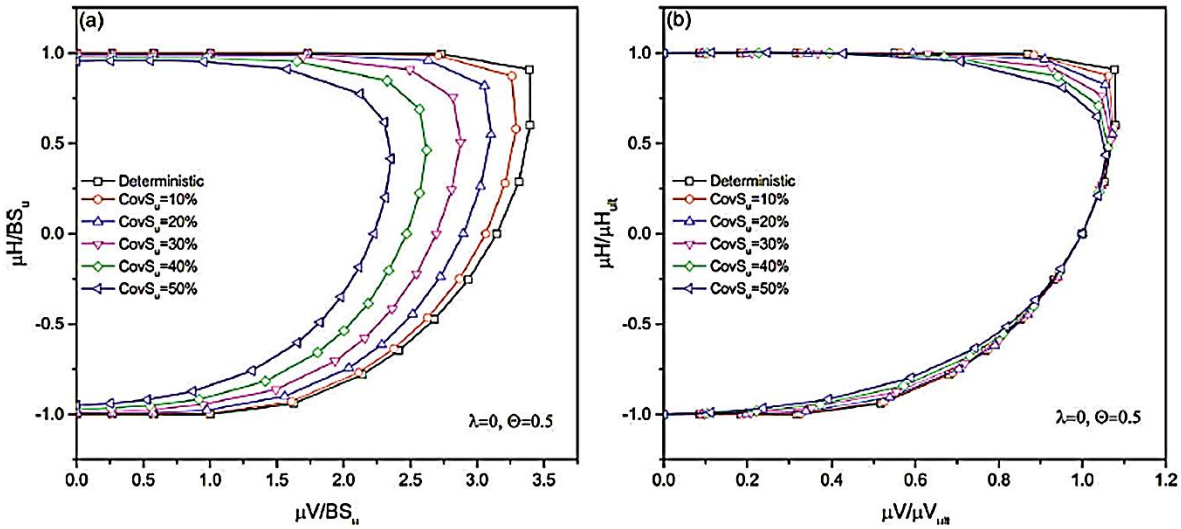

Figure 3.5: The variation of COV with: (a) surfaces of normalized failure loads, and (b) curves of load interaction.

Furthermore, Figure 3.6(a) showed that the size of failure envelopes is enhanced significantly with the increase of the isotropic correlation length; the resulting failure envelopes lie all in the same shape (Figure 3.6(b)).

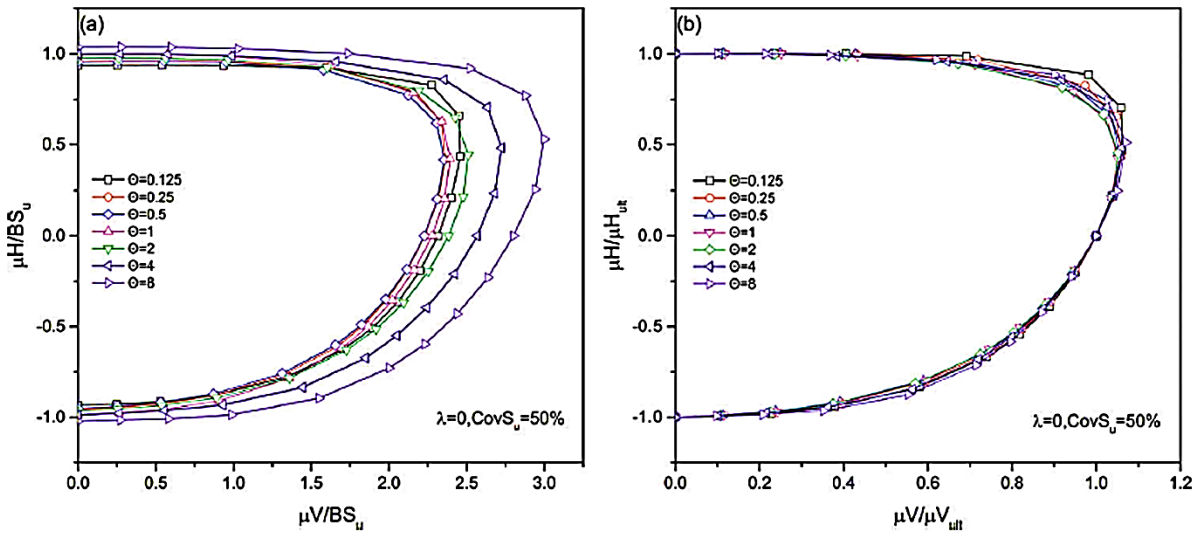

Figure 3.6: The variation of Θ with: (a) surfaces of normalized failure loads, and (b) curves of load interaction.

3.3 Bearing capacity of shallow footings near stabilized slopes

3.3.1 Deterministic analyses for stabilized slopes under purely vertical surface loads

Recently, the effect of pile response used to stabilize slopes on the soil bearing capacity under purely vertical surface load was widely investigated, with respect to a model of serialized centrifuge tests applied to estimate the lateral pile behaviour (Wang & Zhang, 2014). It was indicated that, the pile strength properties and optimal position near the top of slope are the key factors of a positive soil limit load response. The failure mechanism is captured by the displacement localization of the soil around the load surface. Nevertheless, researchers addressed the estimation of quantitative and qualitative correlations pertaining to the bearing capacity and the position of both footing and piles within the slope. Several methods were used; for instance, finite element method (Munawir et al., 2013; Raee et al., 2019), limit equilibrium method (Haghbin & Ghazavi, 2013), finite difference analysis (Sharafi & Sojoudi, 2016) and upper bound limit analysis (Jin et al., 2020). All of these analyses agreed on the fact that, the improvement in bearing capacity is attributed to the increase in the reinforcement rigidity and decrease in the centre-to-centre spacing. This is due to the effect of soil arching between reinforcement columns and the enhancement in the footing response corresponding to the load-settlement relation.

Sharafi and Sojoudi (2016) adopted a small-scale physical modelling technique and numerical finite difference analysis, to account for a loose sandy slope under surface loading (Figure 3.7(a)) with the presence of an interlayer of soft soil bound (Figure 3.7(b)).

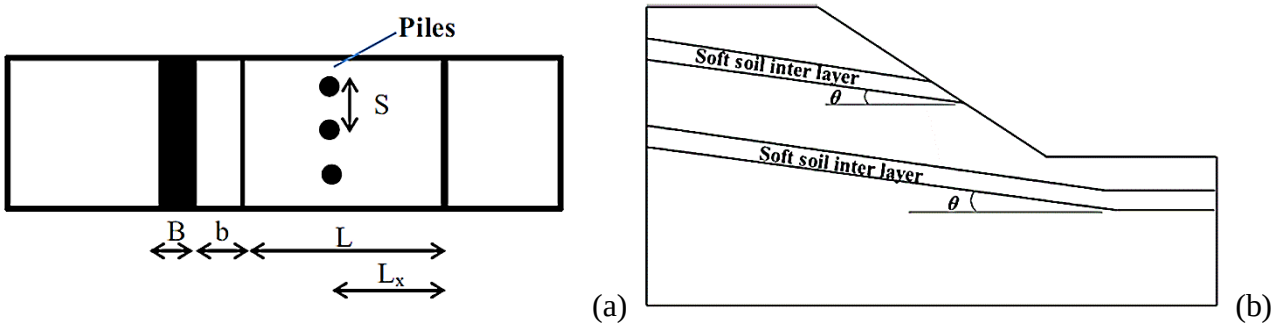

Figure 3.7: Definition of the problem (Sharafi & Sojoudi, 2016).

It is important to mention that the raise in the distance between piles may develop higher failure volume of the slope and lower soil-arching. It was deduced from Figure 3.8 that the slope factor of safety before reinforcement decreases with the increase of the soil interlayer; hence, an opposite tendency was captured for the reinforced slope. Figure 3.9 showed that the optimal pile location is where the improvement in bearing capacity is maximum referring to the case of piles driven closer to the slope crest.

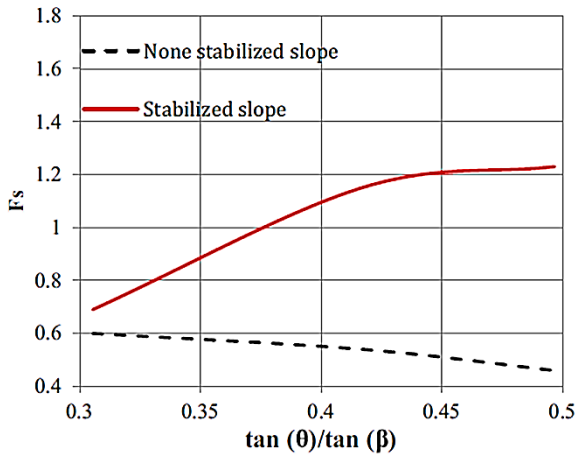

Figure 3.8: Effect of soil interlayer on Fs (Sharafi & Sojoudi, 2016).

Nevertheless, slopes under surface vertical loading cause an increase in lateral displacements and decrease in the confining pressure of soils. Therefore, the sheet pile walls have shown an excellent performance to improve the situation (Ahmed, 2004; Esser & Dingeldein, 2007; Hon & Demcsak, 2010; Sudani et al., 2015). El Sawwaf (2005) investigated the efficiency of adopting a pile row or a sheet pile wall in enhancing the bearing capacity of a strip footing near a sandy slope. Figure 3.10 shows that the strip footing and both retaining structures are placed at the crest of the slope (b/B=0 and d/B=0, respectively). It was noted that the best enhancement of bearing capacity is attributed to the sheet pile

wall; hence, it is noticeable for heights h/B of relatively larger values. This happens due to the increase in the sheet pile resistance with the increase in the embedded height in the stable soil.

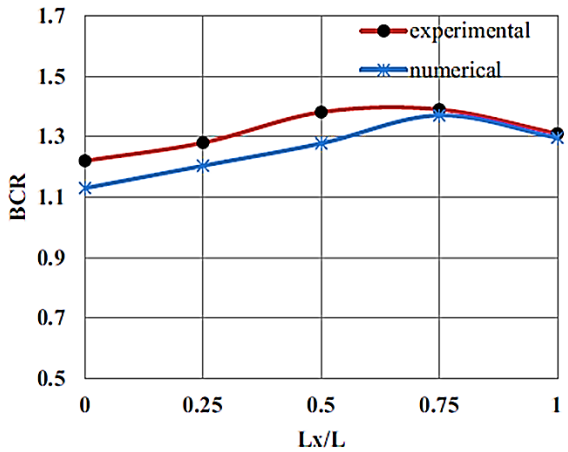

Figure 3.9: Effect of pile location on the bearing capacity improvement (Sharafi & Sojoudi, 2016).

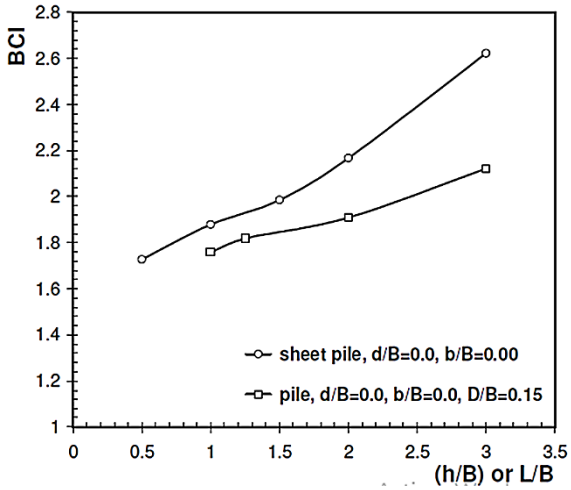

Figure 3.10: Comparison of the best performance between sheet pile walls and pile rows (El Sawwaf, 2005).

3.4 Conclusion

This chapter furnishes a representation of experimental, analytical and numerical methods conducted for the deterministic evaluation of the bearing capacity near slopes. In particular, the effect of inclined loading condition was addressed with respect to several mechanical and geometrical parameters. Furthermore, the failure envelopes are computed to account for the absolute size, which is defined in terms of horizontal and vertical bearing capacity factors in the load space. Thus, the shape of failure envelopes is plotted by loading space parameters, normalized by their ultimates horizontally and vertically.

The traditional deterministic methods assume that the soil properties are the same alongside the field, with providing determined values of soil parameters. Therefore, probabilistic analyses are addressed to give an accurate estimation for the load inclination effect on the generated failure envelopes, with respect to normal and Lognormal distributions of soil shear parameters. According to the published results, the deterministic methods overestimate the limit load. The mean value of this latter, has shown a decreasing trend with the raise in COV_{cu}, whenever Θ is as high as the footing width. The interaction curves showed that, probabilistic curves all fall inside the deterministic one. This is explained by the reduction of the limit load caused by the heterogeneity of the soil.

It is worthwhile noting that, the subject of investigating the response of anti-slide piles to an adjacent foundation, has been widely investigated in the literature. However, the studies addressed only one condition, where the footing load is purely vertical, which gives the opportunity to this thesis to make a step forward in the scientific research and address the case of inclined loading in chapter five.

Chapter 4: Strength reduction analysis on the safety factor of a slope reinforced with one row of piles

4.1 Introduction

Reinforcing slopes with piles to extensively improve the stability has become an innovational technique in geotechnical engineering. In the last few decades, several pressure or displacement based methods have been used to analyze the response of piles, undergoing lateral soil deformations (Ashour & Ardalan, 2012; Ito & Matsui, 1975; Nimityongskul et al., 2018). It should be mentioned that the limit equilibrium based methods don't account for the soil-pile interaction (Laora et al., 2017; Hassiotis et al., 1997; Ito et al., 1981; Poulos, 1995; Yamin & Liang, 2009). Therefore to serve this purpose, numerical computations were highly recommended. The behavior of soil-pile system was studied with considering the effect of 3D sets of pile-soil forces using the FE analysis (Jeong et al., 2003; Kim & Jeong, 2011; Taheri et al., 2015). The kinematic approach of limit analysis has shown that, the optimal location of piles within the slope is where the stabilizing force has a minimum value (Ausilio et al., 2001; Nian et al., 2008; Qin et al., 2017). Nevertheless, the shear strength reduction method SSR has shown accurate solutions for analyzing slopes without reinforcement (Cheng et al., 2007; Griffiths & Lane, 1999; Wei & Cheng, 2009). Thusly, it was extended to study the pile-stabilized slopes by many researchers. Won et al. (2005), as well as Cai and Ugai (2000) used 3D finite difference (SSRFD) and finite element (SSRFE) methods, to locate the slip surface by the maximum shear force developed in piles. Hence, Wei and Cheng (2009) and Yang et al. (2011) used the SSRFD method in 3D to locate the slip surface by the maximum shear strain rate and the maximum pressure on piles, respectively. It was deduced that the method of locating

the slip surface influences significantly the resulting factor of safety of identical slopes analyzed with identical methods.

In this chapter, we investigate the factor of safety of a c-φ slope reinforced with one row of piles using the SSRFE method through OptumG2 code. The utilized method is based on extending the method of analyzing piles suggested by Sluis et al. (2014) to investigate the stability of the slope under various pile center-to-center spacings. It is worthwhile noting that the present study is subject of an oral presentation in an international conference (Bougouffa et al., 2019).

4.2 Principle of Sluis integrated in OptumG2 software

The modeling of piles as plates or node-to-node anchors in plane strain analyses, leads to unavoidable gaps in the soil-pile interaction behavior, as it is supposed to be a 3D problem. The classical 3D methodology relies on, accounting for plate elements according to the equivalent pile row properties per unit width. In which, the interface elements are meant to represent the soil-pile interaction with separating the soil mesh from that of the piles. This leads to small interaction in all sides of the pile, resulting in a limited range of spacings S in terms of the pile diameter Ø (S/Ø < 2 to 3). Moreover, the use of node-to-node anchors assures continues mesh of soil without any soil-pile interaction. This is shown by the independent flow of the soil; in which, it doesn't reflect the real behavior.

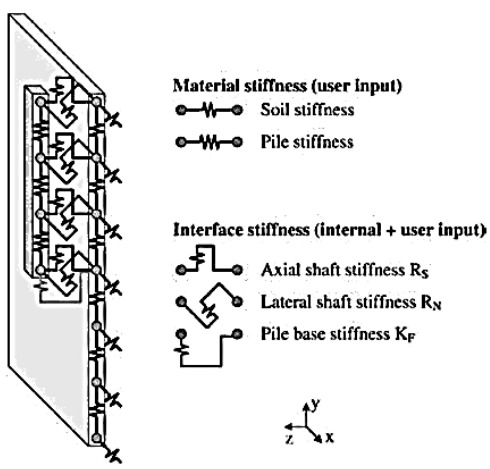

Figure 4.1: The 2D interaction between soil and piles in a row (Sluis et al., 2014).

Sluis et al. (2014) came out with a solution to permit the estimation of the slope stability in 2D with considering unlimited pile spacings. This technique joined both methods to model the piles, with eliminating the drawback to the maximum. The pile properties are taking after the plate element, and a

continuous mesh is inspired from node-to-node connectors. Two different layers are considered for the soil and beam representing the piles. By which the mesh of the beam element is superimposed on the 2D mesh corresponding to the soil. The soil-pile interaction is represented by the connection of the beam with the soil nodes, as shown in Figure 4.1. Therefore, the mesh is duplicated in all the edges and nodes of the pile element along the geometry line pertaining to the soil, representing the elements of interface. Moreover, the loads are transmitted from the pile to the soil through the generation of an elastic semicircle at the pile base of a width $D_{eq}/2$ in order to represent all possible elastic stress points.

4.2.1 The pile row properties by virtue of the out of plane direction

The actual pile properties are expanded into the out of plane spacing, as represented bellow:

$$\hat{E} = EA/D_{eq}S\ [KN/m/m^1],$$
$$D_{eq} = \sqrt{12I/A}\ [m], \tag{4.1}$$

$$\hat{\gamma} = \frac{\gamma A}{S}\ [KN/m/m^1], \tag{4.2}$$

where, E, A, D_{eq}, I, γ are respectively the young's modulus, area of pile, semicircle with a radius of half the equivalent pile width, moment of inertia and unit weight.

4.2.2 The properties pertaining to the soil-pile interface

The interface elements are represented by axial A, lateral L and base B springs, with a finite strength to represent the bearing capacity of piles. Thusly, they are characterized by stiffness K properties as follows:

$$K_A = IFS_A \frac{G_{soil}}{S},$$
$$K_L = IFS_L \frac{G_{soil}}{S}, \tag{4.3}$$
$$K_B = IFS_B \frac{G_{soil}}{S}\frac{D_{eq}}{2},$$

where G_{soil} and IFS_x are respectively the soil shear modulus and corresponding interaction factors that are defined as follows:

$$IFS_A = 2.5\left(\frac{S}{D_{eq}}\right)^{-0.75},$$

$$IFS_L = 2.5\left(\frac{S}{D_{eq}}\right)^{-0.75}, \qquad (4.4)$$

$$IFS_B = 25\left(\frac{S}{D_{eq}}\right)^{-0.75},$$

4.3 Study on the factor of safety pertaining to a pile- stabilized slope

4.3.1 Presentation of the studied problem

In order to avoid the occurrence of a landslide, a factor of strength reduction F_s needs to be evaluated. Following, the shear strength reduction method, the Mohr-Coulomb parameters are reduced; i.e. cohesion c and friction angle φ, as shown in eq. (4.5).

$$F_s = \frac{c}{c_{red}} = \frac{\varphi}{\tan \varphi_{red}}, \qquad (4.5)$$

where c_{red} and φ_{red} are the reduced shear strength parameters. Figure 4.2 visualizes the problem geometry; in which, the slope gradient is of 1 vertical:1.5 horizontal and height of 10 m. Two symmetric boundaries are used to represent a row of three adjacent piles at the middle of the slope L_x= 7.5m. A boundary condition of full fixity at the base and tangential fixity at the sides is adopted. Table (4.1) represents the parameters pertaining to the soil, pile, and interface.

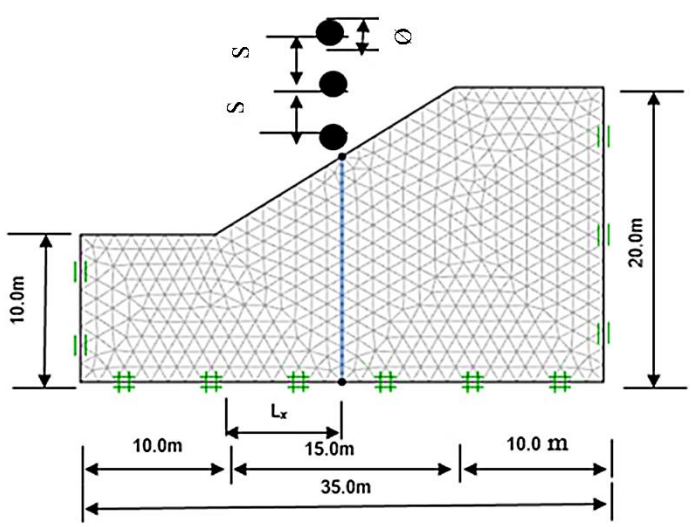

Figure 4.2: The problem geometry associated with FE mesh.

Table 4.1: Material properties.

Material	Elastic modulus E (MPa)	Poisson's ratio ν	Cohesion c (kPa)	Friction angle φ (°)	Unit weight γ (KN/m^3)	Dilation angle ψ (°)
Soil	200	0.25	10	20	20	0
Interface	200	0.25	10	20	-	0
Pile	60000	0.2	-	-	-	-

4.4 Numerical procedures

The 2D finite element software OptumG2 is adopted to reach the average value of F_s corresponding to upper and lower bounds of SSR method. The piles are modeled as linear elastic steel tube with an outer diameter Ø of 0.8m and a center-to-center spacing of S/Ø=2 to 6. Various pile head conditions are taking into account; namely, fixed (neither rotation nor displacements are permitted), hinged (permissible rotation without displacements), free (permissible rotations and displacements) and non-rotated (permissible horizontal displacement without the vertical nor the rotation). Hence, the soil is considered to be elastic perfectly plastic, following the failure criterion of Mohr-Coulomb. A mesh adaptivity of 2000 lower and upper triangular elements is adopted, with three adaptive shear dissipation control.

4.5 Results and discussion

4.5.1 Comparison of the factor of safety

Figure 4.3 shows that, the lower the pile spacing is, the higher the slope steadiness will be. This is explained by the tendency of the reinforcing system to behave similarly as a continuous barrier.

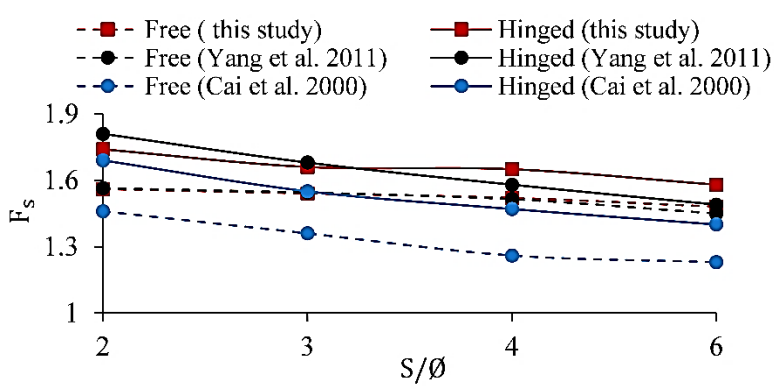

Figure 4.3: Comparison of F_s for various pile head conditions (E_p= 60 GPa).

For both of the free and hinged head piles, F_s increases with the decrease of pile spacing. It should be mentioned that the regularity of the maximum shear force developed by piles for the free head pile differs from the hinged one. Consequently, the best stability is attributed to the hinged head pile by dint of the increase in the corresponding lateral bearing capacity. For both pile head conditions, F_s obtained from Yang et al. (2011) agrees well with the present study, regardless of the underestimation of Cai and Ugai (2000).

4.5.2 Effect of pile rigidity for various head conditions

It is noted from Figure 4.4 that the pressure undergoing on piles is more pronounced for the fixed and hinged head conditions independently of the bending stiffness.

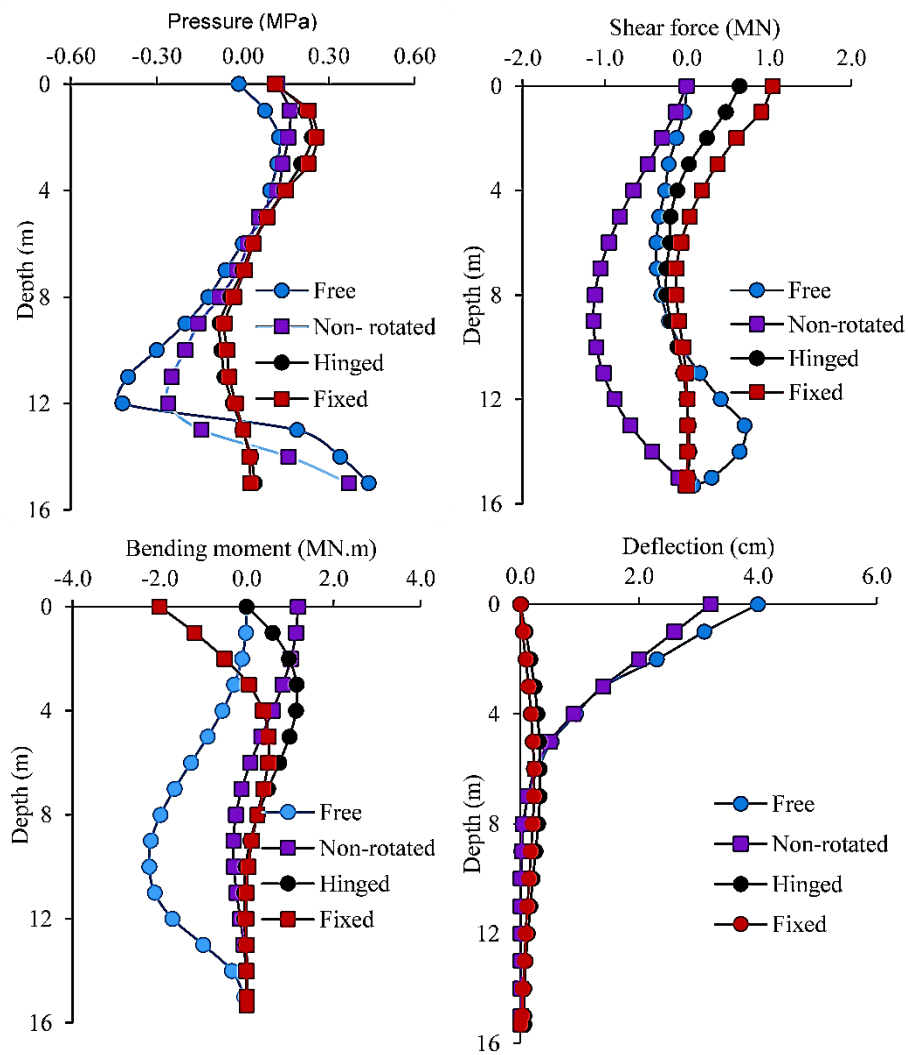

(a) E= 60 GPa

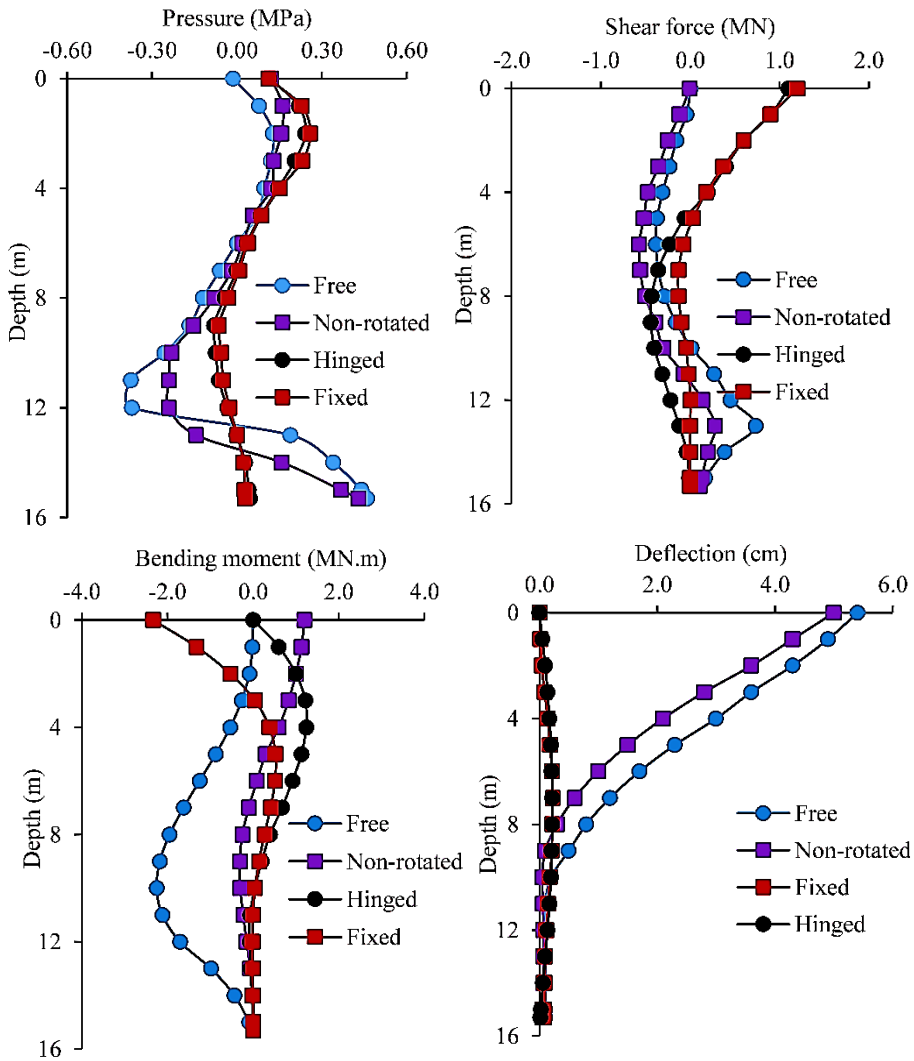

(b) E= 200 GPa

Figure 4.4: Pile behaviour for different pile head conditions and bending stiffnesses (S/Ø=3).

Thus, the negative pressure (directed away from the sloping ground) is reduced to give possibility for the piles to generate the sought reaction force and transmit the lateral mobilized forces from the unstable to the stable layer. Nevertheless, both Free and non-rotated head piles show negative pressure over certain depths (exceeding 5m). This is explained by the fact that, the unconstrained pile movement exceeds the surrounding soil movement, generating an extra thrust to the soil. This phenomenon leads to a noteworthy drop in the stability of the overall system due to the mobilized shear strength of the soil-pile interface. The bending moment is smallest in the hinged head pile; followed in order by those pertaining to the fixed, non-rotated and free conditions.

This note gives the advantage to adopt restrained head conditions rather than the free head piles, because piles are more likely to yield by their bending moment than by their shear force. The increase in the bending stiffness leads to smaller shear forces; therefore, it is important to adopt rigid unrestrained head piles rather than flexible ones in case of the inability to obtain restrained flexible head piles. The deflection is more important in the free head piles followed by the non-rotated case for both bending stiffnesses. However, flexible piles tend to have smaller deflection, which enlightens the necessity of increasing the pile length with the increase in the corresponding stiffness.

4.5.3 Effect of pile spacing for various head conditions

Figure 4.5 shows the behavior of a row of flexible piles (E_p=60 GPa) for various pile spacings and head conditions. It is worthy to mention that, intense pressure on piles leads to the generation of higher resisting forces to failure induced by piles.

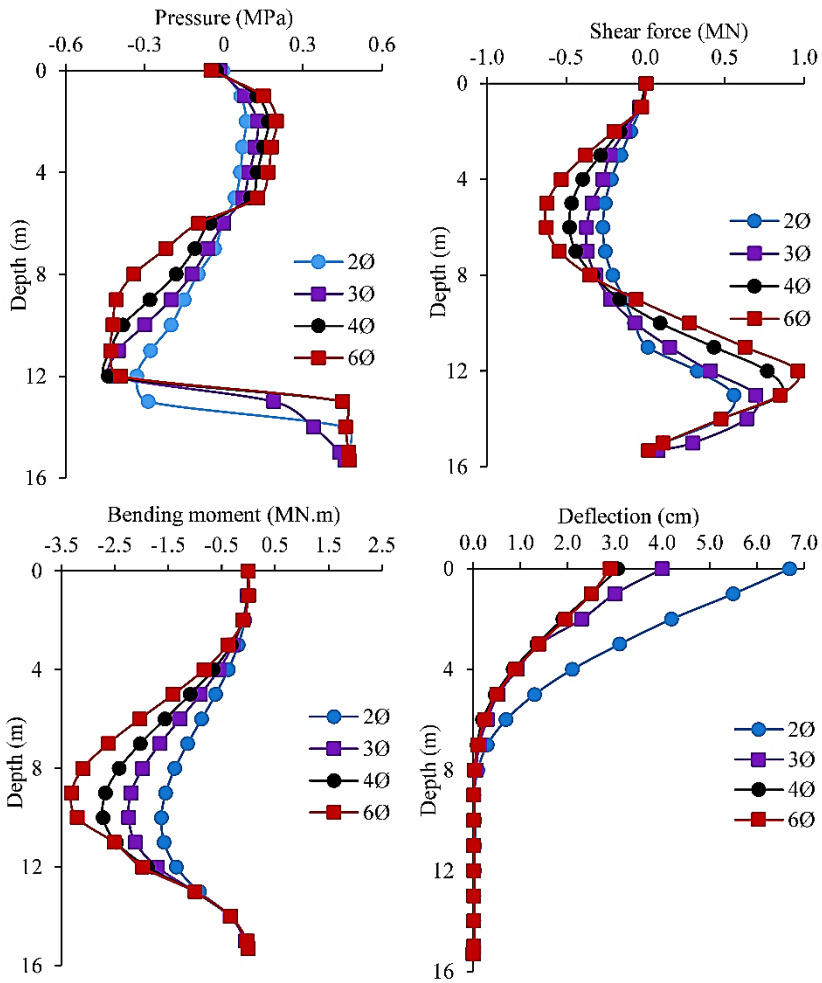

(a) Free

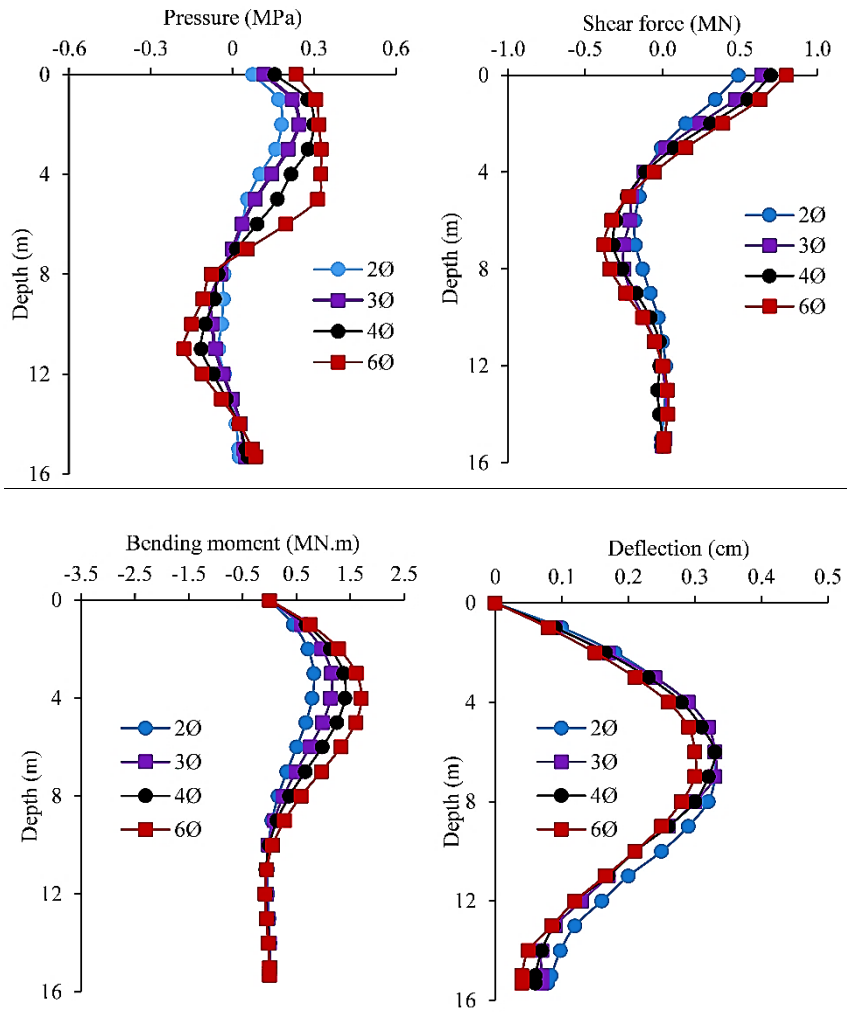

(b) Hinged

Figure 4.5: Pile behaviour for various head conditions and centre-to-centre spacings.

Moreover, the negative pressure reflects the incapability of piles to supply the sought reaction forces to stop the sliding. This tendency increases with the increase in S/Ø. For free head piles, the maximum shear force is attaint at deeper depths corresponding to relatively smaller spacings and the vice versa. In contrast, hinged head piles reach the maximum shear force at the same depth independently of their corresponding spacing. Consequently, free head piles supply maximum bending moments, reached at quite deeper depths comparing with those corresponding to maximum shear forces. Hence, the hinged head piles furnish maximum bending moment at shallower depths. It is noted that, at collapse the pile deflection is more pronounced for relatively smaller spacings (S/Ø=2 to 3). This is due to the act of piles

as a barrier that continues to lean; however, the limit state is not reached before the occurrence of the full deformation and deflection. Moreover, hinged head piles act similarly as rigid piles, due to the generation of insignificant lateral deflections.

4.6 Conclusion

This chapter introduced a method of calculating the stability of a c-φ slope reinforced with one row of piles, based on an earlier study conducted by Sluis et al. (2014). The soil-pile interaction is an important data that should be accounted for; to serve this purpose OptumG2 software is used herein. The pile center-to-center spacing effect on the resulting factor of safety was investigated and compared with those available in the literature.

The study focused on studying the behavior of piles in a row under several conditions; namely, pile head conditions, bending stiffness and pile spacings. The piles in a row tend to act similarly as a continuous wall for relatively small spacings leading to F_s to increase. It should be mentioned that, restrained head conditions are recommended due to the corresponding small bending moments, as the piles tend to yield by their bending moment rather than their shear force. However, the adoption of rigid unrestrained head piles rather than flexible ones is a good choice, by dint of the decrease in shear forces with the increase in pile stiffness. Spacings in the range of $2 \leq S/Ø \leq 3$, provide higher deflection due to the stages the limit state takes to reach the full deformation.

Chapter 5: Probabilistic analysis on pile-stabilized slope under purely vertical loading

5.1 Introduction

The subject of enhancing the bearing capacity and the slope stability, may be applicable with the construction of pile rows. This is due to their role in limiting horizontal deformations underneath the footing and redirecting the failure surface away from the slope (Munawir et al., 2013; Haghbin & Ghazavi, 2013; Sharafi & Sojoudi, 2016; Wang & Cao, 2013). The limit analysis used for this purpose has shown a very sufficient degree of accuracy. Several scholars studied the admissible diameter and spacing between piles (Li et al., 2012; Nian et al., 2008; Rao et al., 2017; Xiao et al., 2016). It was found that the pile location is governed by the choice of the corresponding diameter, and the maximum spacing is related to the minimum interaction between piles. It should be mentioned that the natural soil heterogeneity (inherent variability) is the main source of uncertainty pertaining to soil properties that generates randomly. This definitely requires further probabilistic analyses in order to take into account the theory of random fields in the soil variation. The bearing capacity of a strip footing has been widely addressed in the literature (Ali et al., 2016; Cassidy et al., 2013; Griffiths et al., 2002). The effect of vertical loading on a strip footing situated at the slope crest, has been investigated by (Luo & Bathurst, 2017), using the RFEM. It was concluded that the bearing capacity may be quite affected by the correlation length and coefficient of variation pertaining to the undrained cohesion.

This study investigates a practical range of coefficients of variatioan COV and isotropic correlation lengths Θ pertaining to the soil shear strength. The limit analysis is employed for this purpose, through the finite element code OptumG2 (Krabbenhoft, 2017).

5.2 Definition of the numerical problem

The study considers a cohesive slope (c_u=20 kPa, γ=20 KN/m^3) with an adjacent rough strip footing of B= 1m, situated at the crest (Figure 5.1). Random distribution of the shear strength is applied, in order to reach an accurate solution in terms of probability distributions rather than a unique value of bearing capacity. The undrained shear strength is accounted for as a random field with a lognormal distribution. The stochastic parameters that define the domain are, the mean value μ_{cu}, standard deviation σ_{cu}, coefficient of variation COV_{cu} (describes the dispersion of cohesion around the mean), and the isotropic correlation length $\Theta=\delta_h/B=\delta_v/B$ (refers respectively to the horizontal and vertical distances between two points where the soil properties are strongly related, normalized by the footing width).

This study makes use of Monte Carlo simulations implemented in OptumG2; thusly, the method of Krahunen-Loeve is used to resolve the exponential correlation function (Zhang & Lu, 2004).

At each random field, the limit load is calculated as follows:

$$q_{ui} = \mu_{cu} N_{ci}, \qquad i = 1,2, \dots 1000. \tag{5.1}$$

The limit analysis is adopted using the finite element code OptumG2 (Krabbenhoft, 2017). An associated flow rule is simulated for a Tresca perfectly plastic soil material. Herein, the average undrained bearing capacity is given with respect to theories of plasticity limit integrated in the corresponding upper and lower bounds. Accurate computations are assured for an initial mesh adaptivity of 1000 elements up to a final mesh of 2000 elements. Three adaptive iterations are conducted for the shear dissipation control.

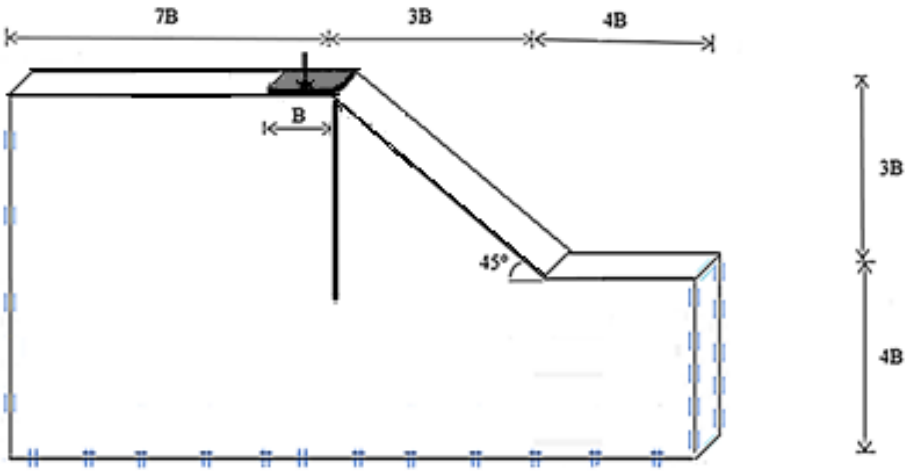

Figure 5.1: Model slope and reinforcing system.

5.3 Comparison of various correlation lengths

Figure 5.2 furnishes a comparison between the plots obtained from the present study and those of Luo and Bathurst (2017).

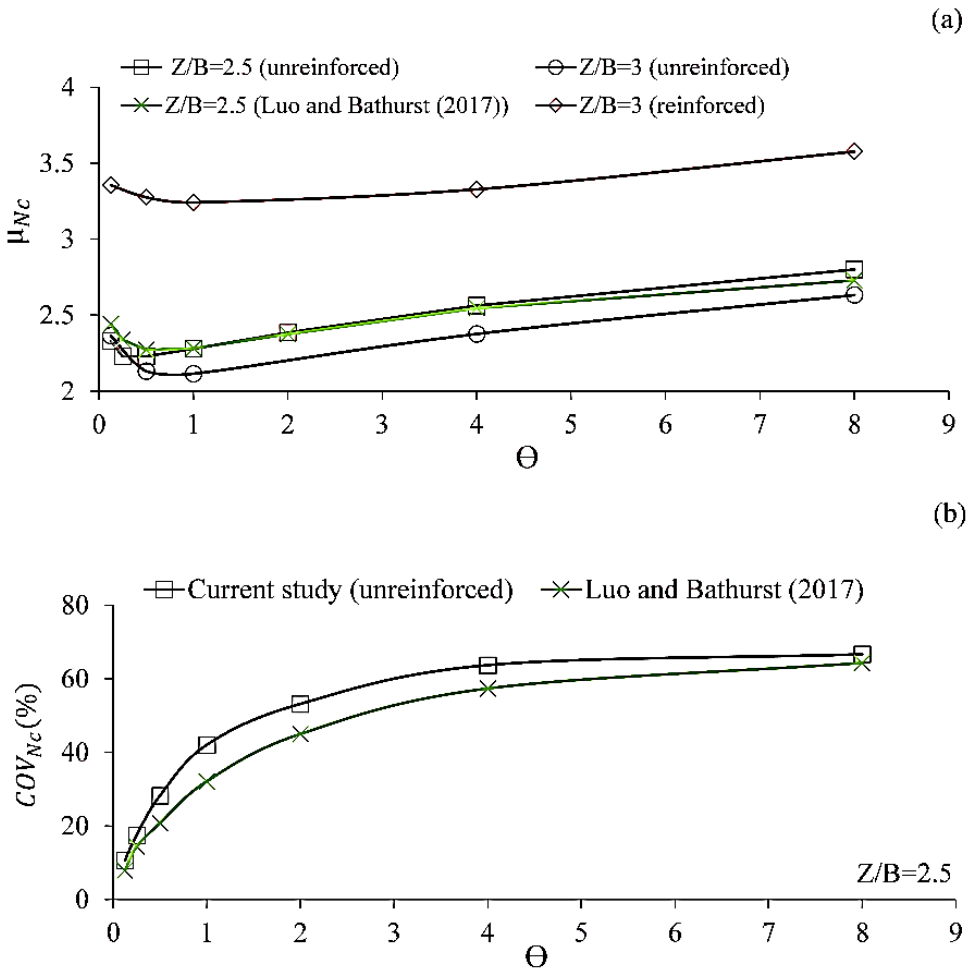

Figure 5.2: Comparison of various correlation lengths, for COV_{cu}=50%: (a) μ_{Nc}, and (b) COV_{Nc}.

The curves are dressed for d/B=0, λ=0 and Z/B=2.5 and 3. A good agreement with the literature is noted for the unreinforced case pertaining to Z/B=2.5. However for Z/B=3 (Figure 5.2(a)), an underestimation of μ_{Nc} is captured; this is due to the raise in the slope instability that follows the increase in its height. Therefore, piles tend to significantly enhance the mean value of the bearing capacity, around 42.19% for Θ=0.125, and 36.12% for Θ=8.

5.4 Stochasttic computations

It is seen from Figure 5.3(a) that μ_{Nc} decreases in value with the increase in Θ, until reaching a critical value of Θ=1 that corresponds to a maximum reduction of μ_{Nc}=2.11 (unreinforced slope) and 3.24 (reinforced slope). Beyond this unfavourable value of Θ, an opposite tendency takes place. Figure

5.3(b) shows that, the spatial correlation length has a great influence on the resulting COV_{Nc}; as this latter, tends to raise with the raise of Θ. It is worthwhile to mention that for higher values of Θ, the coefficient of variation tend to provide constant values.

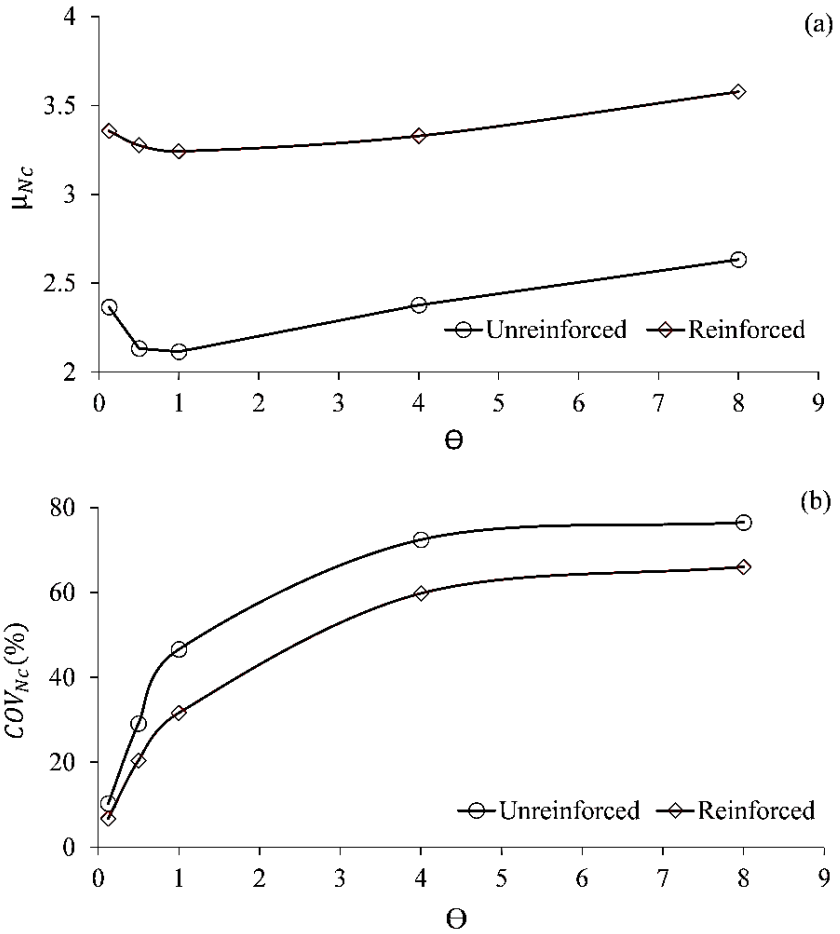

Figure 5.3: Effect of Θ on: (a) μ_{Nc}, and (b) COV_{Nc}.

The influence of $COVc_u$ is captured for Θ=1 (Figure 5.4). It is shown from Figure 5.4(a) that, the increase in COV_{cu} tends to decrease μ_{Nc}. However, the alterations in the reinforced slope are more pronounced, as for COV_{cu}=10% the mean bearing capacity factor is 33.12% higher than that of the unreinforced case, and 53.55% for COV_{cu}=50%. Furthermore, the effect of COV_{cu} on COV_{Nc} (Figure 5.4(b)) becomes more pronounced for larger values. In contrast, both slope cases tend to give identical COV_{Nc} for COV_{cu}= 10%.

The distributions of the complementary cumulative probabilities pertaining to the random bearing capacity $N_{c,rand}$ are dressed for various ranges of COV_{cu} and Θ, as shown in Figure 5.5. The random factors of bearing capacity are calculated using the upper and lower bounds. It is seen that, the unreinforced case provides significantly lower probabilities and conservative random variables X.

This is explained by the noticeable tendency of the reinforced slope to give higher factors $N_{c,random}$. Furthermore, All plots end up to give mean bearing capacity factors that are quite lower than the deterministic results ($N_{c,det}$=4.15 (reinforced), and $N_{c,det}$=3.15 (unreinforced)). Lower values of COV_{cu} tend to approach the deterministic N_c, and the vice versa.

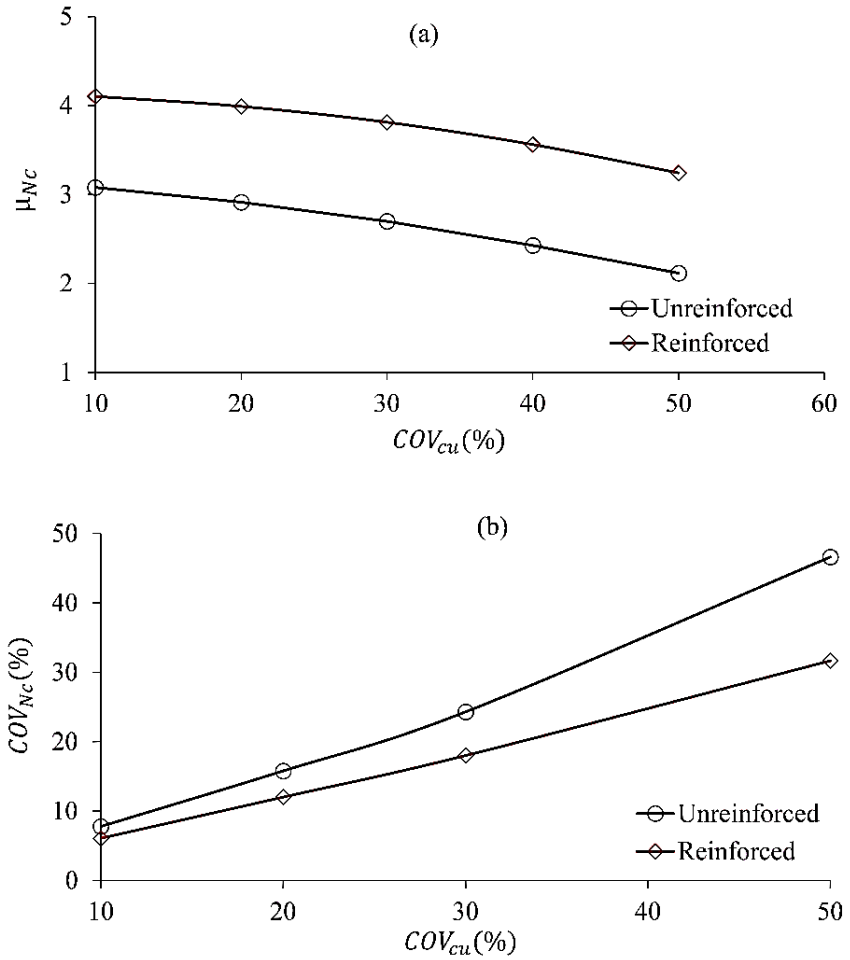

Figure 5.4: Effect of COV_{cu} on: (a) μ_{Nc}, and (b) COV_{Nc}.

It is of interest to mention that, before the crossover happens, the increase in spatial variability lowers the corresponding probabilities, and the opposite is observed beyond this point. This critical reference where all the curves meet refers to the weakest path (zones) within the slope could be obtained from the RFEM. These zones depict the potential failure mechanism as they inevitably pass through lower elements in the distribution of strength values. It is of interest to mention that the shear strength distributions spread out in Figure 5.6 indicates the weak and strong regions, respectively corresponding to the dark blue and shiny colors. Small correlation lengths (i.e. Θ=1) imply a high degree of variability in the soil shear strength; whereas bigger lengths imply more uniformity.

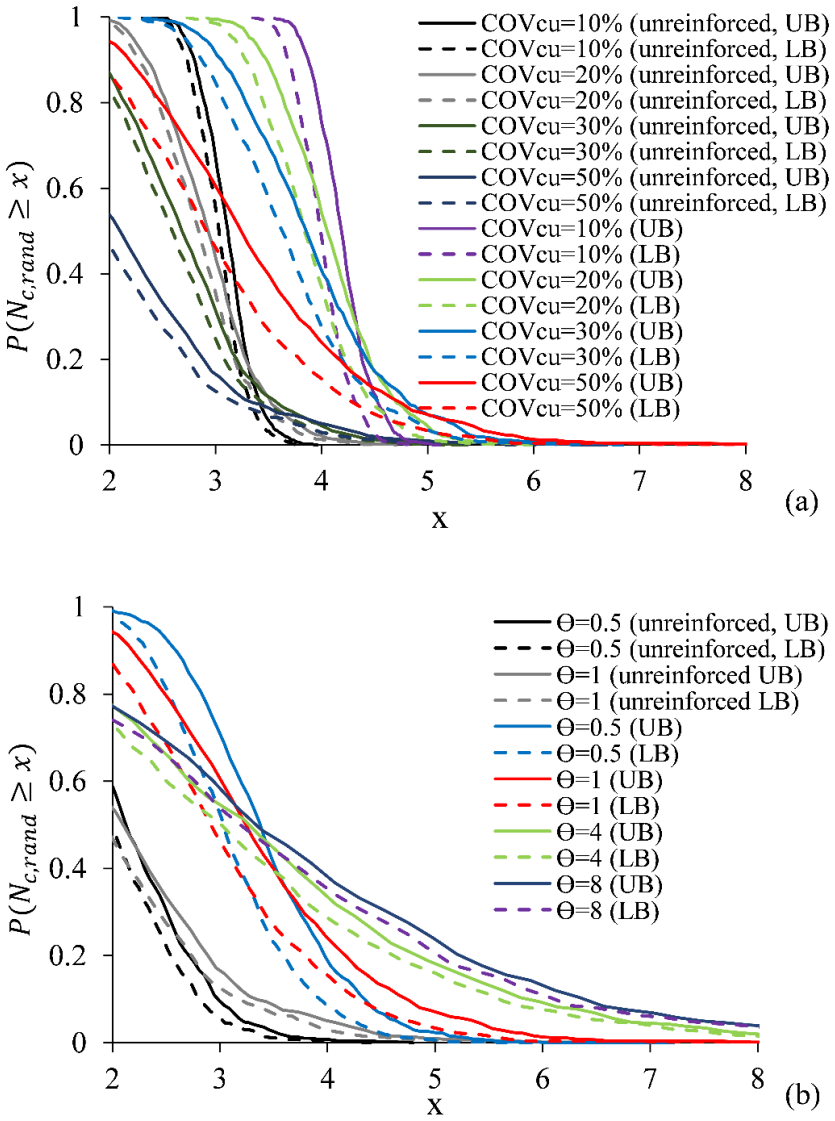

Figure 5.5: Distributions of the complementary cumulative probabilities pertaining to the random bearing capacity $N_{c,rand}$.

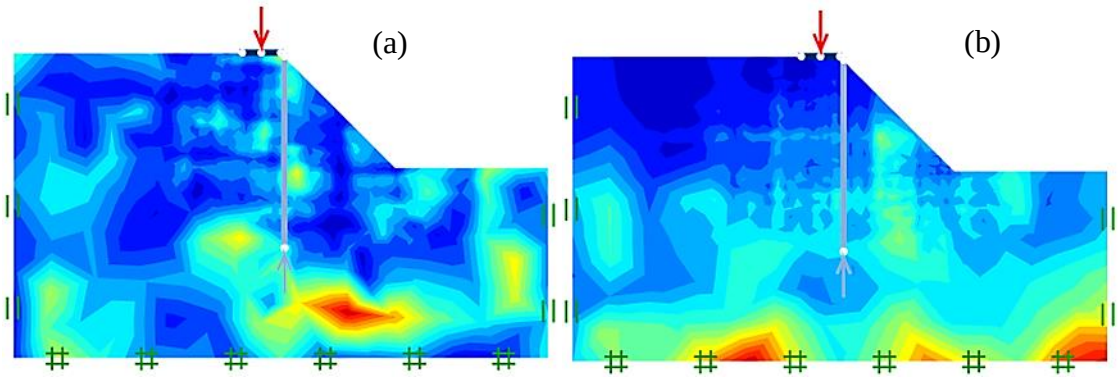

Figure 5.6: Shear strength distribution: (a) Θ=1, and (b) Θ=8.

5.5 Conclusion

The random limit analysis was employed herein, using the finite element code OptumG2 (Krabbenhoft, 2017). The objective was to investigate the response of a row of piles to a strip footing under vertical loading, located near a cohesive slope. Random distributions were applied for the shear strength in order to obtain the limit load in terms of lognormal distributions rather than a unique deterministic one. It was found that, the critical spatial variability parameters are attributed to Θ=1 and COV_{cu}=50%; in which, the pertaining μ_{Nc} is minimum. The piles tend to enhance μ_{Nc} by 33.12% for COV_{cu}=10%, and 53.55% for COV_{cu}=50%. Furthermore, values of COV_{Nc} pertaining to the unreinforced case were seen to be upgrading with the raise of COV_{cu}. It was found from the distributions of the complemetry cumulative probabilities pertaining to the random bearing capacity $N_{c,rand}$ that, the unreinforced case provides significantly lower probabilities and conservative random variables X. Also, before the crossover, the increase in spatial variability lowers the corresponding probabilities. Small correlation lengths (i.e. Θ=1) imply a high degree of variability in the soil shear strength; whereas bigger lengths imply more uniformity.

Chapter 6: Numerical analysis on sheet pile wall reinforcement of a slope with an adjacent inclined loaded strip footing

6.1 Introduction

In terms of limit load pertaining to a footing situated at the crest of a slope, a stability number should be verified. Taylor (1948) proposed an expression for this purpose to reach an accurate estimation of the overall stability. Furthermore, to depict the inclined loaded footing behaviour, load correction factors have been addresses by Hansen (1961) and Vesic (1975). Georgiadis (2010) proposed an analytical equation for failure envelopes by means of normalized loads. This motion accounted only for a quite limited cases, where the slope is undergoing a bearing capacity failure mode. The bearing capacity of a footing at a slope crest may show a significant reduction compared to the case of a horizontal ground (Kusakabe et al., 1981; Meyerhof, 1957; Saran et al., 1989). Therefore, to contribute at the purpose of enhancing the limit load, sheet pile walls have proved a great response to footing settlement and overall steadiness (El Sawwaf, 2005; Esser & Dingeldein, 2007; Sudani et al., 2015). This is due to their effective dynamic response (Gazetas et al., 2016; Lin et al., 2018; Qu et al., 2017).

This chapter aims to presenting a conducted study by Bougouffa et al. (2020). In which, a sheet pile wall is employed to reinforce a slope with an adjacent strip footing, in order to provide a new estimation of the bearing capacity. As well as, another accepted study for publication made on load inclination factors under various slope conditions. Computational series of two dimensional FE limit analysis are conducted, using OptumG2 code (Krabbenhoft, 2017).

6.2 Problem definition

The undrained bearing capacity of a footing situated on a sheet pile reinforced slope, is calculated as follows:

$$q_u = N_c^* B c_u, \quad N_c^* = N_c i_{c\beta}, \tag{6.1}$$

where N_c, B and c_u are respectively the factor of bearing capacity, width of strip footing, and undrained shear strength. It should be emphasized that the load inclination $i_{c\beta}$ is obtained from dividing the limit load of inclined loaded footing on a slope $q_{u(\theta\neq0,\ \beta\neq0)}$, by that of the vertical loaded footing on a horizontal ground $q_{u(\theta=0,\ \beta=0)}$:

$$i_{c\beta} = q_{u(\theta\neq0,\beta\neq0)} / q_{u(\theta=0,\beta=0)}, \tag{6.2}$$

where θ and β are respectively, the load and slope inclination angles. The bearing capacity improvement is expressed by a non-dimensional factor BCI:

$$BCI = {}^{q_{us}}/_{q_u}, \tag{6.3}$$

where q_{us} and q_u are respectively, the undrained limit load of the stabilized slope and the unstabilized one. The slope domain is shown in Figure 6.1(a), with a footing of width B=1m. The parametric study investigates the influence of various parameters. Specifically, the relative footing distances of λ=0-2 (measured from its edge to the slope crest), slope height ratios of Z/B=0.5-4, slope angles of β=15-45°, height of sheet pile wall ratios of L/B=1-5 and sheet pile wall distance ratios of d/B=0-2 (measured from the reinforcement to the slope edge).

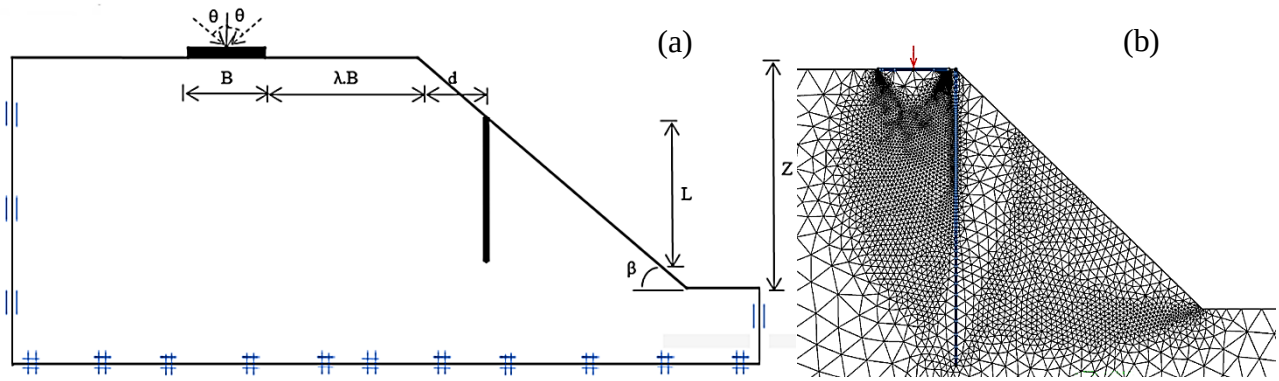

Figure 6.1: Definition of the problem: (a) geometry, and (b) mesh adaptivity.

6.3 Numerical approach

The plane strain FE code OptumG2 (Krabbenhoft, 2017) is adopted to model the entire slope domain, due to the absence of both geometry and load symmetry. The soil is simulated as rigid plastic material, following the failure criterion of Tresca, with associated flow rule. The sheet pile wall reinforcement

and the rough strip footing are simulated as rigid beam elements. Figure 6.1(a) shows that, the base of the model is fully fixed, while the sides are only of a horizontally fixity.

The accurate estimation of the limit load is furnished by dint of the average corresponding to the upper (UB) and lower (LB) bounds of the limit analysis. An initial mesh of 2000 triangle elements is employed; thusly, it is increased up to a final mesh of 8000 elements (Figure 6.1(b)). Four adaptive iterations are used for the shear dissipation control. The probe loading technique is used for the assessment of the limit load q_u. This is done by amplifying a load multiplier q_{mult} from its initial state until attaining failure, by dint of a failure multiplier η:

$$q_u = \eta q_{mult}. \tag{6.4}$$

6.4 Numerical analysis of load inclination factors under various slope angles

The investigations of load inclination factors of a strip footing using limit analysis should be verified using further elastoplastic calculations, in order to assure the credibility of the adopted method. For this reason, Figure 6.2 presents the load-displacement curves plotted for a slope angle, soil Young's modulus, and shear strength ratio respectively of, β=40°, E_u=30 MPa and $c_u/\gamma B$=2.5 (γ=20 KN/m^3). The curves represent normalized applied loads V/Bc_u in terms of the pertaining displacements U/B, for L/B=3. The ultimate failure load is generated when the pressure below the strip footing is stabilized. It is shown that, the average plots of limit analysis are in an excellent agreement with those corresponding to the elastoplastic analysis. The ultimate failure load is remarkably affected by the load inclination angle θ and the ratio d/B. For d/B=0, the resistance to the lateral soil displacement heading towards the sloping ground is maximum. This is interpreted by the noteworthy improvement in failure loads. For purely vertical loading, the failure load of d/B=0 (V/Bc_u=4.7) is witnessing a raise of 29.83% compared to the unstabilized case, where V/Bc_u=3.62. However, when the sheet pile wall is driven farther from the crest (i.e., d/B=1), the bearing capacity doesn't show any enhancement. This is interpreted by the corresponding failure loads that are indistinguishable from those of the unstabilized case. Consequently, the limit load is reached at minor ratios of U/B.

Figure 6.3 shows the disparity in the bearing capacity factors N_c* in terms of different load inclinations. The plots corresponding to the case before reinforcement are computed for reasons of comparison with the literature. It is noted that, the current plots (unreinforced case) agree well with Hansen's solution (1961); in contrast, Vesic (1975) represents a notable underestimation of N_c^*. The effectiveness of locating the sheet pile wall at the crest d/B=0, is pronounced by the high tendency of N_c*. This latter is showing an improvement that is only 8.56% lower than Prandtl's (1920).

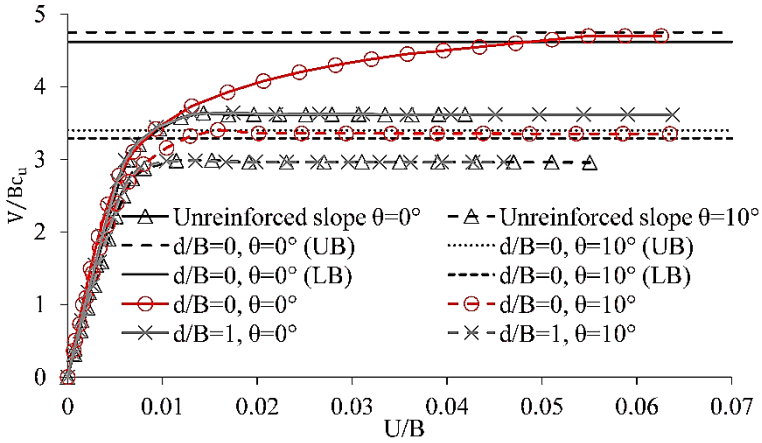

Figure 6.2: Effect of d/B ratios on load-displacement plots, for β=40°, and θ=0° and 10°.

Furthermore, an analytical expression (eq. (6.4)) is derived for $i_{c\beta}$ pertaining to the case without reinforcement. The expression is showing an excellent agreement with the average limit analysis, as shown in Figure 6.3.

$$i_{c\beta} = \frac{4.47\pi}{0.28\beta + \theta + 4.09\pi}. \qquad (6.5)$$

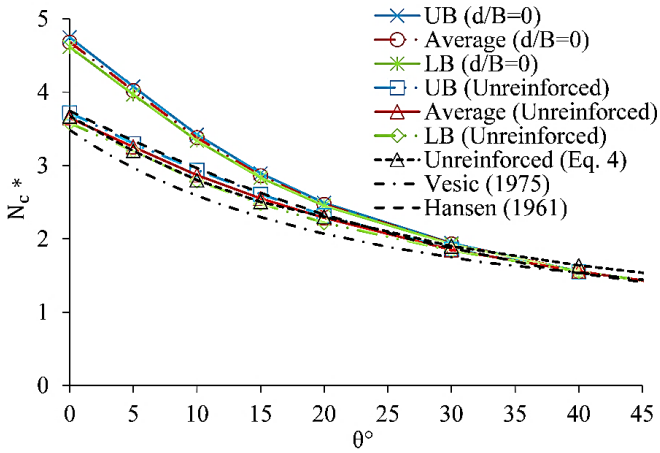

Figure 6.3: Variation of N_c* factors with θ, for β=40°.

6.4.1 Effect of sheet pile wall location on $i_{c\beta}$

Figure 6.4(a-b-c-d) illustrates the disparity in $i_{c\beta}$ with respect to different locations of the sheet pile wall. The plots are captured for slope angles varying from 15° to 45°. It is noted that $i_{c\beta}$ drops with the raise of θ, β, and d/B ratios until crossing over a specific angle of θ=30°. Beyond which (θ≥30°), $i_{c\beta}$ acts similarly as the slope before reinforcement, irrespectively of d/B ratios. This is explained by the existence of a substantial active earth pressure, where the mobilized passive resistance generated by the sheet pile wall is nil. However, the passive resistance attains its maximum at θ=0° for d/B=0; thus, $i_{c\beta}$ undergoes a decreasing trend from 1 (β=15°) to 0.88 (β=45°). Subsequently, $i_{c\beta}$ raises by

11.11% (β=15°) to 29.41% (β=45°) compared to their respective cases of the unreinforced slope. Thereafter, an original expression of $i_{c\beta}$ is derived for d/B≤0.5 and 15°≤β≤45°:

$$i_{c\beta} = \frac{3.2d/B + 20}{0.3\beta d/B + 0.08\beta + \theta + 18.7}. \quad (6.6)$$

It is worthwhile to mention that it is indicated in Figure 6.4 that the plots obtained from eq. (6.5) are almost identical to those of the current analysis (limit analysis).

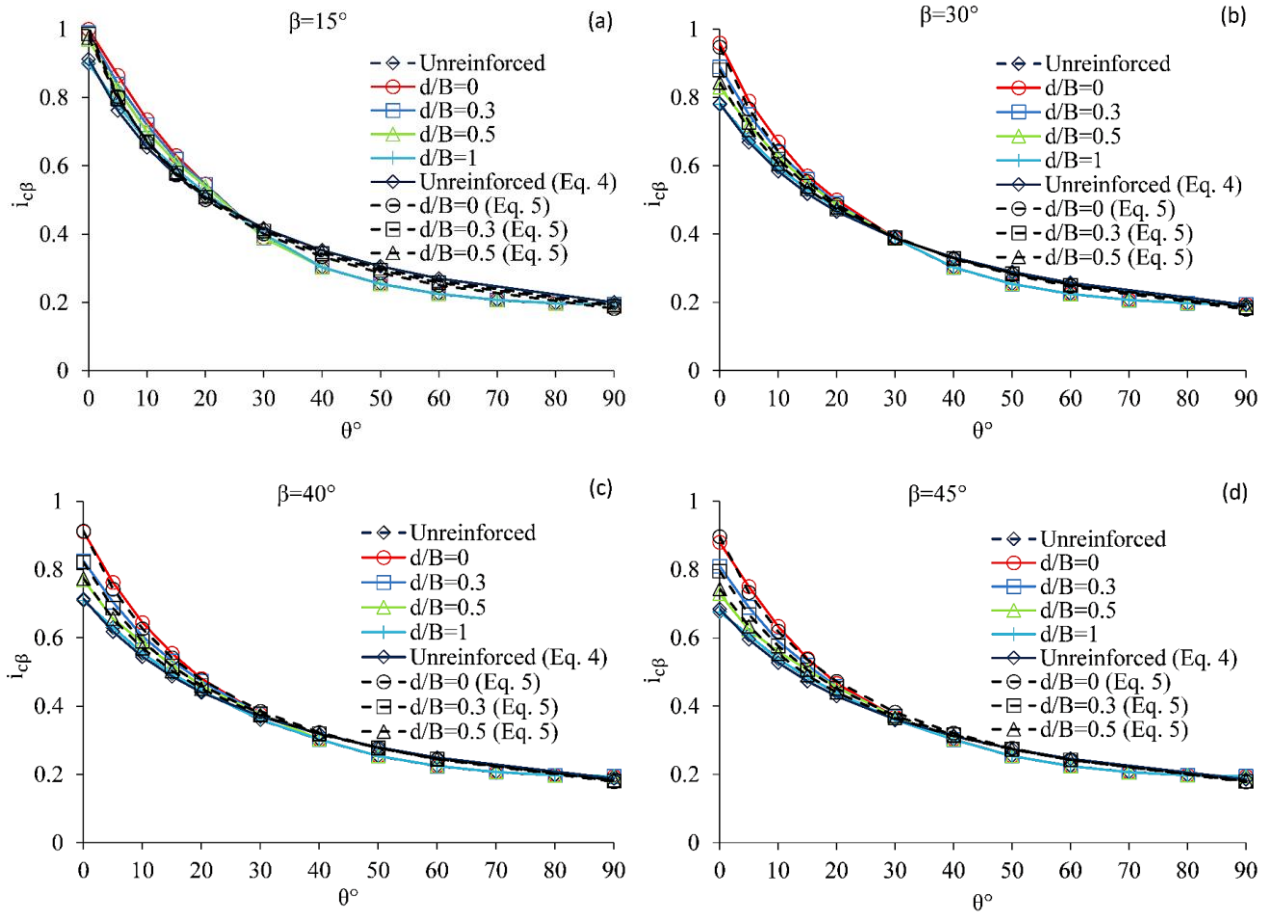

Figure 6.4: Effect of various ranges of θ and d/B on $i_{c\beta}$, captured for various slope angles.

6.4.2 Failure mechanism

Figure 6.5 shows that the incremental shear strains below the footing are captured to define the failure mechanisms. It is clear that for θ=0°, the wedge-shaped elastic zone that is directly underneath the strip footing is quite deeper compared to θ>0°. By dint of the presence of slope reinforcement at d/B=0, a noteworthy passive resistance is generated to dominate the spreading of the active earth pressure. The failure surface is not even crossed for the case of d/B=1. It is noted that, the shear zone

is shallower for θ>0°, as well as its width that narrows with the drop of d/B ratios. This is interpreted by the steadiness of the lower soil layer that repulses the failure plane.

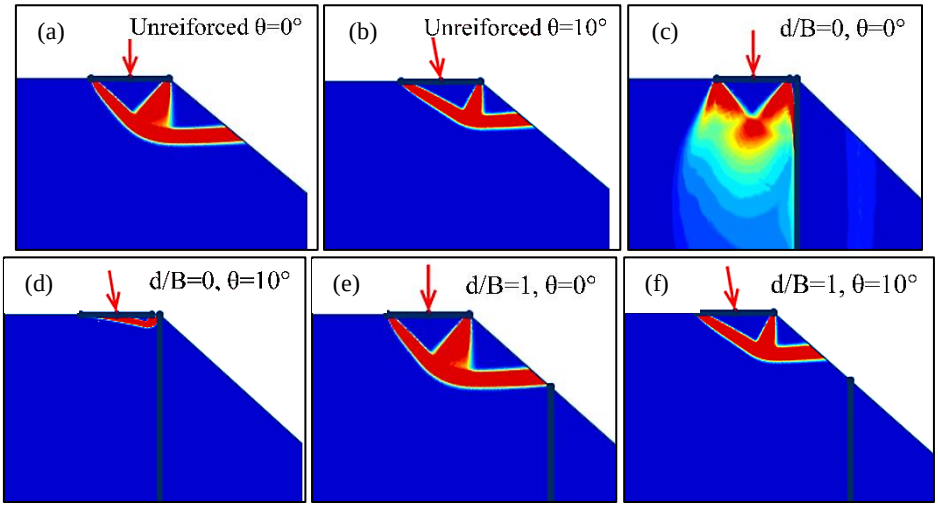

Figure 6.5: Pattern of failure captured for β=40°, 0°≤θ≤10°, and d/B=0 and 1.

6.5 Numerical analysis of the load inclintion effect on failure loads under various reinforcement conditions

Figure 6.6 shows a comparison of the ultimate bearing capacity between the employed method of limit analysis and the classical elastoplastic analysis, for reasons of reliability. The soil undrained shear strength ratio, unit weight and young's modulus are respectively of $c_u/(\gamma B)$ =2.5, γ=20 KN/m^3, and E_s=30 MPa. Hence, the thickness and young's modulus of the sheet pile wall are respectively of t=0.2 m, E=30 and 200 GPa. It is noted from Figure 6.6(a) that, the ultimate bearing capacity is not possibly influenced by the flexural rigidity of the reinforcement. This is due to the similar normalized failure loads resulting from various reinforcement stiffnesses. The failure load corresponding to the average of UB and LB of the limit analysis falls exactly at that of the elastoplastic analysis. It is indicated in Figure 6.6(b) that, the increase of L/B from 1 to 5 leads to an increase of the bearing capacity factors (V/Bc_u). Beyond this interval (L/B>5) failure loads are undergoing a constant trend. It is indicated that the UB and LB solutions in Figure 6.7(a) provide factors of bearing capacity as high as $N_{c(UB)}$=5.198 and $N_{c(LB)}$= 5.082. This signifies that, the average value N_c= 5.14 is similar to the exact one provided by Prandtl (1920). Regardless the underestimation of failure loads resulted from Vesic's equation (1975), the present study is in good agreement with solutions of Meyerhof and Hansen, especially for small horizontal loads. Figure 6.7(b) shows failure envelopes of a footing at the slope crest.

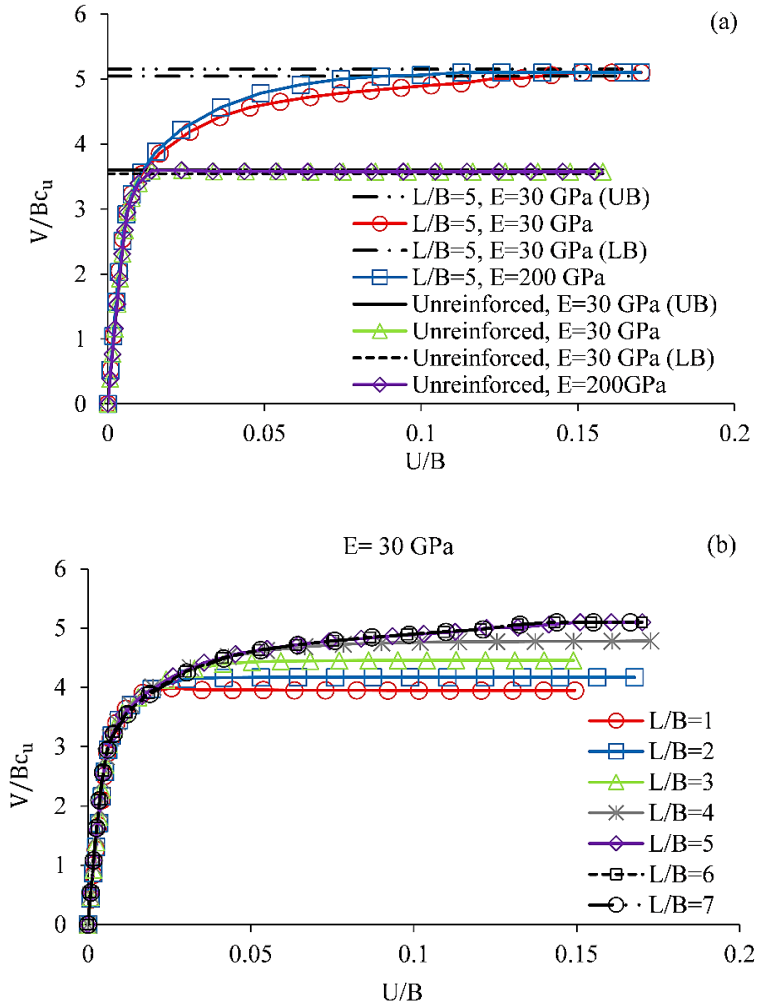

Figure 6.6: Load-displacement plots captured for β=45°, θ=0°, λ=0 and d/B=0: (a) effect of the flexural rigidity of the reinforcement, (b) effect of various ratios of L/B.

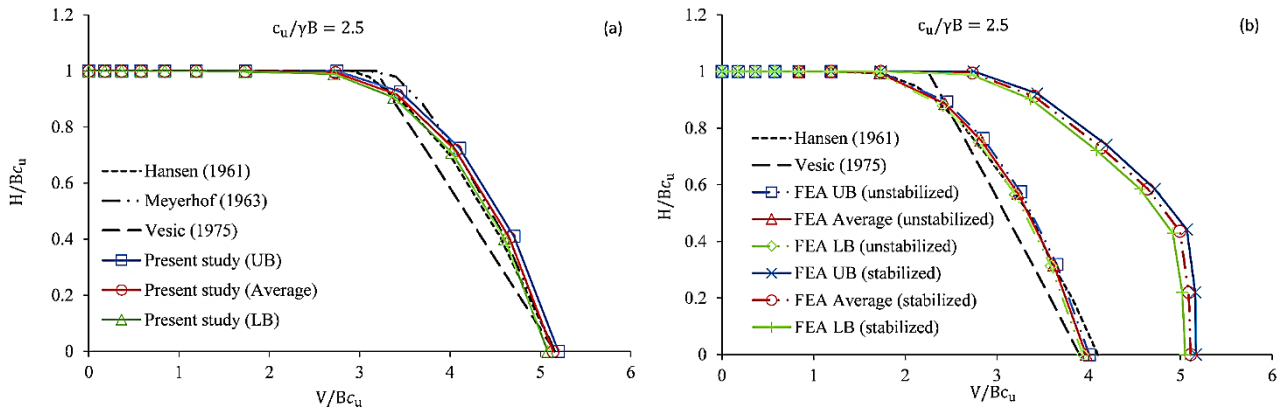

Figure 6.7: Failure plane captured for a footing situated on (a) horizontal ground surface, and (b) slope of β=30°.

It is shown that regardless the solutions of Vesic, the current average results of the unreinforced slope agree well with Hansen for relatively high load angles. It is of interest to mention that, the employed

Analysis is conducted for a sheet pile wall of L/B=5. The corresponding ultimate vertical load is of V_0=5.11Bc_u, which it is about 28.72% greater than the unstabilized case (V_0=3.97Bc_u) and only 0.58% lesser than that of Prandtl (1920).

6.5.1 Effect of various sheet pile wall locations d/B within the slope

Figure 6.8 addresses the relation between BCI and θ, for various ranges of d/B. It is noted that, the bearing capacity is quite enhanced for 0.2 ≤d/B≤ 0.4, which drives the factor BCI to increase. Thus, BCI drops with the increase of θ, specifically for 0°<θ<30°. For θ≥30°, BCI tends to stabilize regardless the range of d/B; this is due to the large active earth pressure that influences N_c factors, and drive them to be equal to those of the unstabilized case. The failure mechanism might be quite enhanced for d/B=0.2 as shown in Figure 6.9(a-b). The elastic wedge shape below the footing gets narrower, and the shear zone headed to the slope is stopped by dint of the reinforcement passive resistance. However, d/B>0.4 might increase the stability of the slope but wouldn't cross the failure plane generated by the footing.

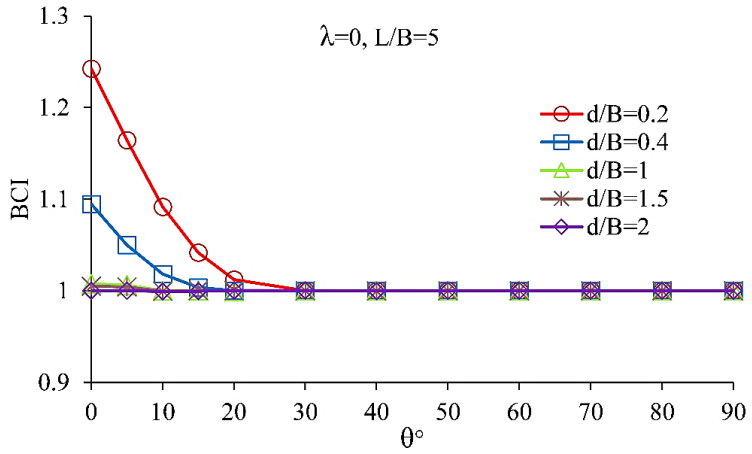

Figure 6.8: Bearing capacity improvement in terms of various normalized sheet pile locations, for $c_u/\gamma B$=1, λ=0, and β=40°.

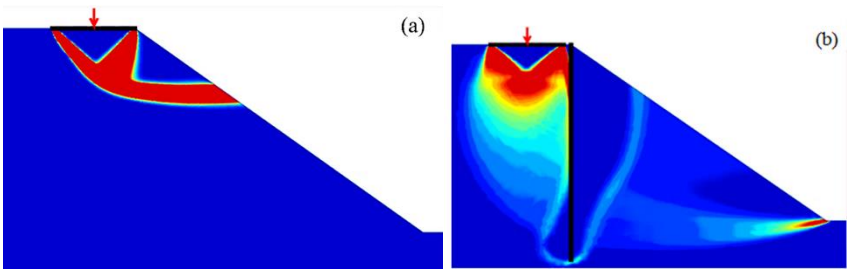

Figure 6.9: The pattern of failure captured for β=40°, θ=0° and λ=0: (a) unreinforced slope and (b) reinforced slope, with L/B=5.

The normalized failure load surfaces are shown in Figure 6.10(a). The unstabilized slope has N_c as high as 3.17, which is similar to the result obtained by Georgiadis (2010). For negative θ, vertical and

horizontal failure loads raise the pertaining size, until reaching θ=-15° (V/Bc_u=3.26 and H/Bc_u=-0.87). Beyond which, they come across the unstabilized curve; leading to a failure mechanism to construct at the crest without being affected by the reinforcement. In contrast, Figure 6.10(b) shows that the load interaction curves are conservative for d/B=0.2 and 0.4; while for d/B> 0.4 they tend towards the unstabilized slope. Thereafter, a simple expression is derived for load interaction curves pertaining to a=d/B≤1 and θ≥0°:

$$h = (0.11a + 0.96)v^{(-1.47a^2+3.75a+2)} - 0.01a + 1.02 \qquad (6.7)$$

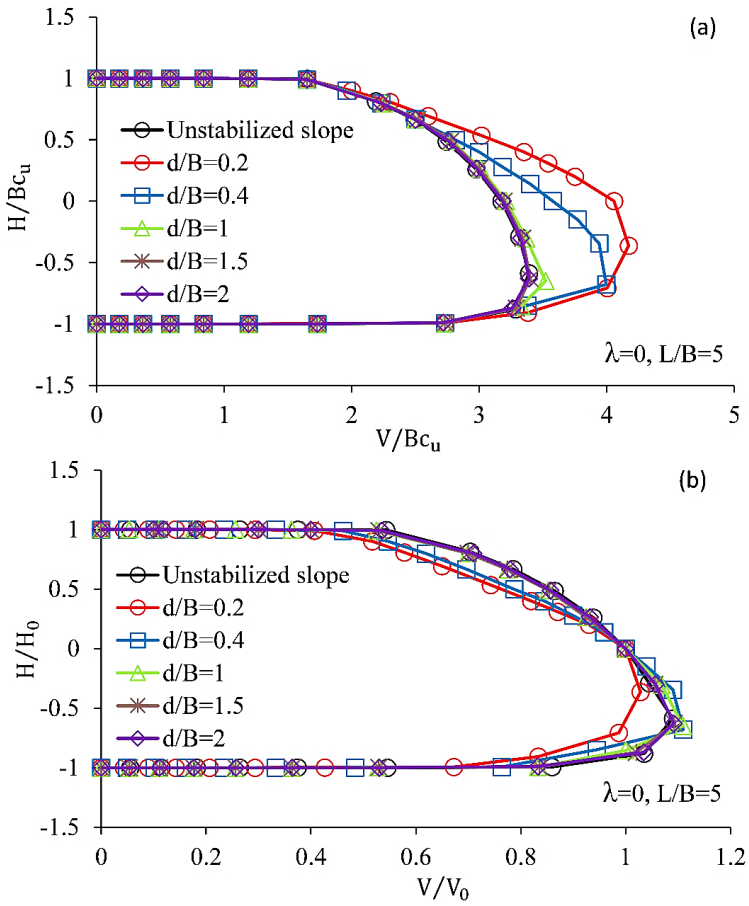

Figure 6.10: Effect of various sheet pile positions, captured for $c_u/\gamma B$=1 and β=45°: (a) normalized failure load planes, and (b) load interaction surfaces.

6.5.2 Effect of various sheet pile wall heights

Both bearing capacity and overall failure types are function of angle θ° and a slope angle less than 45°. Figure 6.11 indicates that at θ=10°, a sheet pile of L/B=5 leads to an improvement of 1.41 times that of the slope without reinforcement. This occurs by dint of the raise in the embedded portion within the stable layer. Consequently, minus lateral deformations of soil and rotation of sheet pile wall are assured. Mostly, the extreme BCI comes around 10°≤θ≤20°. After the peak, the bearing capacity failure mode takes place at relatively great θ values; the overall failure mode happens for

lower values of θ°. It is illustrated in Figure 6.12(a) that, L/B=5 raises the vertical load to the maximum (4.18Bc_u), by which, the reinforcement passive resistance returns to be utmost. Nevertheless, the vertical load that leads to failure is as high as 2.73Bc_u, almost 65.45% greater than the unreinforced slope (1.65Bc_u). A noteworthy drop is noted from the failure envelopes expansion pertaining to L/B=1 and 2. Figure 6.12(b) shows that, the shape of failure envelopes for both positive and negative angles is undergoing a contradictory trend. This tendency indicates the extent of shear surface within the slope that gets far down for shorter sheet pile walls. But then again, shear zones are restricted and shallower for L/B=5.

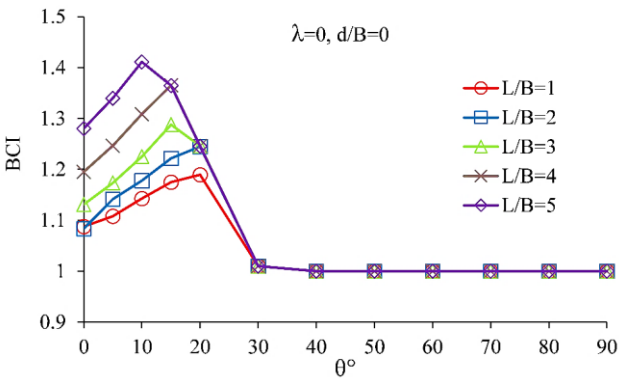

Figure 6.11: Bearing capacity improvement in terms of various sheet pile heights L/B, captured for $c_u/\gamma B$=1, λ=0, and β=40°.

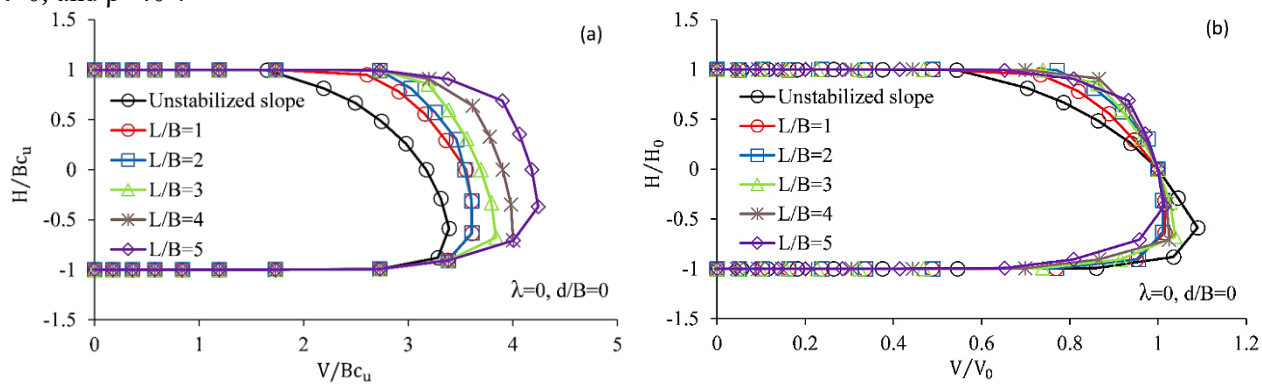

Figure 6.12: Effect of various sheet pile heights, captured for $c_u/\gamma B$=1 and β=45°: (a) normalized failure load planes, and (b) load interaction surfaces.

6.5.3 Effect of various normalized footing distances

Figure 6.13 shows that, BCI reaches its maximum when the footing is right at the crest, since the passive resistance is quite increased at this stage. For λ=0, the angle θ exerts a critical effect in a wider range 0°≤θ≤20°, compared to λ>0 (0°≤θ≤10°). Therefore, the ultimate BCI is related to θ=10° for λ=0, and to θ<10° for λ=1 and 2; this indicates the existence of an overall failure type. However, this latter, is considered quite limited for λ=0 (unstabilized slope) as shown in Figure 6.9. Furthermore, Figure 6.14(a) indicates that high values of λ raise the size of failure envelopes.

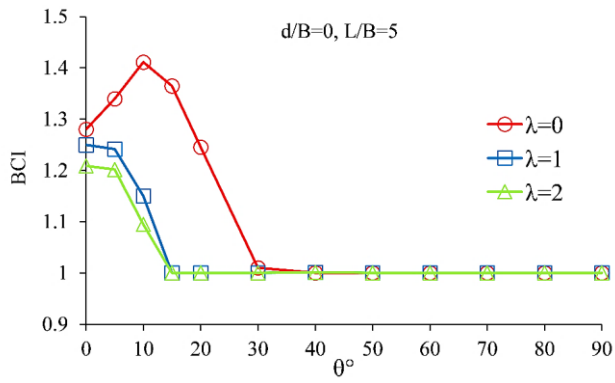

Figure 6.13: Bearing capacity improvement in terms of various normalized footing distances, captured for $c_u/\gamma B=1$, d/B=0, and β=40°.

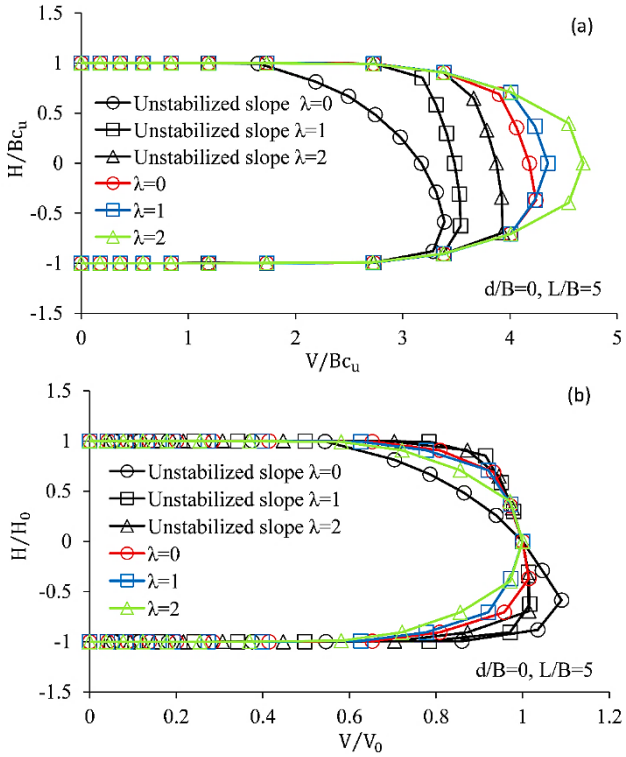

Figure 6.14: Effect of various normalized footing distances, captured for $c_u/\gamma B=1$ and β=45°: (a) normalized failure load surfaces, and (b) load interaction curves.

The bearing capacity factor pertaining to the stabilized slope with λ=0 is of 4.18, which is 81.32% close to the horizontal ground surface; whereas for λ=2 (N_c=4.68) it is 91.05%. Nevertheless, the shape of failure envelopes is affected by the sheet pile wall, as shown in Figure 6.14(b); whereas, positive and negative loads are leaning in a tight band, dissimilarly to the unstabilized slope. Hence, higher λ values of the unstabilized case tend to lean load interaction curves towards lower λ for the stabilized case.

6.5.4 Effect of various shear strength ratios $c_u/\gamma B$

It is illustrated in Figure 6.15(a-b-c) that, three ratios are considered $c_u/\gamma B$= 1, 2.5 and 5 for β=15°, 30° and 45°. The overall failure mode tend to reduce the normalized failure loads for $c_u/\gamma B$=1. Thusly, the reduction persists with the increase of β. For β=15°, the footing ultimate vertical load capacity pertaining to the stabilized slope raises by 15.65% from the unstabilized one. Nevertheless, for β=30°, the enhancement is up to 24.06% relevant to $c_u/\gamma B$=1, and 26.98% relevant to $c_u/\gamma B$=2.5 and 5. As well as for the case of β=45°, a raise of 31.86% is captured for $c_u/\gamma B$=1 and 42.86% relevant to $c_u/\gamma B$=2.5 and 5.

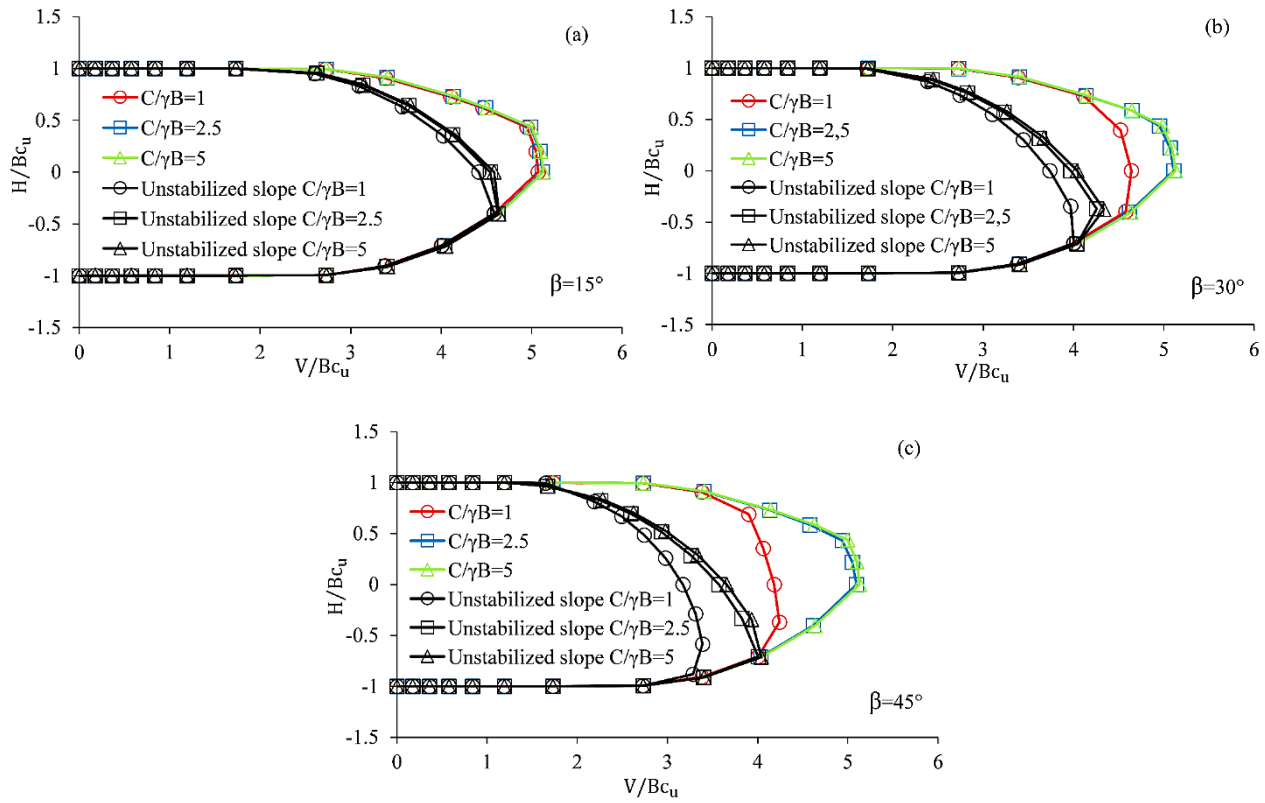

Figure 6.15: Effect of various $c_u/\gamma B$ ratios on normalized failure surfaces, captured for: (a) β=15°, (b) β=30°, and (c) β=45°.

It is noted from Figure 6.16(a-b-c) that β=15° leads to a unique shape of failure envelopes regardless of $c_u/\gamma B$ ratios, as the bearing capacity is not affected by the reinforcement. In contrast, failure envelopes lean similarly for β=30° and 45° ($c_u/\gamma B$=2.5 and 5). However, the raise in β leads to an increase in load interaction curves of $c_u/\gamma B$=1.

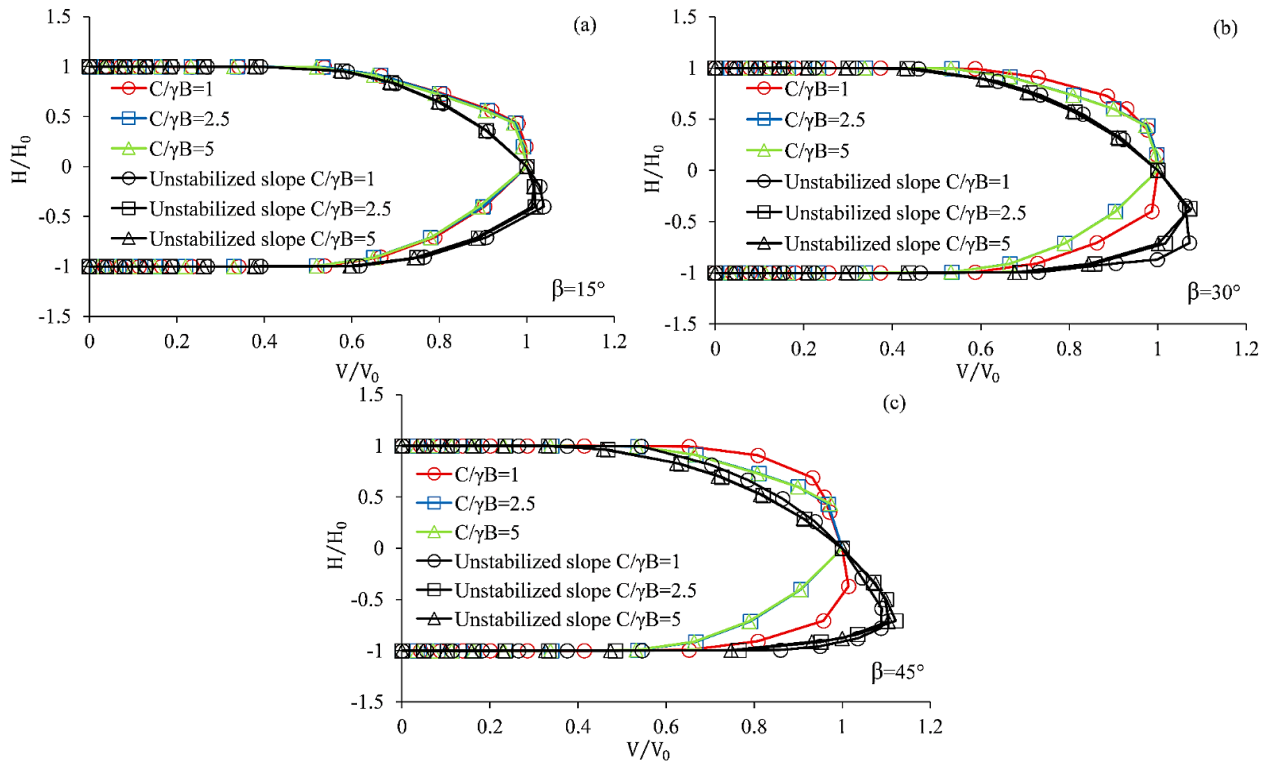

Figure 6.16: Effect of various $c_u/\gamma B$ ratios on load interaction curves, captured for: (a) β=15°, (b) β=30°, and (c) β=45°.

6.5.5 Effect of various slope heights

The stability number N_s obtained from Taylor (1948), is defined by means of the slope ultimate height Z_0 and safety factor F_s ($N_s = F_s\gamma Z_0/c_u$). In the current study N_s is of 5.52 (β<54°), which is slightly conservative compared to Taylor's (N_s=5.33). Figure 6.17(a-b) shows that the computed curves decrease with the raise in Z/B ratios.

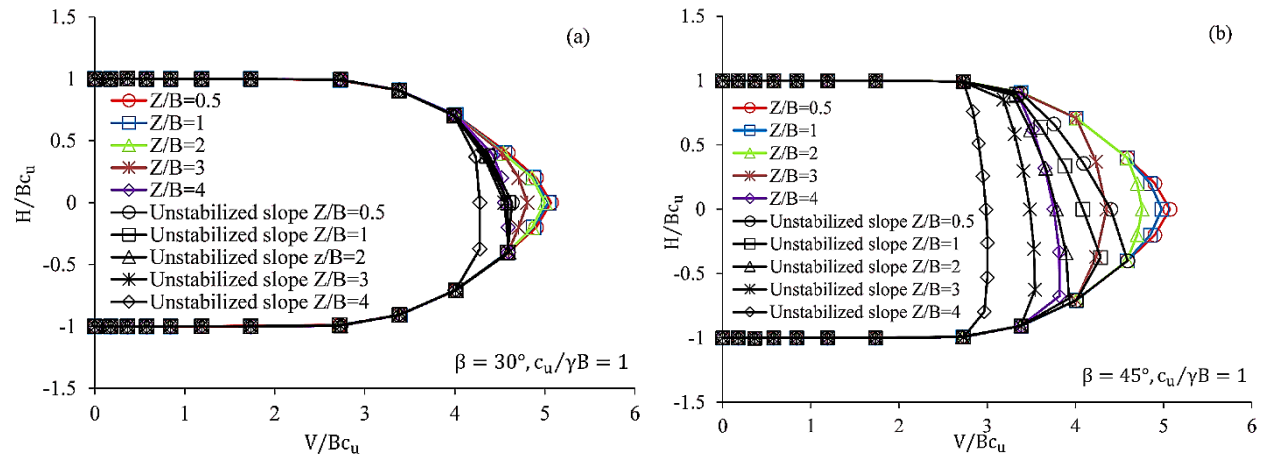

Figure 6.17: Effect of various Z/B ratios on normalized failure surfaces, captured for λ=1: (a) β=30°, and (b) β=45°.

A bearing capacity failure mode is developed for the case relevant to Z/B<3 and β=30°, regardless of the inclination angle θ. Hence, an overall mode happens for Z/B≥3 pertaining to θ<10°. β=45° may generate an overall mode for all cases independently of Z/B and θ. Figures 6.18(a) and 6.19(a) show an overall failure mechanism for β=30° and Z/B=3, at exactly θ=0°. Figures 6.18(b) and 6.19(b) show a bearing capacity failure mechanism relevant to θ=10°.

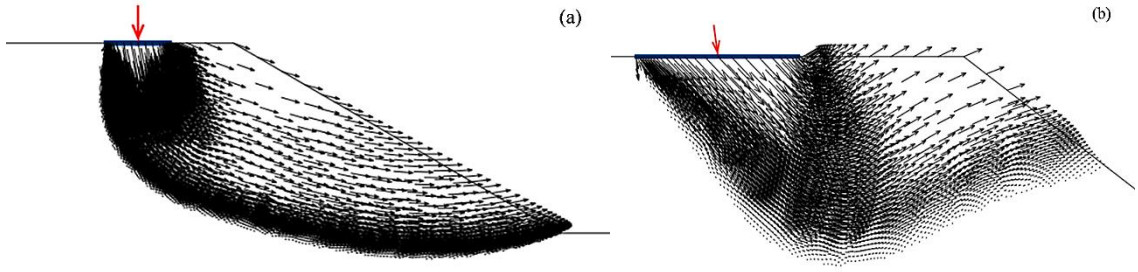

Figure 6.18: The pattern of failure pertaining to the unstabilized slope for Z/B=3, λ=1, $c_u/\gamma B$=1 and β=30°: (a) overall failure at θ=0°, and (b) bearing capacity failure at θ=10°.

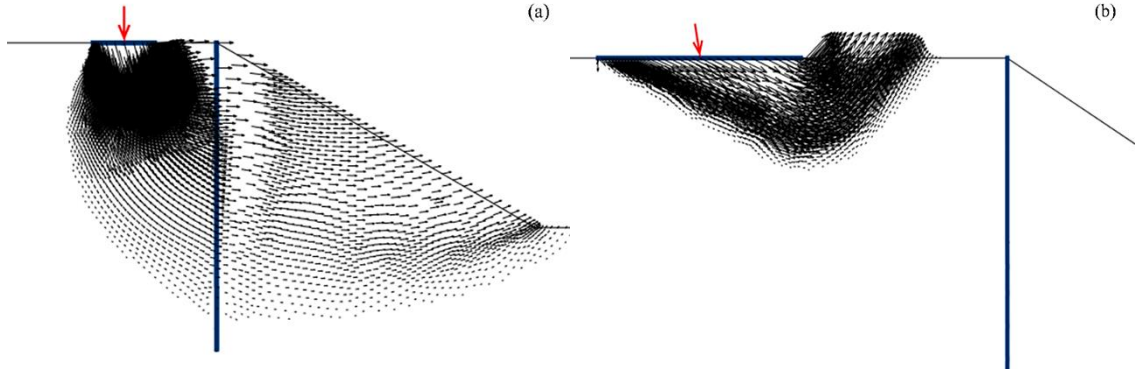

Figure 6.19: The patter of failure pertaining to the stabilized slope for Z/B=3, λ=1, $c_u/\gamma B$=1 and β=30°: (a) overall slope failure at θ=0°, and (b) bearing capacity failure at θ=10°.

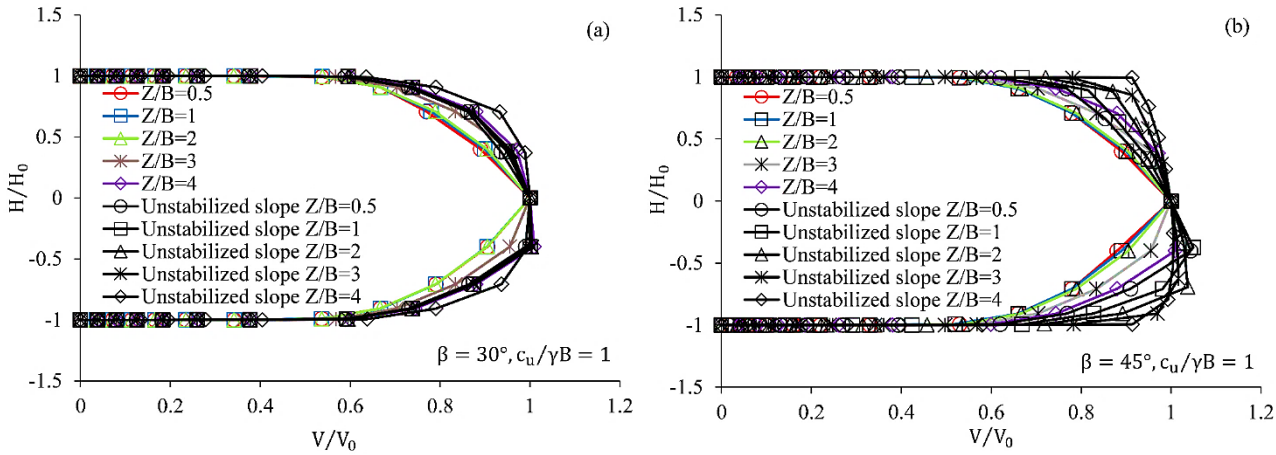

Figure 6.20: Effect of various Z/B ratios on load interaction curves, captured for λ=1: (a) β=30°, and (b) β=45°.

Figure 6.20(a-b) indicates that, the shape of failure envelopes of Z/B<3 is undistinguishable for β=30° and 45°. Z/B≥3 assures greater normalized failure loads, even though the corresponding size of failure envelopes shown in Figure 6.17 is lower. It is noted that the safest estimation of load interaction curves is related to the stabilized slope.

6.6 Conclusion

The 2D finite element limit analysis implemented in OptumG2 code (Krabbenhoft, 2017) was adopted to consider a rough strip footing subjected to a combined loading at a crest of a cohesive slope. In order to serve at the purpose of enhancing the corresponding limit load, a sheet pile wall reinforcement technique was employed. The factors of load inclination $i_{c\beta}$ and improvement in bearing capacity BCI were captured for each load inclination angle θ°. Thusly, failure envelopes were dressed to predict the relevant size and shape, as well as the type of failure mechanism.

The factor $i_{c\beta}$ drops with the raise of θ, d/B and β until reaching failure at θ=30°. Beyond which, a crossover takes place independently of β, due to the attaint of a similar footing failure with that of the unstabilized case. Quite original expressions of $i_{c\beta}$ were derived for the slope before and after reinforcement. The ratios of d/B, L/B, $c_u/\gamma B$ and Z/B showed a significant influence on the ultimate vertical load capacity, as well as on the size and shape of failure envelopes. This results in great failure load surfaces pertaining to cases where the overall stability is assured. A sheet pile of L/B=5 and λ=0 leads to the maximum improvement in the bearing capacity. Nevertheless, the type of failure mechanism is governed by the footing location, load inclination and slope angle. This happens for β<45° due to the reveal of overall and bearing capacity failure types that are in terms of θ°. For θ<10°, the failure mode pertaining to Z/B≥3 and $c_u/\gamma B$=1 is that of the overall. This latter happens for all cases of Z/B pertaining to β=45°, independently of the load inclination. In contrast, β<45° associates the bearing capacity mode for θ≥10° and Z/B<3 regardless the inclination angle θ°.

General conclusion and perspectives

The prediction of the behaviour and safety factors of slopes reinforced with a row of piles or sheet pile wall, relies on the accurate consideration of the soil-pile interaction. The sliding induced pressure exerted on the passive part of piles is function of the pertaining properties; namely, soil-pile stiffness and strength. The criteria that defines the structural failure is attributed to the strength of the pile material itself. By which, failure is governed by the pile centre-to-centre spacing, diameter, location within the slope, length, soil mechanical properties, and the presence of a surface load condition.

The main objective of this thesis, is to contribute to the deterministic and probabilistic studies of the subject pertaining to the steadiness and safety of slopes, subjected to an inclined loading condition at the surface. This is done by considering the reinforcement technique of discrete and continues vertical structures. The numerical contributions are addressing several problems; namely, safety improvement of a c-φ slope, combined effect of surface inclined loading and purely cohesive sloping ground, bearing capacity enhancement of an inclined loaded strip footing, as well as, the influence of spatial variability of soil parameters on the pile response.

The first Chapter of this thesis, is mainly addressing a bibliographical synthesis of already conducted studies in the literature. Foremost, chapter one is presenting basic notions and principles of slope analyses based on the sought purpose; might be safety problems, bearing capacity problems or random field generation. The slope failure is induced by different causes; for instance, the self-weight, surface loading (shallow foundation at the slope crest) or soil spatial variability. It was found that, all the approaches are relying on the same principle of stability estimation. Basically, they depend on locating the slip surface firstly, then determining the active stresses in order to compute the factor of safety. The bearing capacity of shallow foundations is taken into consideration by means of Terzaghi's superposition principle (1943). Whereas, the bearing capacity is determined by virtue of correction factors. In addition, the accuracy of probabilistic level is determined by dint of the generation of a rigorous random field. Therefore, the Monte-Carlo simulation addresses quite

complex problems by combining all random combinations of soil parameters. Thusly, the resulting data are of the form of probability distribution and cumulative distribution functions.

Analytical and numerical methods reported in the literature for the stability assessment of a slope stabilized by a row of piles, are presented in **Chapter two**. The limit equilibrium method is primarily consisting of two sections: pressure and displacement based methods. The advantage of numerical methods (shear strength and limit analyses) over the classical method of equilibrium is that, the soil-pile interaction is fully considered. Moreover, the calculations are carried out without necessarily locating previously the slip surface. In addition, the pile bending stiffness and head conditions are taken into account in the assessment of the factor of safety.

The third chapter presents the deterministic and stochastic studies performed earlier for the determination of the limit load with combining two effects, sloping ground and surface load condition. It should be mentioned that, the case of a reinforced slope was considered by different scholars only under purely vertical loading condition. The elastoplatic approach provides the ability of tracking the history of deformations and stresses. In contrast; the limit analysis is concentrated on the accurate estimation of the limit load based on the corresponding static and kinematic approaches. Furthermore, this chapter presented the most influencing parameters on the bearing capacity under soil spatial variability condition; for instance, mean value, correlation length and coefficient of variation.

The second part is addressing the presentation of numerical contributions conducted within the objective of this dissertation. The problem of reinforcing a slope with/without an adjacent shallow footing to ensure an overall enhancement in slope stability, is considered as a complex problem. Whereas, a robust numerical tool to conduct either deterministic or probabilistic analyses is necessary. This thesis relies on the efficiency of OptumG2 code (Krabbenhoft, 2017), as it permits the simulation of pile rows in two dimensional finite element analyses, following the principle of Sluis (2014). Thusly, it permits to depict the full failure process, by tracking the effect of all possible load inclinations applied on the slope surface. It is of interest to mention that, the simulation of soil spatial variability following random field theories is one of the concepts of OptumG2 code.

First of all, **Chapter four** provides a study conducted on the stability enhancement of a c-φ slope with a row of piles. The finite element shear strength reduction method integrated in OptumG2 was used. The elastoplastic approach was adopted by dint of taking into consideration the pile head conditions, bending stiffness and pile spacing. The computations were conducted to determine the

maximum mobilized pressure acting on piles; as well as, the distribution of the shear force, deflection and bending moment along the pile row. It was found that the shear force pertaining to the case of restrained head piles, is larger and the deflection is lower compared to the free head condition. In which, it leads by its turn to a maximum factor of safety. Hence, pile rigidity doesn't really show an influence on F_s, due to the similar resulting reaction force for both cases. The slip surface undergoes a decreasing trend in depth with the increase of pile spacing under the free head condition; while it leans similarly under the hinged head condition.

Chapter five is representing an original study on the problem of bearing capacity pertaining to shallow footings. The limit analysis integrated in OptumG2 is employed to analyze the behaviour of a rigid strip footing on a cohesive slope, under the condition of vertical and inclined loading. This study considered the effect of reinforcing the slope by a row of anti-slide piles to improve the undrained bearing capacity. The failure envelopes are dressed in terms of the average of upper and lower bound solutions. The bearing capacity improvement and both size and shape of failure envelopes were detected for each pile spacing, length, diameter and location. The plots were captured under positive and negative load inclinations, with different footing locations. It was found that, piles driven at the slope crest raise significantly the bearing capacity improvement factor BCI, specifically at $5° \leq \theta \leq 10°$, pertaining to S/B=0.5 (BCI=1.39). Thenceforth, the failure through piles in a row is significantly limited for Ø=0.2B and L=5B. In which, it refers to the best case with an improvement of the factor of load inclination $i_{c\beta}$ as high as 32.79%, compared to the reference case (slope without piles). The failure loads, indicate that the critical bearing capacity factor is attributed to $\theta=30°$. This leads to a minimum bearing capacity factor improvement of 14.97%. It was concluded that, conservative failure envelopes are corresponding to a footing setback of $\lambda=0$, as the pertaining factor $i_{c\beta}$ drops remarkably.

The effect of special variability of soil characteristics on the bearing capacity of a rigid strip footing subjected to purely vertical loading, is studied using the probabilistic analysis. The study showed that, the stochastic parameters influencing N_c and the probability of failure P_f are the shear strength mean value, coefficient of variation and isotropic correlation length. The software OptumG2 serves at the purpose of, simulating the spatial variability of soil following the theory of random fields using the limit analysis, in order to obtain direct limit load computations. This is considered as an advantage over the elastoplastic analysis where the time criteria is much extended. It was found that, the critical correlation length and coefficient of variation that attributes maximum reduction in the mean bearing capacity, are respectively of $\Theta=1$ and $COV_{cu}=50\%$. It is important to mention that, the pile

reinforcement tends to enhance remarkably the bearing capacity factor by 53.55% compared to the reference case (without reinforcement).

Furthermore, A two dimensional deterministic study was conducted and represented in **Chapter six**, to depict the behaviour of a sheet pile wall, under various slope angles. The sheet pile wall has shown a great effect in dominating the extent of failure surface towards the sloping ground and improve the overall stability. A new evaluation of the undrained bearing capacity was determined in terms of most efficient pile wall parameters; as well as, the slope geomechanic and geometric parameters. It was found that, the maximum slope stability is related to larger failure load surfaces. In which, they are attributed to L/B=5, d/B=0 and λ=2. The slope angle is the one responsible to define the failure pattern. Whereas, $\beta<45°$ indicates an overall failure pattern relevant to $\theta<10°$, pertaining to a slope height of $Z/B\geq3$ and shear strength ratio of $c_u/\gamma B=1$. In contrast, the bearing capacity failure type is relevant to cases where $\theta\geq10°$ and all cases of $Z/B<3$. It should be mentioned that, for the case corresponding to a slope angle of $\beta=45°$, the overall failure type is independent of the ratio Z/B.

Another study was carried out in the same perspective, to investigate the rate of improvement in the factor $i_{c\beta}$ for various slope angles. The rigid strip footing is situated exactly at the slope crest imitating the case of bridge abutments. The study investigated the suitable pile wall position under various degrees of β. It was concluded that the load inclination factor is function of d/B, θ and β. Thusly new expressions of $i_{c\beta}$ were derived to take into consideration the slope before and after reinforcement. It was noted that, $i_{c\beta}$ drops remarkably with the raise in its influencing parameters till the point where θ is of 30° (the critical state). d/B=0 is the optimal position that assures maximum passive resistance. This is explained by the improvement in the ultimate vertical load capacity that is 91.44% ($\beta=40°$) close to the case of the horizontal surface provided by Prandtl (1920).

References

Ahmed, F. (2004). *Stability of strip footings adjacent to concrete sheet pile walls*. D. Eng. thesis of Lamar University-Beaumont.

Ali, A., Lyamin, A. V., Huang, J., Li, J. H., Cassidy, M. J., & Sloan, S. W. (2017). Probabilistic stability assessment using adaptive limit analysis and random fields. *Acta Geotechnica*, *12*(4), 937–948.

Ali, A., Lyamin, A. V., Huang, J., Sloan, S. W., & Cassidy, M. J. (2016). Effect of spatial correlation length on the bearing capacity of an eccentrically loaded strip footing. *6th Asian-Pacific Symposium on Structural Reliability and Its Applications-APSSRA 2016*, 312–317.

As'ad, M., Murni, D., Yulvi, Z., & Agoes, S. M. D. (2013). Bearing Capacity on Slope Modelling with Composite Bamboo Pile Reinforcement. *International Journal of Engineering and Advanced Technology*.

Ashour, M., & Ardalan, H. (2012). Analysis of pile stabilized slopes based on soil–pile interaction. *Computers and Geotechnics*, *39*, 85–97.

Ausilio, E., Conte, E., & Dente, G. (2001). Stability analysis of slopes reinforced with piles. *Computers and Geotechnics*, *28*(8), 591–611.

Baazouzi, M., Benmeddour, D., Mabrouki, A., & Mellas, M. (2016). 2D numerical analysis of shallow foundation rested near slope under inclined loading. *Procedia Engineering*, *143*, 623–634.

Bauer, G. E. (1981). Bearing capacity of footings in granular slopes. *Proc. 10th ICSMFE*, *2*, 33–36.

Biarez, J. (1965). Equilibre limite des talvs et barrages de terre. *Annales de l'Institut Tech. Du Batiment Travaux Pub.*, *211*.

Bishop, A. W. (1955). The use of the slip circle in the stability analysis of slopes. *Geotechnique*, *5*(1), 7–17.

Bolton, M. D., & Lau, C. K. (1993). Vertical bearing capacity factors for circular and strip footings on Mohr–Coulomb soil. *Canadian Geotechnical Journal*, *30*(6), 1024–1033.

Bougouffa, I., Mellas, M., & Baheddi, M. (2019). Probabilistic Analysis of Slopes by Finite Element Method. In B. Pradhan (Ed.), *GCEC 2017* (Vol. 9, pp. 379–392). Springer Singapore.

Bougouffa, I., Mellas, M., Mabrouki, A., & Baheddi, M. (2019). *Two-dimensional strength reduction analysis of a slope reinforced with piles*. Paper presented at the 4th Eurasian conference on Civil and Enviromental Engineering, Avcilar, Turkey.

Bougouffa, I., Mellas, M., Mabrouki, A., Krabbenhoft, K., & Baheddi, M. (2020). Numerical analysis of the bearing capacity of inclined loaded strip footings supported on sheet pile wall stabilized slopes. *Australian Geomechanics*, *55*(2), 79–89.

Brahmi, N., Ouahab, M. Y., Mabrouki, A., Benmeddour, D., & Mellas, M. (2018). Probabilistic analysis of the bearing capacity of inclined loaded strip footings near cohesive slopes. *International Journal of Geotechnical Engineering*.

Bransby, M. F., & Randolph, M. F. (1998). Combined loading of skirted foundations. *Géotechnique*, *48*(5), 637–655.

Broms, B. B. (1964). Lateral resistance of piles in cohesionless soils. *Journal of the Soil Mechanics and Foundations Division*, *90*(3), 123–156.

Cai, F., & Ugai, K. (2000). NUMERICAL ANALYSIS OF THE STABILITY OF A SLOPE REINFORCED WITH PILES. *Soils and Foundations*, *40*(1), 73–84.

Caquot, A. (1954). Equilibre des massifs à frottement interne. Stabilité des terres pulvérulents et cohérents. *Geotechnique*, *4*, 43.

Cassidy, M. J., Uzielli, M., & Tian, Y. (2013). Probabilistic combined loading failure envelopes of a strip footing on spatially variable soil. *Computers and Geotechnics*, *49*, 191–205.

Castelli, F., & Motta, E. (2010). Bearing capacity of strip footings near slopes. *Geotechnical and Geological Engineering*, *28*(2), 187–198.

Chatzigogos, C. (2007). *Comportement sismique des fondations superficielles: Vers la prise en compte d'un critère de performance dans la conception*. Thèse de doctorat de l'école Polytechnique.

Chen, F., Cheng, L., Zhou, T., Chen, X., & Zhang, W. (2019). Probabilistic Assessment on Stability of Slopes Reinforced with Piles Considering Spatial Variability of Soil Properties. *IOP Conference Series: Earth and Environmental Science*, *304*(4).

Chen, G., Zou, L., Wang, Q., & Zhang, G. (2020). Pile-spacing calculation of anti-slide pile based on soil arching effect. *Advances in Civil Engineering*.

Chen, L. T., & Poulos, H. G. (1997). Piles subjected to lateral soil movements. *Journal of Geotechnical and Geoenvironmental Engineering*, *123*(9), 802–811.

Chen, W.-F. (2013). *Limit analysis and soil plasticity*. Elsevier.

Cheng, Y. M., Lansivaara, T., & Wei, W. B. (2007). Two-dimensional slope stability analysis by limit equilibrium and strength reduction methods. *Computers and Geotechnics*, *34*(3), 137–150.

Choudhury, D., & Subba Rao, K. S. (2006). Seismic bearing capacity of shallow strip footings embedded in slope. *International Journal of Geomechanics*, *6*(3), 176–184.

Chow, Y. K. (1996). Analysis of piles used for slope stabilization. *International Journal for Numerical and Analytical Methods in Geomechanics*, *20*(9), 635–646.

Dembicki, E. (1974). Model tests on bearing capacity of foundations on slopes. *Proc. Danube-European Conf. on SMFE*, 147–153.

Di Laora, R., Maiorano, R. M. S., & Aversa, S. (2017). Ultimate lateral load of slope-stabilising piles. *Géotechnique Letters*, *7*(3), 237–244.

Dong-ping, D., Liang, L., & Lian-heng, Z. (2017). Limit-equilibrium method for reinforced slope stability and optimum design of antislide micropile parameters. *International Journal of Geomechanics*, *17*(2).

El Sawwaf, M. A. (2005). Strip footing behavior on pile and sheet pile-stabilized sand slope. *Journal of Geotechnical and Geoenvironmental Engineering*, *131*(6), 705–715.

Erickson, H. L., & Drescher, A. (2002). Bearing capacity of circular footings. *Journal of Geotechnical and Geoenvironmental Engineering*, *128*(1), 38–43.

Esser, A. J., & Dingeldein, J. E. (2007). Failure of Tieback Wall Anchors due to Corrosion. *Case Studies In Earth Retaining Structures*, 1–10.

Fellenius, W. (1927). Earth stability calculations assuming friction and cohesion on circular slip surfaces. *Ernst: Berlin, Germany*.

Fenton, G. A., & Griffiths, D. V. (2008). *Risk assessment in geotechnical engineering* (Vol. 461). John Wiley & Sons.

Frydman, S., & Burd, H. J. (1997). Numerical studies of bearing-capacity factor Nγ. *Journal of Geotechnical and Geoenvironmental Engineering*, *123*(1), 20–29.

Gazetas, G., Garini, E., & Zafeirakos, A. (2016). Seismic analysis of tall anchored sheet-pile walls. *Soil Dynamics and Earthquake Engineering*, *91*, 209–221.

Georgiadis, K. (2010). The influence of load inclination on the undrained bearing capacity of strip footings on slopes. *Computers and Geotechnics*, *37*(3), 311–322.

Giroud, J. P. (1971). Force portante d'une fondation sur une pente. *Theories et Methodes de Calcul NO. 142, 283/284*.

Gong, W., Li, J., & Li, L. (2018). Limit analysis on seismic stability of anisotropic and nonhomogeneous slopes with anti-slide piles. *Science China Technological Sciences*, *61*(1), 140–146.

Gong, W., Tang, H., Wang, X., & Juang, C. H. (2019). Probabilistic analysis and design of stabilizing piles in slope considering stratigraphic uncertainty. *Engineering Geology*, *259*.

Gourvenec, S. (2007). Failure envelopes for offshore shallow foundations under general loading. *Géotechnique*, *57*(9), 715–728.

Graham, J., Andrews, M., & Shields, D. H. (1988). Stress characteristics for shallow footings in cohesionless slopes. *Canadian Geotechnical Journal*, *25*(2), 238–249.

Green, A. P. (1954). The plastic yielding of metal junctions due to combined shear and pressure. *Journal of the Mechanics and Physics of Solids*, *2*(3), 197–211.

Griffiths, D. V., & Fenton, G. A. (1993). Seepage beneath water retaining structures founded on spatially random soil. *Geotechnique*, *43*(4), 577–587.

Griffiths, D. V., Fenton, G. A., & Manoharan, N. (2002). Bearing capacity of rough rigid strip footing on cohesive soil: Probabilistic study. *Journal of Geotechnical and Geoenvironmental Engineering*, *128*(9), 743–755.

Griffiths, D. V., & Lane, P. A. (1999). Slope stability analysis by finite elements. *Geotechnique*, *49*(3), 387–403.

Haghbin, M., & Ghazavi, M. (2013). Bearing capacity of footings on pile-stabilized slopes. *Transactions of Civil Engineering*, *37*, 257–269.

Hansen, B. (1961). A general formula for bearing capacity. *Danish Geotechnical Institute, Bulletin*, *11*, 38–46.

Hansen, J. B. (1970). A revised and extended formula for bearing capacity. *Danish Geotechnical Institute, Bulletin*, *28*, 5–11.

Hassiotis, S., Chameau, J. L., & Gunaratne, M. (1997). Design method for stabilization of slopes with piles. *Journal of Geotechnical and Geoenvironmental Engineering*, *123*(4), 314–323.

He, Y., Hazarika, H., Yasufuku, N., Han, Z., & Li, Y. (2015). Three-dimensional limit analysis of seismic displacement of slope reinforced with piles. *Soil Dynamics and Earthquake Engineering*, *77*, 446–452.

Hon, R. K., & Demcsak, M. R. (2010). Design and construction of an underpinning and earth-retaining system for Lehigh Valley Hospital building. *Earth Retention Conference 3*, 342–351.

Houlsby, G. T., & Puzrin, A. M. (1999). The bearing capacity of a strip footing on clay under combined loading. *Proceedings of the Royal Society of London. Series A: Mathematical, Physical and Engineering Sciences*, *455*(1983), 893–916.

Huang, J., Kelly, R., Li, D., Zhou, C., & Sloan, S. (2016). Updating reliability of single piles and pile groups by load tests. *Computers and Geotechnics*, *73*, 221–230.

Huang, J., Lyamin, A. V., Griffiths, D. V., Krabbenhoft, K., & Sloan, S. W. (2013). Quantitative risk assessment of landslide by limit analysis and random fields. *Computers and Geotechnics*, *53*, 60–67.

Huang, Y. H. (2014). Slope stability analysis by the limit equilibrium method: Fundamentals and methods. *American Society of Civil Engineers*.

Ito, T., & Matsui, T. (1975). Methods to estimate lateral force acting on stabilizing piles. *Soils and Foundations*, *15*(4), 43–59.

Ito, T., Matsui, T., & Hong, W. P. (1981). Design method for stabilizing piles against landslide: One row of piles. *Soils and Foundations*, *21*(1), 21–37.

Jeong, S., Kim, B., Won, J., & Lee, J. (2003). Uncoupled analysis of stabilizing piles in weathered slopes. *Computers and Geotechnics*, *30*(8), 671–682.

Jiang, C., Li, T., Zhou, K., Zhao, C., Li, C., Zhou, Z., Lin, L. I. U., & Ce, S. H. A. (2016). Reliability analysis of piles constructed on slopes under laterally loading. *Transactions of Nonferrous Metals Society of China*, *26*(7), 1955–1964.

Jin, L., Feng, Y., Zhang, H., & Feng, Q. (2020). The use of improved radial movement optimization to calculate the ultimate bearing capacity of a nonhomogeneous clay foundation adjacent to slopes. *Computers and Geotechnics*, *118*.

Kayser, M., & Gajan, S. (2014). Application of probabilistic methods to characterize soil variability and their effects on bearing capacity and settlement of shallow foundations: State of the art. *International Journal of Geotechnical Engineering*, *8*(4), 352–364.

Keskin, M. S., & Laman, M. (2013). Model studies of bearing capacity of strip footing on sand slope. *KSCE Journal of Civil Engineering*, *17*(4), 699–711.

Kim, Y., & Jeong, S. (2011). Analysis of soil resistance on laterally loaded piles based on 3D soil–pile interaction. *Computers and Geotechnics*, *38*(2), 248–257.

Kimura, T., Kusakabe, O., & Saitoh, K. (1985). Geotechnical model tests of bearing capacity problems in a centrifuge. *Géotechnique*, *35*(1), 33–45.

Kourkoulis, R., Gelagoti, F., Anastasopoulos, I., & Gazetas, G. (2012). Hybrid method for analysis and design of slope stabilizing piles. *Journal of Geotechnical and Geoenvironmental Engineering*, *138*(1), 1–14.

Krabbenhoft, K. (2017). Optum computational engineering (OptumG2). *Computer Software*.

Krabbenhoft, K., Lyamin, A. V., Hjiaj, M., & Sloan, S. W. (2005). A new discontinuous upper bound limit analysis formulation. *International Journal for Numerical Methods in Engineering*, *63*(7), 1069–1088.

Kusakabe, O., Kimura, T., & Yamaguchi, H. (1981). Bearing capacity of slopes under strip loads on the top surfaces. *Soils and Foundations*, *21*(4), 29–40.

Lebegue, Y. (1973). Essais de fondations superficielles sur talus. *Proceedings, 8th International Conference on Soil Mechanics and Foundation Engineering*, *4*(3), 313.

Lee, C. Y., Hull, T. S., & Poulos, H. G. (1995). Simplified pile-slope stability analysis. *Computers and Geotechnics*, *17*(1), 1–16.

Li, C., Chen, W., Song, Y., Gong, W., & Zhao, Q. (2020). Optimal location of piles in stabilizing slopes based on a simplified double-row piles model. *KSCE Journal of Civil Engineering*, *24*(2), 377–389.

Li, L., & Liang, R. Y. (2014a). Limit equilibrium based design approach for slope stabilization using multiple rows of drilled shafts. *Computers and Geotechnics*, *59*, 67–74.

Li, L., & Liang, R. Y. (2014b). Reliability-based design for slopes reinforced with a row of drilled shafts. *International Journal for Numerical and Analytical Methods in Geomechanics*, *38*(2), 202–220.

Li, X., Pei, X., Gutierrez, M., & He, S. (2012). Optimal location of piles in slope stabilization by limit analysis. *Acta Geotechnica*, *7*(3), 253–259.

Lin, Y., Cheng, X., Yang, G., & Li, Y. (2018). Seismic response of a sheet-pile wall with anchoring frame beam by numerical simulation and shaking table test. *Soil Dynamics and Earthquake Engineering*, *115*, 352–364.

Loukidis, D., Chakraborty, T., & Salgado, R. (2008). Bearing capacity of strip footings on purely frictional soil under eccentric and inclined loads. *Canadian Geotechnical Journal*, *45*(6), 768–787.

Luo, N., & Bathurst, R. J. (2017). Reliability bearing capacity analysis of footings on cohesive soil slopes using RFEM. *Computers and Geotechnics*, *89*, 203–212.

Mabrouki, A., Benmeddour, D., Frank, R., & Mellas, M. (2010). Etude numérique de la capacité portante d'une fondation filante au bord d'une pente. *Journées Nationales de Géotechnique et Géologie de l'ingénieur JNGG*, *1*, 489–496.

Maréchal, O. (1999). Portance de fondations superficielles établies à proximité de talus et soumises à des charges inclinées et excentrées. *Thèse de Doctorat de L'école Centrale de Nantes-Discipline*.

Martin, C. M. (2003). User Guide for ABC-Analysis of Bearing Capacity, Version 1.0. *OUEL Report No. 2261/03. Department of Engineering Science, University of Oxford*.

Massih, D. Y. A., & Soubra, A.-H. (2010). Effet de la variabilité spatiale du sol dans l'étude du comportement des fondations superficielles filantes. *Revue Française de Géotechnique*, *130*, 41–50.

Meyerhof, G. G. (1951). The ultimate bearing capacity of foundations. *Geotechnique*, *2*(4), 301–332.

Meyerhof, G. G. (1963). Some recent research on the bearing capacity of foundations. *Canadian Geotechnical Journal*, *1*(1), 16–26.

Meyerhof, G. G. (1957). The ultimate bearing capacity of foundations on slopes. *Proc., 4th Int. Conf. on Soil Mechanics and Foundation Engineering*, *1*, 384–386.

Michalowski, R. (1997). An estimate of the influence of soil weight on bearing capacity using limit analysis. *Soils and Foundations*, *37*(4), 57–64.

Nian, T. K., Chen, G. Q., Luan, M. T., Yang, Q., & Zheng, D. F. (2008). Limit analysis of the stability of slopes reinforced with piles against landslide in nonhomogeneous and anisotropic soils. *Canadian Geotechnical Journal*, *45*(8), 1092–1103.

Nian, T.-K., Jiang, J.-C., Wang, F.-W., Yang, Q., & Luan, M.-T. (2016). Seismic stability analysis of slope reinforced with a row of piles. *Soil Dynamics and Earthquake Engineering*, *84*, 83–93.

Nimityongskul, N., Kawamata, Y., Rayamajhi, D., & Ashford, S. A. (2018). Full-Scale Tests on Effects of Slope on Lateral Capacity of Piles Installed in Cohesive Soils. *Journal of Geotechnical and Geoenvironmental Engineering*, *144*(1).

Nonveiller, E. (1965). The stability analysis of slopes with a slip surface of general shape. *Proc. of 6th. ICSMFE.*, 522–525.

Ouahab, M., Mabrouki, A., Mellas, M., & Benmeddour, D. (2017). Inclination Factors for Strip Footings on Non-Homogeneous Clay. *Soil Mechanics & Foundation Engineering*, *54*(3).

Phoon, K.-K., & Kulhawy, F. H. (1999). Characterization of geotechnical variability. *Canadian Geotechnical Journal*, *36*(4), 612–624.

Pirone, M., & Urciuoli, G. (2018). Analysis of slope-stabilising piles with the shear strength reduction technique. *Computers and Geotechnics*, *102*, 238–251.

Popescu, R., Prevost, J.-H., & Deodatis, G. (1997). Effects of spatial variability on soil liquefaction: Some design recommendations. *Geotechnique*, *47*(5), 1019–1036.

Poulos, H. G. (1995). Design of reinforcing piles to increase slope stability. *Canadian Geotechnical Journal*, *32*(5), 808–818.

Prandtl, L. (1920). Über die härte plastischer körper. *Nachrichten von Der Gesellschaft Der Wissenschaften Zu Göttingen, Mathematisch-Physikalische*, 74–85.

Qin, C. B., Chian, S. C., & Wang, C. Y. (2017). Kinematic analysis of pile behavior for improvement of slope stability in fractured and saturated Hoek–Brown rock masses. *International Journal for Numerical and Analytical Methods in Geomechanics*, *41*(6), 803–827.

Qu, H. L., Luo, H., Liu, L., & Liu, Y. (2017). Analysis of dynamic coupling characteristics of the slope reinforced by sheet pile wall. *Shock and Vibration*.

Raee, E., Hataf, N., Barkhordari, K., & Ghahramani, A. (2019). The effect of rigidity of reinforced stone columns on bearing capacity of strip footings on the stabilized slopes. *International Journal of Civil Engineering*, *17*(6), 673–685.

Randolph, M. F., & Houlsby, G. T. (1984). The limiting pressure on a circular pile loaded laterally in cohesive soil. *Geotechnique*, *34*(4), 613–623.

Rao, P., Zhao, L., Chen, Q., & Li, L. (2017). Limit analysis approach for accessing stability of three-dimensional (3-D) slopes reinforced with piles. *Marine Georesources & Geotechnology*, *35*(7), 978–985.

Sanping, Z., & Robert, L. (2002). Stability analysis of drilled shafts reinforced slope. *Soils and Foundations*, *42*(2), 93–102.

Saran, S., Sud, V. K., & Handa, S. C. (1989). Bearing capacity of footings adjacent to slopes. *Journal of Geotechnical Engineering*, *115*(4), 553–573.

Sayed, S., Dodagoudar, G. R., & Rajagopal, K. (2010). Finite element reliability analysis of reinforced retaining walls. *Geomechanics and Geoengineering: An International Journal*, *5*(3), 187–197.

Schweckendiek, T. (2006). Structural reliability applied to deep excavations. *Coupling Reliability Methods with Finite Elements*.

Sharafi, H., & Sojoudi, Y. (2016). Experimental and numerical study of pile-stabilized slopes under surface load conditions. *International Journal of Civil Engineering*, *14*(4), 221–232.

Shields, D. H. (1977). Bearing capacity of foundations near slopes. *Proc. of 9th ICSMFE*, *1*, 715–720.

Shields, D. H., & Garnier, J. (1989). Foundations at the top of slopes. *Demello Volume of the 12th International Conference of the International Society of Soil Mechanics and Foundation Engineers*.

Sieffert, J.-G., & Bay-Gress, C. (2000). Comparison of European bearing capacity calculation methods for shallow foundations. *Proceedings of the Institution of Civil Engineers-Geotechnical Engineering*, *143*(2), 65–74.

Sluis, J. M. M., Besseling, F., & Stuuworld, P. H. H. (2014). Modelling of a pile row in a 2D plane strain FE-analysis. In *Numerical Methods in Geotechnical Engineering* (pp. 277–282).

Srivastava, A., & Babu, G. S. (2009). Effect of soil variability on the bearing capacity of clay and in slope stability problems. *Engineering Geology*, *108*(1–2), 142–152.

Sudani, G. A., Brake, N., & Jao, M. (2015). Stability of footings adjacent to pile walls. *International Journal of Geomechanics*, *15*(6).

Taheri, O., Moayed, R. Z., & Nozari, M. (2015). Lateral Soil-Pile Stiffness Subjected to Vertical and Lateral Loading. *Journal of Geotechnical and Transportation Engineering*, *1*(2).

Taiebat, H. A., & Carter, J. P. (2002). Bearing capacity of strip and circular foundations on undrained clay subjected to eccentric loads. *Geotechnique*, *52*(1), 61–64.

Tang, W. H. (1984). Principles of probabilistic characterization of soil properties. In *Geotechnical Safety and Reliability* (pp. 39–39).

Taylor, D. (1948). *Fundamentals of soil mechanics*. Chapman And Hall.

Taylor, D. W. (1937). Stability of earth slopes. *J. Boston Soc. Civil Engineers*, *24*(3), 197–247.

Terzaghi, K. (1943). Theoretical Soil Mechanics. *John Wiley & Sons, New York*.

Ukritchon, B., Whittle, A. J., & Sloan, S. W. (1998). Undrained limit analyses for combined loading of strip footings on clay. *Journal of Geotechnical and Geoenvironmental Engineering*, *124*(3), 265–276.

Vanmarcke, E. (1983). *Random fields: Analysis and synthesis*. The MIT press.

Vesic, A. S. (1973). Analysis of ultimate loads of shallow foundations. *Journal of Soil Mechanics & Foundations Div*, *99*(1), 45–76.

Vesic, A. S. (1975). Bearing capacity of shallow foundations. *Foundation Engineering Handbook (Ed. H. F. Winterkorn and H. Y. Fang), 121–47*.

Viggiani, C. (1981). Ultimate lateral load on piles used to stabilize landslides. *Proc. 10th Int. Conf. on SMFE*, *3*, 555–560.

Wang, L. P., & Zhang, G. (2014). Progressive failure behavior of pile-reinforced clay slopes under surface load conditions. *Environmental Earth Sciences*, *71*(12), 5007–5016.

Wang, Y., & Cao, Z. (2013). Expanded reliability-based design of piles in spatially variable soil using efficient Monte Carlo simulations. *Soils and Foundations*, *53*(6), 820–834.

Wei, W. B., & Cheng, Y. M. (2009). Strength reduction analysis for slope reinforced with one row of piles. *Computers and Geotechnics*, *36*(7), 1176–1185.

Won, J., You, K., Jeong, S., & Kim, S. (2005). Coupled effects in stability analysis of pile–slope systems. *Computers and Geotechnics*, *32*(4), 304–315.

Xiao, S. (2020). Improved limit analysis method of piled slopes considering the pile axial forces. *Proceedings of the Institution of Civil Engineers-Geotechnical Engineering*, 1–8.

Xiao, S., He, H., & Zeng, J. (2016). Kinematical limit analysis for a slope reinforced with one row of stabilizing piles. *Mathematical Problems in Engineering*.

Yamin, M., & Liang, R. Y. (2009). Limiting equilibrium method for slope/drilled shaft system. *International Journal for Numerical and Analytical Methods in Geomechanics*.

Yamin, M., & Liang, R. Y. (2010). Limiting equilibrium method for slope/drilled shaft system. *International Journal for Numerical and Analytical Methods in Geomechanics*, *34*(10), 1063–1075.

Yang, M., & Deng, B. (2019). Stability study of slope reinforced with piles under steady unsaturated flow conditions. *Computers and Geotechnics*, *109*, 89–98.

Yang, S., Ren, X., & Zhang, J. (2011). Study on embedded length of piles for slope reinforced with one row of piles. *Journal of Rock Mechanics and Geotechnical Engineering*, *3*(2), 167–178.

Yang, X. L., & Zhang, S. (2020). Stability analysis of 3D cracked slope reinforced with piles. *Computers and Geotechnics*, *122*.

Zhalehjoo, N., Chenari, R. J., & Pouya, K. R. (2012). Evaluation of bearing capacity of shallow foundations using random field theory in comparison to classic methods. In *Geocongress: State of the Art and Practice in Geotechnical Engineering* (pp. 2971–2980).

Zhang, D., & Lu, Z. (2004). An efficient, high-order perturbation approach for flow in random porous media via Karhunen–Loeve and polynomial expansions. *Journal of Computational Physics*, *194*(2), 773–794.

Zhang, J., Wang, H., Huang, H. W., & Chen, L. H. (2017). System reliability analysis of soil slopes stabilized with piles. *Engineering Geology*, *229*, 45–52.